The *Blepharisma stoltei* macronuclear genome: towards the origins of whole genome reorganization

Minakshi Singh[1], Kwee Boon Brandon Seah[1], Christiane Emmerich[1], Aditi Singh[1], Christian Woehle[2], Bruno Huettel[2], Adam Byerly[3], Naomi Alexandra Stover[4], Mayumi Sugiura[5], Terue Harumoto[5], Estienne Carl Swart[1,*]

1. Max Planck Institute for Biology, Tuebingen, Germany
2. Max Planck Genome Center Cologne, Max Planck Institute for Plant Breeding, Cologne, Germany
3. Department of Computer Science and Information Systems, Bradley University, Peoria IL, USA
4. Department of Biology, Bradley University, Peoria, IL, USA
5. Nara Women's University, Nara, Japan

* Corresponding author

Abstract

Both the function and origin of genome reorganization, in which germline genomes are transformed into somatic genomes, are great biological mysteries. In ciliates, ubiquitous microbial eukaryotes with both somatic and germline nuclei in the same cell, tens of thousands of internally eliminated sequences (IESs) scattered throughout the genome are excised. *Blepharisma* represents one of the two earliest diverging ciliate classes, and has unique, dual pathways of somatic nuclear development, making it ideal for investigating the functioning, origins and evolution of these processes. Here, we report the somatic genome assembly of *Blepharisma stoltei* strain ATCC 30299 (41 Mb), arranged as numerous alternative telomere-capped minichromosomes, tens to hundreds of kilobases long. This genome encodes eight PiggyBac transposase homologs liberated from transposons. All are subject to purifying selection, but just one, the putative IES excisase, has a complete catalytic amino acid triad. We proposed that PiggyBac homologs may have been ancestral excisases that enabled extensive genome reorganization.

Abbreviations

- MIC - micronucleus
- MAC - macronucleus
- IES - interspersed eliminated sequence
- MDS - macronuclear-destined sequence
- PacBio - Pacific Biosciences
- CLR - continuous long read (PacBio)
- CCS - circular consensus sequence (PacBio)
- HiFi - High-fidelity read (PacBio)
- ATAS - alternative telomere addition site
- PBLE - PiggyBac-like element
- PGBD - PiggyBac element-derived
- Pgm - PiggyMac
- PgmL - PiggyMac-like

Introduction

Acquisition of new organelles defines and is responsible for the origins of eukaryotes [1]. Ciliates represent one of a couple of eukaryotic lineages with more than one kind of nucleus within individual cells [2]. Profound differences between the ciliate nuclei and the genomes they contain now exist, with some parallels to the germline-soma distinction in multicellular organisms [3]. Ciliate nuclear and genomic dimorphism provides a special opportunity to observe the consequences of evolution of a specialized organelle clearly derived from a general one and for studying the evolution of new, functionally differentiated genes that enable this unusual situation.

The processes responsible for large-scale developmental DNA elimination [4] in ciliate nuclei are under active study, but what the responsible ancestral molecules were remains to be determined. Knowledge of the molecules responsible for ciliate genome reorganization is dominated by *Tetrahymena* and *Paramecium* (class Oligohymenophorea), with additional input from *Oxytricha*, *Stylonychia* and *Euplotes* (class Spirotrichea) [5,6], whereas this remains to be investigated in the remaining nine or so classes. To gain fresh insights into genome reorganization and tackle questions about its origin we focused on the ciliate species *Blepharisma stoltei*. Together with its sister-class, Karyorelictea, the class Heterotrichea, to which this *B. stoltei* belongs, represent the earliest branching ciliate lineages, more distantly related to current model ciliates than those models are to each other [7]. Furthermore, *Blepharisma* exhibits distinctive alternative somatic developmental pathways, which have potential utility in disentangling processes involved in genome reorganization from preceding ones that may indirectly influence it.

Blepharisma is a distinctive genus of single-celled ciliates (Figure 1) known for the red, light-sensitive pigment, blepharismin, in the sub-pellicular membranes of representative species [8],

and unusual nuclear/developmental biology (Figure 2) [9]. To date molecular investigations and genomics of ciliates have predominantly focused on oligohymenophoreans and spirotrichs (Figure 3, Table S1). In recent years, publication of a draft genome for the heterotrich ciliate, *Stentor,* has facilitated revival of this genus for investigations of cellular regeneration [10–12]. However, significant hurdles still need to be overcome to investigate genome reorganization in *Stentor coeruleus* since requisite cell mating has not been observed in the reference somatic genome strain (personal communication, Mark Slabodnick), and very high lethality has been reported for other strains in which mating occurred [13]. We therefore focused on *Blepharisma* which is amenable to such investigations, with controlled induction of mating, and, critically, procedures for investigating cellular and nuclear development have been established from more than a century of meticulous cytological research [8,14–25].

The *Blepharisma stoltei* strains used in the present study were originally isolated in Germany (strain ATCC 30299) and Japan (strain HT-IV), with the former continuously cultured for over fifty years, and the latter for over a decade. The cells are comparatively straightforward to maintain, e.g., stable cultures can be established in a simple salt medium on a few grains of rice passaged every few months. Due to their distinctive pigmentation and large size several *Blepharisma* species are excellent subjects for introducing cell biology concepts to non-specialists, and are thus readily available for educational purposes from commercial suppliers like Carolina Biological Supply Company (USA). They are ideal subjects for behavioral and developmental investigations, e.g., as voracious predators of smaller ciliates and other unicellular species, and also exhibit pronounced phenotypic plasticity, including forming cysts and giant, cannibal cells under suitable conditions [8].

Like all ciliates [3], *Blepharisma* cells have two types of nuclei: a macronucleus (MAC) which is very large and transcriptionally active during vegetative growth, and a small, generally

transcriptionally inactive micronucleus (MIC), which serves as the germline. Each *Blepharisma* cell has one MAC and several MICs (Figure 1A, B). In vegetative propagation (asexual replication) of *Blepharisma*, cell fission results in about half of the MAC pinching off which is then distributed to each of the resulting daughter cells together with the mitotically divided MICs. Upon starvation, *Blepharisma* cells, like other ciliates, are also capable of conjugation and the associated sexual processes. Essential for developmental investigations, the intricate ballet of nuclear movements and morphological changes occurring during *Blepharisma* conjugation is well-documented [9] (Figure 2). During this process about half of the MICs in each of the cells undergo meiosis (meiotic MICs) and the rest do not (somatic MICs) (Figure 2B). One of the meiotic MICs eventually gives rise to two haploid gametic nuclei. One gametic MIC (the migratory nucleus) from each conjugating cell is exchanged with that of its partner. In parallel in partnered cells, subsequent fusion of the migratory and stationary haploid nuclei generates a zygotic nucleus (synkaryon), and after successive mitotic divisions gives rise to both new MICs and new MACs (known as anlagen). The new MACs continue to mature, eventually growing in size and DNA content [9].

Conveniently for investigations of development and genome reorganization, *Blepharisma* is one of only two ciliate genera, along with *Euplotes* [26–29], where conjugation has been shown to be mediated through pheromone-like substances called gamones. *Blepharisma* has two mating types, distinguished by their gamone production. Mating type I cells release gamone 1, a ~30 kDa tyrosine-rich [30] glycoprotein [31,32]; mating type II cells release gamone 2, calcium-3-(2'-formylamino-5'-hydroxybenzoyl) lactate, a small-molecule effector [33]. *Blepharisma* cells commit to conjugation when complementary mating types recognize each other's gamones, with the cells remaining paired while meiosis and fertilization occur and eventually new MACs begin to form.

As in model ciliates, during *Blepharisma* anlagen development, MIC-specific sequences are removed from a MIC genome copy to form a functional MAC genome (Seah, et al. in prep.). The new MAC genomes of model ciliate species are largely free of mobile elements and other forms of “junk” DNA contained in the MIC genome [34]. In the best studied ciliates, a form of genome reorganization assisted by small RNAs (sRNAs) is thought to occur [5]. Specific genome segments limited to the MIC, termed internally eliminated sequences (IESs), are excised by domesticated transposases, and may have originated from transposons [3,5,35,36]. Large scale genome-wide DNA amplification accompanies the genome reorganization process, producing thousands of copies in mature MACs of larger ciliate species [3,34].

We were motivated to investigate genome reorganization in *Blepharisma*, as, unlike model ciliates, these cells can produce two kinds of anlagen, and particularly because one of the two pathways of their development skips the complex series of mitoses, meioses, nuclear exchanges and fertilization [9] (Figure 2). Primary anlagen mature in the conventional manner from zygotic nuclei. Somatic MICs which have not undergone meiosis can give rise to secondary anlagen, which can develop into mature macronuclei [9]. This occurs frequently in strains with a high frequency of selfing (conjugation among cells within a clonal population), in preference to development of primary macronuclear anlagen [9]. This alternative pathway of MAC development has also been observed experimentally after removal of primary macronuclear anlagen by microsurgery [9]. As conjugation progresses, the old (maternal) MACs are progressively degraded [9]. Since the *B*. *stoltei* MIC genome has numerous IESs which interrupt genes (Seah et al. in prep.), in principle, to produce functional, mature MAC genomes, it is essential that reorganization of DNA occurs in both primary and secondary anlagen.

Here we provide essential macronuclear genome and developmental, transcriptomic resources for *B. stoltei* and present the first investigations of possible molecules involved in its genome

reorganization. Like *Stentor coeruleus* [10], *Blepharisma stoltei* genes have the shortest known spliceosomal introns, predominantly 15 or 16 nt long. From long-read sequencing the *B. stoltei* MAC genome appears to be organized in the form of numerous minichromosomes. Among the MAC-encoded transposase genes we identified in *Blepharisma* were PiggyBac transposase homologs, which, as far as we are aware, have not been reported in any ciliates other than *Paramecium* and *Tetrahymena*. A few *Blepharisma* PiggyBac homologs are substantially upregulated in MAC development, including one with a complete catalytic triad which is the main candidate IES excisase. Consistent with ancient origins of genome reorganization in ciliates, *Blepharisma* shares pronounced development-specific upregulation of homologs known to be involved in this process, notably Dicer-like and Piwi proteins responsible for sRNA biogenesis. *Blepharisma* therefore represents an invaluable outgroup for investigations of the evolution of genome reorganization.

Results

A compact, extensively fragmented genome

The draft *Blepharisma stoltei* ATCC 30299 MAC genome is compact, at 41 Mb, and AT rich (66%), like most sequenced ciliate MAC genomes, and relatively complete (Figure 3; Table S1, 2, Figure S1). From joint variant calling of reads from strains ATCC 30299 and HT-IV mapped to this assembly, strain ATCC 30299 appears to be virtually homozygous, with only 1277 heterozygous single-nucleotide polymorphisms (SNPs) observed compared to 193725 in strain HT-IV (i.e., individual heterozygosity of 3.08×10^{-5} vs. 4.67×10^{-3} respectively). Low SNP levels were likely beneficial for the overall assembly contiguity, since heterozygosity poses significant algorithmic challenges for genome assembly software [37]. For brevity's sake, we refer to this

draft genome as the *Blepharisma* MAC genome (and likewise "*Blepharisma*" for the associated strain). Though the final assembly comprises 64 telomere-to-telomere sequences, it is not possible to define conventional chromosome ends given the extensive natural fragmentation of the *Blepharisma* MAC genome (characterized in the next section), hence we refer to them simply as "contigs".

The basic telomere unit of *B*. *stoltei* is a permutation of CCCTAACA, like its heterotrich relative *Stentor coeruleus* [10] (Figure S2). However, a compelling candidate for a telomerase ncRNA (TERC) could not be found in either *Blepharisma* or *Stentor* using Infernal [38] and RFAM models (RF00025 - ciliate TERC; RF00024 - vertebrate TERC). Thus, it was not possible to delimit the ends of the repeat. Heterotrichs may use a different kind of ncRNA, or one which is very divergent from known TERCs. In contrast to the extremely short (20 bp) macronuclear telomeres of spirotrichs like *Oxytricha* with extreme MAC genome fragmentation [39], sequenced *Blepharisma* macronuclear telomeres are moderately long (Figure S2A), with a mode of 209 bp (i.e., 26 repeats of the 8 bp motif), extending to a few kilobases.

Approximately one in eight reads in the *Blepharisma* HiFi library were telomere-bearing and distributed across the entire genome (Figure 4A), using a moderately strict definition of possessing at least three consecutive telomeric repeats. In contrast, the telomere-bearing reads of the model ciliate *Tetrahymena thermophila* predominantly map to chromosome ends (Figure S3A), and only one in fifty nine *Tetrahymena* CLR reads are telomere-bearing, as identified by three consecutive telomeric subunit repeats (i.e., 3×CCCCAA).

Typically, only a minority of mapped reads are telomere-bearing at individual internal contig positions, and so we term them alternative telomere addition sites (ATASs) (Figure 4A). We identified a total of 46705 potential ATASs in *Blepharisma* by mapping PacBio HiFi reads onto

the MAC reference, and searching for partially mapped reads that contained telomeric repeats in the unmapped (clipped) segments without any intervening sequence between the mapped segment and the beginning/end of the telomeric repeat. The majority of these sites (38686) were represented by only one mapped HiFi read.

The expected distance between telomeres, and hence the average MAC DNA molecule length, is about 130 kb. This is consistent with the raw input MAC DNA lengths, which were mostly longer than 10 kb and as long as 1.5 Mb (Figure S3C, D), and our observation that a small fraction (1.3%) of *Blepharisma*'s HiFi reads are bound by telomeres on both ends. Excluding the length of the telomeres, these telomere-bound reads may be as short as 4 kb (Figure S2B). Given the frequency of telomere-bearing reads, we expect many additional two-telomere DNA molecules longer than 12 kb, the approximate maximum length of the HiFi reads (Figure S3C, D).

Since the lengths of the sequenced two-telomere DNA molecules on average imply that they encode multiple genes, we propose classifying them as "minichromosomes". This places them between the length of "nanochromosomes" of ciliates like *Oxytricha* and *Stylonychia*, which typically encode single genes and are on the order of a few kilobases long [39,40], and MAC chromosomes of *Paramecium tetraurelia* and *Tetrahymena thermophila* which are hundreds of kilobases to megabases long [41–43]. Recently it was reported that the *Paramecium bursaria* MAC genome is considerably more fragmented than those of other previously examined *Paramecium* species [44]. The DNA molecules from *P. bursaria* have thus also been classified as minichromosomes [44].

Alternative telomere addition sites in the MAC genome tend to be intergenic in model ciliates like *Oxytricha trifallax* [39]. In *Blepharisma*, we found more intergenic ATASs (28309) than intragenic

ones (18396). As intergenic regions only make up 10.1 Mb of the assembly, the intergenic frequency of ATASs is about five-fold higher (2.81 per 1 kb) than intragenic frequency (0.562 per 1 kb). The presence of intragenic ATASs raises the question how the cell tolerates or deals with mRNAs encoding partial proteins transcribed from 3' truncated genes. Since the sequence data was from a clonal population, it is not possible to tell how much ATAS variability there is within individual cells. However, it is conceivable that their positional variation in single cells reflects that of the population. In this case, together with redundancy from massive DNA amplification there would likely be sufficient intact copies of every gene.

Beyond the first 2-5 bp corresponding to the junction sequences, the average base composition on the chromosome flanking ATAS junctions shows an asymmetrical bias (Figure 4B). From position +6 onwards there is an enrichment of T to about 40% and A to 35-39%, compared to the genome-wide frequencies of 33% each. At position +19 to +23, there is a slight decrease in T to 37-39%. AT values gradually decline back to about 35% each by position +150. Correspondingly, G and C are depleted downstream of ATAS junctions, dropping to a minimum of 8.6% and 11% respectively around position +37, compared to the genome-wide average of 17% each. AT enrichment and GC depletion upstream of ATAS junctions are less pronounced.

If breakage and chromosome healing were random, we would not expect such an asymmetry. This suggests that there is a nucleotide bias, whether in the initiation of breaks, telomere addition, or in the processing of breaks before telomere addition. However, we have not yet identified any conserved motif like the 15 bp chromosome breakage site (CBS) in *Tetrahymena* [45] nor a short 10-bp sequence periodicity in base composition like in *Oxytricha trifallax* [46]. Therefore, telomere addition in *B. stoltei* appears to involve base-pairing of short segments of about 2 bp between the telomere and chromosome, with a bias centered on the "CT" in the

telomere unit, and an asymmetrical preference for AT-rich sequences on the chromosomal side of the junction.

Tiny spliceosomal introns

The *Blepharisma stoltei* ATCC 30299 macronuclear genome is gene-dense (25,711 predicted genes), with short intergenic regions, tiny introns and untranslated regions (UTRs) (Figure 5A). In contrast to *Stentor* which, unusually for ciliates, uses the standard genetic code, *B. stoltei* uses an alternative genetic code with UGA codons reassigned from stops to tryptophan (Figure S5).

Like *Stentor* [10], most (82%) *Blepharisma* genes have no introns. In line with genome compactness, during our inspections we also observed numerous overlapping poly(A)-tailed RNA-seq reads on opposite strands derived from convergently transcribed gene pairs. The correlation of the lengths of different noncoding region classes (intergenic regions, introns and UTRs) can be explained by them being subject to common, neutral evolutionary processes [47].

Blepharisma introns are mostly (97%) 15 or 16 nucleotides (nt) long, like those of *Stentor* (Figure 5B). Though intron reduction (7389 introns predicted in the reference *B. stoltei* MAC genome, i.e., 0.29 introns per gene) is not as extreme as some other microbial eukaryotes, like *Giardia lamblia* [48], where almost all have been lost, both *Blepharisma* and *Stentor* have much fewer introns relative to other ciliates (e.g., intron densities of 1.6, 2.3 and 4.8 introns per gene in *Paramecium*, *Oxytricha* and *Tetrahymena*, respectively [49]) and to the putative, relatively intron-rich eukaryotic common ancestor [50], along with their extreme length reduction.

Blepharisma 15 nt introns possess a characteristic branch-point “A”, as would be expected in classical models of lariat formation during mRNA splicing (Figure 5C). 16 nt introns almost invariably have an “A” at either 10 or 11 nt downstream of the donor site (i.e., only one of 499 does not, but has “A” at 9 nt), although this is not obvious in the consensus sequence logo because the position is variable (Figure S6D). Similarly, 17 nt introns all possess “A” at 10-12 nt downstream of the donor site. Only a few intron bases, 5-8 and 12, of *Blepharisma*’s 15 nt introns are relatively unconstrained (Figure 5C). This leaves little room for the presence of any additional regulatory elements in the mRNA or underlying DNA.

Extensive duplications of transmembrane protein genes

A notable extended ~220 kb region encoding 53 genes belonging to a single orthologous group (orthogroup), OG0000085 is present on Contig_1 (Figure 5A). Four additional OG0000085 genes are present at the opposite end of Contig_1, and 24 copies are found on other contigs, often clustered together (Figure 5D). The DNA coverage across this region is lower (74×) than the rest of Contig_1 (185×). Though there is uncertainty in the exact extent, given the sheer volume of reads involved, the assembled sequences certainly correspond to highly repetitive regions of the MAC genome. At the junction between the lower and higher coverage regions more than 30 HiFi reads link the two regions of coverage, and a similar number of telomere-bearing reads are in close proximity. At the junction we also observe at least two potential locations of IESs, corresponding to regions that may be partially IES/partially MDS.

Large clusters of genes from particular orthogroups can be found on additional contigs (Figure 5D). In total 551 (2%) of predicted *B. stoltei* genes belong to the orthogroups with the largest clusters per contig. Some of the largest contiguous clusters of genes from these orthogroups are situated at the ends of contigs, suggesting they may have caused assembly breaks beyond

them. One contig, split off from other connected components in the assembly graph, predominantly encodes genes from a single orthogroup (contig_64, 43× coverage; Figure 5D; Figure S7). Further increases in read length and accuracy may allow assemblers to fully resolve these in future. Curiously, all the orthogroups corresponding to the largest contiguous clusters of genes appear to be transmembrane proteins, or decayed remnants thereof. The nature of these proteins is described in Supplemental Text ("Properties of proteins encoded by extensive duplications").

Features of gene expression during new MAC development

To gain an overview of the molecular processes during genome reorganization in *Blepharisma* we examined gene expression trends across a developmental time series. Complementary mating strains of *B. stoltei* were treated with gamones of the opposite mating type, before mixing to initiate conjugation [9,51]. Samples for morphological staging and RNA-seq were taken at intervals from the time of mixing ("0 hour" time point) up to 38 hours (Figure S8). The progression of nuclear morphological development and the proportion of cells in each stage at various time points is illustrated in Figure S9.

During conjugation in *Blepharisma*, meiosis begins around 2 h after conjugating cell pairs form and continues up to around 18 h, by when gametic nuclei generated by meiosis have been exchanged (Figure 2A, B, Figure S9). This is followed by karyogamy and mitotic multiplication of the zygotic nucleus (22 hours). At the 26 h time point, new, developing primary MACs can be observed in the conjugating pairs, in the form of large, irregular bodies (Figure 2A, Figure S9). These macronuclear anlagen mature into the new MACs of the exconjugant cell by 38 h, after which cell division generates two daughter cells. Smaller secondary MACs, derived directly from

MICs without all the intermediate nuclear stages, can also be seen from 22 hours to 30 hours, but eventually disappear, giving sole way to the primary MACs (Figure 2A, Figure S9).

Examining gene expression at 26 hours, when the majority of cells are forming a new MAC (Figure S9), we observe two broad trends: relatively stable constitutive gene expression (Table S5; Data S3), e.g., an actin homolog (ENA accession: BSTOLATCC_MAC19444) and a bacteria-like globin protein (BSTOLATCC_MAC21846), versus pronounced development-specific upregulation (Table S6; Data S3), e.g., a histone (BSTOLATCC_MAC21995) an HMG box protein (BSTOLATCC_MAC14030), and a translation initiation factor (eIF4E, BSTOLATCC_MAC5291).

We eschewed a shallow Gene Ontology (GO) enrichment analysis in favour of close scrutiny of a smaller subset of genes strongly upregulated during new MAC formation which we expect are more relevant to molecular biologists. For this, computational gene annotations in combination with BLASTP searches and examination of literature associated with homologs was used. Ranking the relative gene expression at 26 hours vs. the average expression of starved, gamone treated, and 0 hour cells, in descending order, reveals numerous genes of interest in the context of genome reorganization, including homologs of proteins known to be involved in genome reorganization in model ciliate species (Table S6).

Among the top 100 genes ranked this way (69× to 825× upregulation) nine contain PFAM transposase domains: DDE_Tnp_1_7, DDE_3, MULE and DDE_Tnp_IS1595 (e.g., BSTOLATCC_MAC2188, BSTOLATCC_MAC14490, BSTOLATCC_MAC18054, BSTOLATCC_MAC18052, respectively). We also observe small RNA (sRNA) biogenesis and transport proteins, i.e., a Piwi protein (BSTOLATCC_MAC5406) and a Dicer-like protein (BSTOLATCC_MAC1138; see also “Supplemental text”, “Homologs of small RNA-related

proteins involved in ciliate genome reorganization" and Figure S12), and a POT1 telomere-binding protein homolog (POT1.4; BSTOLATCC_MAC1496; Supplemental Text "Telomere-binding protein paralogs"). Numerous homologs of genes involved in DNA repair and chromatin are also present among these highly developmentally upregulated genes ("Supplemental text", "Development-specific upregulation of proteins associated with DNA repair and chromatin" and "Supplemental text", "Development-specific histone variant upregulation"). The presence of proteins involved in either transcription initiation or translation initiation among these highly upregulated genes suggests a possible manner to coordinate the regulation of development-specific gene expression ("Supplemental text", "Development-specific upregulation of proteins associated with initiation of transcription and translation").

PiggyBac homologs in *Blepharisma* are candidate IES excisases

In *Paramecium tetraurelia* and *Tetrahymena thermophila*, PiggyBac transposases are responsible for IES excision during genome reorganization occurring in the developing new MAC [52,53]. These transposases appear to have been domesticated, i.e., their genes are no longer contained in transposons but are encoded in the somatic genome where they provide a necessary function in genome development [52,53]. PiggyBac belongs to the DDE/D-superfamily of transposases due to the presence of a protein domain containing the catalytic triad of 3 aspartic acid residues (DDD), where the third residue can also be a glutamate (E). PiggyBac homologs typically have a DDD catalytic triad, rather than the more common DDE triad of other DDE/D transposases [54]. The DDD catalytic motif is present in the PiggyMac (Pgm) of *Paramecium* and the *Tetrahymena* PiggyBac homologs Tpb1 and Tpb2 [53,55]. Among ciliates, domesticated PiggyBac transposases have so far only been reported in the model oligohymenophorean genera *Paramecium* and *Tetrahymena*, and have not been detected in either the MAC or MIC genomes of the spirotrich *Oxytricha trifallax* [39,56].

We detected more transposase domains (9 distinct PFAM identifiers) in *B. stoltei* than any of the other ciliate species we examined (Figure 6A). Seven of these domains are also found in at least one other ciliate species. Using HMMER searches with the PFAM domain characteristic of PiggyBac homologs, DDE_Tnp_1_7 (PF13843), we found eight homologs in *B. stoltei* ATCC, none of which were flanked by terminal repeats identified by RepeatModeler. We also found PiggyBac homologs in *B. stoltei* HT-IV and *B. japonicum* R1072. Reminiscent of *Paramecium tetraurelia*, which, among ten PiggyMac homologs, has just one homolog with a complete catalytic triad [55], the DDD triad is preserved in just a single *B. stoltei* ATCC 30299 PiggyBac homolog (Figure 6B; Contig_49.g1063, BSTOLATCC_MAC17466). This gene is strongly upregulated during development from 22 to 38 hours after formation of heterotypic pairs, when new MACs develop and IES excision is required (Figure 6B). Furthermore, there are significant similarities in the basic properties of *Blepharisma* and *Paramecium* IESs, which will be reported in detail in the subsequent *B. stoltei* MIC genome paper (Seah et al., in prep.). Consequently, adopting the *Paramecium* nomenclature, we refer to our primary candidate IES excisase as *Blepharisma* PiggyMac (BPgm) and the other homologs as BPgm-Likes (BPgmLs).

PiggyMac homologs are also present in other heterotrich ciliates but have not yet been described because of genome assembly or annotation challenges. Using BPgm as a query sequence, we found convincing homologs containing the conserved catalytic DDD-motif in a genome assembly of the heterotrichous ciliate *Condylostoma magnum* (TBLASTN e-value 2e-24 to 2e-37). While we failed to detect the DDE_Tnp_1_7 domain in predicted genes of the heterotrich *Stentor coeruleus*, we were able to detect a relatively weak adjacent TBLASTN matches split across two frames in its draft MAC genome (e-value 7e-15; SteCoe_contig_741 positions 6558-5475). After joining ORFs corresponding to this region and translating them, we obtained a more convincing DDE_Tnp_1_7 match with HMMER3 (e-value 2e-24). This either

corresponds to a pseudogene or a poorly assembled genomic region. It is also possible that additional PiggyBac homologs were missed in unassembled *Stentor* MAC genome regions.

In addition, we searched for PiggyMac homologs in the MAC genome of the pathogenic oligohymenophorean ciliate *Ichthyophthirius multifiliis* [57]. TBLASTN searches using the *T. thermophila* Tpb2 as a query returned no hits. A HMMER search using hmmscan with a six-frame translation of the *I. multifiliis* MAC genome against the PFAM-A database also did not return any matches with independent E-values (i-E-value) less than 1. We note that based on BUSCO analyses (Figure S1) the *I. multifiliis* genome appears to be less complete than other ciliates we examined. So, a better genome assembly will be needed to investigate the possibility that PiggyBac homologs are encoded elsewhere in this MAC genome.

Other than the PFAM DDE_Tnp_1_7 domain, three of the *Blepharisma* PiggyBac homologs also possess a short, characteristic cysteine-rich domain (CRD) (Figure 6C). This domain is essential for Pgm activity and *Paramecium* IES excision [58]. PiggyBac CRDs have been classified into three different groups [58]. In *Blepharisma*, the CRD consists of five cysteine residues arranged as CxxC-CxxCxxxxH-Cxxx(Y)H (where C, H, Y and x respectively denote cysteine, histidine, tyrosine and any other residue). Two *Blepharisma* homologs possess this CRD without the penultimate tyrosine residue, while the third contains a tyrosine residue before the final histidine. This -YH feature towards the end of the CxxC-CxxCxxxxH-Cxxx(Y)H CRD is shared by all the PiggyBac homologs we found in *Condylostoma*, as well as the PiggyBac-like element (PBLE) from the bat *Myotis lucifugus* (Piggybat) and the human PiggyBac element-derived (PGBD) proteins PGBD2 and PGBD3. In contrast, PiggyBac homologs from *Paramecium* and *Tetrahymena* have a CRD with six cysteine residues arranged in the variants of the motif CxxC-CxxC-Cx{2-7}Cx{3,4}H, and group together with human PGDB4 and *Spodoptera frugiperda* PBLE (Figure 6C).

Previous experiments involving individual or paired gene knockdowns of most of the ten *Paramecium tetraurelia* PiggyMac(-like) paralogs lead to substantial IES retention, even though only one PiggyMac gene (PGM) has the complete catalytic triad, indicating that all these proteins are functional [55]. To examine whether PiggyMac homologs in *Paramecium* are functionally constrained we examined non-synonymous (d_N) to synonymous substitution rate (d_S) ratios ($\omega = d_N/d_S$) for pairwise codon sequence alignments within and between species, with the latter using two closely related *Paramecium* species (*P*. *tetraurelia* and *P*. *octaurelia*). All the d_N/d_S values for pairwise comparisons of each of the catalytically incomplete *P. tetraurelia* PgmLs versus the complete Pgm, were less than 1, ranging from 0.01 to 0.25 (Table S7). All d_N/d_S values for pairwise comparisons between *P. tetraurelia* and *P. octaurelia* PiggyBac orthologs were also substantially less than 1, ranging from 0.02 to 0.11 (Table S8). Since d_N/d_S= 1 indicates genes evolving neutrally [59], none of these genes are likely pseudogenes, and all are subject to similar strong purifying selection.

Since only one of the eight homologs has the complete DDD catalytic triad characteristic of functional PiggyBac transposases, this is the only possible catalytically active PiggyMac in *B. stoltei*. The *in vitro* catalytic activity of the *T. ni* PiggyBac transposase is abolished when any of the catalytic residues are substituted by alanine [60]. Conversely, we expect all *Blepharisma* PiggyMac homologs with an incomplete catalytic triad to be catalytically inactive. In pairwise comparisons of each of the catalytically incomplete homologs versus the complete one d_N/d_S ranges from 0.0076 to 0.1351 (Table S9). As these estimates fall in a similar range to those obtained for *Paramecium* PiggyMac/PiggyMac-likes, this indicates that the *B. stoltei* PiggyMac homologs are predominantly subject to comparable purifying selection and unlikely to be pseudogenes, but may have differentiated and acquired new functional roles.

A common origin for PiggyBac transposases in ciliates

To determine whether the *Blepharisma* PiggyBac homologs share a common ciliate ancestor, or whether they arose from independent acquisitions in major ciliate groups, we explored a range of phylogenetic methods. We created a phylogeny of 155 sequences of DDE_Tnp_1_7 domains of PiggyBac homologs which are representatives of putative domesticated transposases from the genus *Blepharisma* (*B. stoltei* ATCC 30299, *B. stoltei* HT-IV, *B. japonicum*), *Condylostoma magnum*, *Paramecium* spp., *Tetrahymena thermophila*, together with PiggyBac-like element (PBLE [61]) transposases from a stramenopile species, an archaeplastid species, several opisthokont species and an amoebozoan, homologs of the human PiggyBac-derived 1 gene (PGBD1), PGBD3, PGBD4 and PGBD5 homologs (Figure 7; Data S1). The three BPgms from the three *Blepharisma* strains whose MAC genomes we sequenced form a monophyletic clade, with the BPgmLs 1 and 2 as outgroups. The BPgmLs 3,4,5,6 and 7 are grouped together with the *Condylostoma* Pgms (each of which appears to have a complete catalytic triad). These two clades form a heterotrich-specific group in the phylogeny. We observe that the ciliate Pgms and PgmLs largely cluster to form a single clade. *T. thermophila* Tpb7 is an exception which appears to group together with homologs of PGBD5 from *H. sapiens, G. gallus* and *D. rerio* but has an aBayes support value of 0.84, much lower than the mode (1.0) and average (0.91) for this phylogeny. The other exceptions are two fungal PBLEs and two red algal PBLEs with low aBayes support within the predominantly monophyletic ciliate clade.

We applied tree topology tests to ascertain the likelihood of a monophyletic clade of ciliate Pgms and PgmLs. Constrained trees were compared by different methods including bootstrap proportion using the RELL method [62], a one-sided Kishino-Hasegawa test, a Shimodaira-Hasegawa test [63,64], estimating confidence using expected likelihood weights [65], and an approximately unbiased test [66] (Table S10). A tree with the constraint of monophyly for all

ciliate Pgms and PgmLs lacks support in comparison to an unconstrained tree with all the ciliate Pgms and PgmLs and eukaryotic PBLEs. After excluding *T. thermophila* Tpb7, a tree constrained with a clade consisting of the remaining ciliate Pgms and PgmLs is supported by all tests. In other words, the ciliate PiggyBac homologs except Tpb7 likely originated in a ciliate common ancestor.

Discussion

The genus *Blepharisma* represents one of the earliest diverging ciliate lineages, the heterotrichs, forming an outgroup to the best-studied and deeply divergent oligohymenophorean and spirotrich ciliates [7]. *Blepharisma* species thus provide an excellent vantage point to compare unique processes that have accompanied the evolution of nuclear and genomic dimorphism in ciliates, particularly the extensive genomic reorganization that occurs during the new macronucleus (MAC) development. Comparisons between *Blepharisma* and other ciliates also enable deeper consideration of the potential state of the ciliate common ancestor. The annotated draft *B. stoltei* ATCC 30299 MAC genome and associated transcriptomic data provide the basis for comparative studies of key characteristics of genome reorganization processes.

A minichromosomal architecture with pronounced telomere addition site variation

Ciliate MAC genome architectures span from longer DNA molecules in the oligohymenophoreans *Paramecium tetraurelia* and *Tetrahymena thermophila*, which are more similar to conventional eukaryotic chromosomes, to numerous, predominantly single-gene nanochromosomes of spirotrichs like *Oxytricha trifallax* and *Euplotes crassus* [3]. The *B. stoltei* ATCC 30299 MAC genome organization (and like that of *Paramecium bursaria* [44]) lies

between these two extremes with many minichromosomes representing numerous alternative telomere addition sites. This form of natural sequence heterogeneity creates significant new challenges for generating single representative consensus sequences, because genome assembly methods assume chromosome boundaries are generally consistent, as they are in multicellular eukaryote models, down to the terminology used to describe them [78]. Fortunately, the reference *Blepharisma* MAC genome is largely homozygous, promoting contiguity in the final, 41 Mb assembly of 64 two-telomere-capped contigs. Nevertheless, plenty of room for refinement remains, including development of new ways to better assemble, describe and organize the constituents of genomes with such extreme sequence variability.

Despite the abundance of *Blepharisma* MAC genome telomeres, we did not detect a typical ncRNA gene corresponding to the telomerase RNA component (TERC) of the ribozyme responsible for telomere synthesis in the MAC genome. We suspect this is due to ncRNAs presenting a far greater challenge to detect than protein-coding genes and the presence of highly divergent ncRNA with insufficient similarity to the handful of taxonomically-restricted TERCs identified in oligohymenophorean and spirotrich ciliates and other eukaryotes so far. On the other hand, five homologs of POT1, the canonical telomere-binding protein, are present (Figure S4). One of these is highly upregulated when the new MAC genome is forming, and presumably like model ciliates the DNA is fragmented and replicated, requiring further telomere synthesis and telomere-binding proteins.

A potentially catalytically active PiggyMac is present in *Blepharisma*

In current models of IES excision, MIC-limited sequences are demarcated by deposition of methylation marks on histones in an sRNA-dependent process [5]. These sequences are then

recognized by domesticated transposases whose excision is supported by additional proteins, including those that recognize these marks [5]. Together with MIC sequencing and from the same time course we employed in the present study for RNA-seq we have observed abundant, development-specific sRNA production in *Blepharisma* like that in other ciliates (Seah et al. in prep), and so we examined the expression of potential genes responsible for their biogenesis, along with other genes highly upregulated during new MAC formation. Homologs of proteins implicated in ciliate genome reorganization were present among the genes most highly differentially upregulated during new MAC development, notably including Dicer-like and Piwi proteins, and domesticated transposases.

Following this study, we will report detailed analyses of a draft *B. stoltei* ATCC 30299 MIC genome, which possesses abundant and typically TA-bound IESs (Seah et al. in prep). In oligohymenophorean ciliates *Tetrahymena* and *Paramecium* there is a considerable body of evidence that PiggyBac homologs are responsible for IES excision [35,52,53,55,79]. The responsible IES excisases in the less-studied spirotrich ciliates, *Oxytricha*, *Stylonychia* and *Euplotes*, are not as evident. In *Oxytricha* the TBE transposases are considered to be involved in IES excision, but, unlike the MAC genome-encoded primary IES excisase (Tpb2) in *Tetrahymena* and all the *Paramecium* PiggyMacs and PiggyMac-likes, are encoded by full-length transposons present in the MIC genome, but absent from the MAC [74]. The considerable heterogeneity in *Oxytricha* IES boundaries and “unscrambling” of a large subset of them [56], together with the observation of pronounced developmental upregulation of numerous additional MAC- and MIC-encoded transposases raises the possibility that additional transposases other than those of TBEs could also be involved in IES excision [39,56]. Knowledge of IESs in other ciliates is sparse (primarily confined to the phyllopharyngean *Chilodonella uncinata* [80,81]), and, as far as we are aware, no specific IES excisases have been proposed for them.

Since the oligohymenophorean ciliate PiggyBac homologs are clear IES excisases, we sought and found eight homologs of these genes in the *B. stoltei* ATCC 30299 MAC genome. *Blepharisma* is the first ciliate genus aside from *Tetrahymena* and *Paramecium* in which such proteins have been reported. Additional searches revealed clear PiggyBac homologs in *Condylostoma magnum*, and a weaker pair of matches in *Stentor coeruleus*, suggesting that these are a common feature of heterotrich ciliates. Reminiscent of *Paramecium tetraurelia*, in which just one of the nine PiggyBac homologs, PiggyMac, has a complete DDD catalytic triad [55], a single *B. stoltei* PiggyBac homolog has a complete DDD catalytic triad. The gene encoding this protein in *B. stoltei* ATCC 30299 is highly upregulated during MAC development, together with two other homologs that lack a complete catalytic triad. As is characteristic of PiggyBac homologs, each of these three homologs also has a C-terminal, cysteine-rich, zinc finger domain, which most closely resemble those of *Condylostoma magnum* homologs. The organization of the heterotrich PiggyBac homolog zinc finger domains appears to be more similar to that of comparable domains of *Homo sapiens* PGBD2 and PGBD3 homologs than that of the zinc finger domains in *Paramecium* and *Tetrahymena* PiggyBac homologs (which are more similar to the *Homo sapiens* PGBD4 zinc fingers [58]).

In *Paramecium*, since the discovery of multiple PiggyBac homologs (PiggyMac-likes), there have been questions about their role, since, aside from PiggyMac, they all have incomplete catalytic triads, and are thus likely catalytically inactive, but nevertheless their gene knockdowns lead to pronounced IES retention [55]. It has therefore been proposed that the PiggyMac-likes may function as heteromeric multi-subunit complexes in conjunction with PiggyMac during DNA excision [55]. On the other hand cryo-EM structures available for moth PiggyBac transposase support a model in which these proteins function as a homodimeric complex *in vitro* [82]. Furthermore, the primary *Tetrahymena* PiggyBac, Tpb2, is able to perform cleavage *in vitro*, without the assistance of other PiggyBac homologs [53]. In other eukaryotes, domesticated

PiggyBacs without complete catalytic triads are thought to be retained by virtue of useful DNA-binding roles [83]. One possibility for such purely DNA-binding transposases in ciliates could be in competitively regulating (taming) the excision of DNA by the catalytically active transposases. Future experimental analyses of the BPgm and the BPgm-likes could aid in resolving the conundrums and understanding of possible interactions between catalytically active and inactive transposases.

Domesticated PiggyBac homologs are the main candidate IES excisases in *Blepharisma*

In addition to the PiggyBac homologs, we also found MAC genome-encoded transposases with the PFAM domains “DDE_1”, “DDE_3”, “DDE_Tnp_IS1595” and “MULE” in *Blepharisma* (Figure 6., Supplementary results, “Additional domesticated transposases “). All the genes encoding proteins with these domains lack flanking terminal repeats characteristic of active transposons, suggesting these genes are further classes of domesticated transposases. In *Blepharisma* and numerous other organisms, the DDE_1 domains co-occur with CENPB domains. Two such proteins represent totally different proposed exaptations in mammals (centromere-binding protein) and fission yeast (regulatory protein) [68–70]. Given the great evolutionary distances involved, there is no specific reason to expect that the *Blepharisma* homologs have either function. None of the three proteins with co-occurring DDE_1 and CENPB domains have a complete catalytic triad, making it unlikely that these are active transposases or IES excisases, though all three are noticeably upregulated during MAC development. Six proteins with the PFAM domain DDE_3 are also encoded by *Blepharisma* MAC genes, of which five possess a complete catalytic triad. DDE_3 domains are also characteristic of TBE transposases in *Oxytricha* and Tec transposases in *Euplotes*. All the “DDE_3” protein genes are upregulated during conjugation in *B. stoltei*, and are expressed at particularly high levels during development

of the new MAC. A number of DDE_Tnp_IS1595 and MULE domain-containing proteins have complete catalytic triads and also show pronounced upregulation during *B. stoltei* MAC development.

Upon excision, classical cut-and-paste transposases in eukaryotes typically leave behind additional bases, notably including those of the target-site duplication that arose when they were inserted, forming a “footprint” [84]. PiggyBac homologs are unique in performing precise, “seamless” excision in eukaryotes [85], conserving the number of bases at the site of transposon insertion after excision, a property that makes them popular for genetic engineering [82]. *Tetrahymena* Tpb2 is the one exception among PiggyBac homologs associated with imprecise excision in this eukaryote [53]. Since intragenic IESs are abundant in *Blepharisma*, like *Paramecium* and unlike *Tetrahymena*, it is essential that these are excised precisely without addition or removal of nucleotides, which, at best, could result in translation of additional amino acids and, at worst, translation frameshifts.

Though there are clearly numerous additional domesticated transposases with complete catalytic triads and whose genes are substantially upregulated during *Blepharisma* development, whether they are capable of excision, and if this is precise, needs to be established. *Tetrahymena* has distinct domesticated transposases that excise different subsets of IESs, namely those that are predominant, imprecisely excised and intergenic (by Tpb2) [53], versus those that are rare, precisely excised and intragenic (by Tpb1 and Tpb6) [79,86]. We could envisage if the additional *Blepharisma* domesticated transposases are still capable of excision, but not a precise form, an involvement in excision of a subset of the numerous intergenic IESs. Thus, while we cannot rule out the involvement of other possible domesticated transposases and PiggyMac-likes, currently *B. stoltei* PiggyMac is the primary candidate IES excisase.

A possible PiggyBac homolog ciliate common ancestor

In light of the discovery of PiggyMacs in heterotrichous ciliates, we investigated whether the last common ancestor of ciliates also possessed a PiggyMac. Phylogenetic analyses, together with tree topology tests, indicate that the oligohymenophorean and heterotrichous PiggyMacs and PiggyMac-likes form a monophyletic clade. The lack of PiggyBac homologs in other ciliate classes such as the Spirotrichea, and potentially the oligohymenophorean *Ichthyophthirius multifiliis* (with the caveat of apparent lower genome completeness), raises the question whether the PiggyMacs were lost in these lineages or were gained independently from the same source by both heterotrichs and a subset of oligohymenophoreans. We think the former is more likely. However, the alternative cannot be completely dismissed, because non-model ciliates, where the genome assembly quality allows reliable gene and domain annotations, have only been sparsely sampled.

Future directions

The *B. stoltei* ATCC 30299 MAC genome together with a corresponding MIC genome (Seah et al., in prep.) pave the way for future investigations of a peculiar, direct pathway to new MAC genome development which skips the upstream complexity of meiotic and fertilization-associated nuclear developmental processes of the standard pathway [9]. The pair of *B. stoltei* strains we have are both now low frequency selfers, in which the conventional, indirect MAC development pathway dominates. Comparisons with fresh, high frequency *Blepharisma* selfers collected from the wild will facilitate comparative gene expression analyses with the direct MAC development pathway, which will assist in distinguishing expression upregulation due to meiotic and mitotic processes preceding indirect new MAC development. As a representative of one of the two deepest branching ciliate lineages, the assembled somatic genome will facilitate

investigations beyond those reported here into the enigmatic origins of nuclear and genomic dualism within single cells.

Materials and Methods

Strains and localities

The strains used and their original isolation localities were: *Blepharisma stoltei* ATCC 30299, Lake Federsee, Germany [24]; *Blepharisma stoltei* HT-IV, Aichi prefecture, Japan; *Blepharisma japonicum* R1072, from an isolate from Bangalore, India [22].

Cell cultivation, harvesting and cleanup

For genomic DNA isolation *B. stoltei* ATCC 30299 and HT-IV cells were cultured in Synthetic Medium for *Blepharisma* (SMB) [87] at 27˚C. Belpharismas were fed *Chlorogonium elongatum* grown in Tris-acetate phosphate (TAP) medium [88] at room temperature. *Chlorogonium* cells were pelleted at 1500 g at room temperature for 3 minutes to remove most of the TAP medium, and resuspended in 50 mL SMB. 50 ml of dense *Chlorogonium* was used to feed 1 litre of *Blepharisma* culture once every three days.

Blepharisma stoltei ATCC 30299 and HT-IV cells used for RNA extraction were cultured in Lettuce medium inoculated with *Enterbacter aerogenes* and maintained at 25˚C [89].

Blepharisma cultures were concentrated by centrifugation in pear-shaped flasks at 100 g for 2 minutes using a Hettich Rotanta 460 centrifuge with swing out buckets. Pelleted cells were washed with SMB and centrifuged again at 100 g for 2 minutes. The washed pellet was then transferred to a cylindrical tube capped with a 100 µm-pore nylon membrane at the base and immersed in SMB to filter residual algal debris from the washed cells. The cells were allowed to diffuse through the membrane overnight into the surrounding medium. The next day, the

cylinder with the membrane was carefully removed while attempting to minimize dislodging any debris collected on the membrane. Cell density after harvesting was determined by cell counting under the microscope.

DNA isolation, library preparation and sequencing

B. stoltei macronuclei were isolated by sucrose gradient centrifugation [4]. DNA was isolated with a Qiagen 20/G genomic-tip kit according to the manufacturer's instructions. Purified DNA from the isolated MACs was fragmented, size selected and used to prepare libraries according to standard PacBio HiFi SMRTbell protocols. The libraries were sequenced in circular consensus mode to generate HiFi reads.

Total genomic DNA from *B. stoltei* HT-IV and *B. stoltei* ATCC 30299 was isolated with the SigmaAldrich GenElute Mammalian genomic DNA kit. A sequencing library was prepared with a NEBnext FS DNA Library Prep Kit for Illumina and sequenced on an Illumina HiSeq 3000 sequencer, generating 150 bp paired-end reads.

Total genomic DNA from *B. japonicum* was isolated with the Qiagen MagAttract HMW DNA kit. A long-read PacBio sequencing library was prepared using the SMRTbell® Express Template Preparation Kit 2.0 according to the manufacturers' instructions and sequenced on an PacBio Sequel platform with 1 SMRT cell. Independently, total genomic DNA form *B. japonicum* was isolated with the SigmaAldrich GenElute Mammalian genomic DNA kit and an sequencing library was prepared with the TruSeq Nano DNA Library Prep Kit (Illumina) and sequenced on an Illumina NovaSeq6000 to generate 150 bp paired-end reads.

Gamone 1/ Cell-Free Fluid (CFF) isolation and conjugation activity assay

B. stoltei ATCC 30299 cells were cultured and harvested and concentrated to a density of 2000 cells/mL according to the procedure described in “Cell cultivation, Harvesting and Cleanup”. This concentrated cell culture was incubated overnight at 27˚C. The next day, the cells were harvested, and the supernatant collected and preserved at 4˚C at all times after extraction. The supernatant was then filtered through a 0.22 µm-pore filter. BSA (10 mg/mL) was added to produce the final CFF at a final BSA concentration of 0.01%.

To assess the activity of the CFF, serial dilutions of the CFF were made to obtain the gamone activity in terms of units (U) [90].The activity of the isolated CFF was 2^{10} U.

Conjugation time course and RNA isolation for high-throughput sequencing

B. stoltei cells for the complementary strains, ATCC 30299 and HT-IV, were cultivated and harvested by gentle centrifugation to achieve a final cell concentration of 2000 cells/ml for each strain. Non-gamone treated ATCC 30299 (A1) and HT-IV cells (H1) were collected (time point: -3 hours). Strain ATCC 30299 cells were then treated with synthetic gamone 2 (final concentration 1.5 µg/mL) and strain HT-IV cells were treated with cell-free fluid with a gamone 1 activity of ~2^{10} U/ml for three hours (Figure S8).

Homotypic pair formation in both cultures was checked after three hours. More than 75% of the cells in both cultures formed homotypic pairs. At this point the samples A2 (ATCC 30299) and H2 (HT-IV) were independently isolated for RNA extraction as gamone-treated control cells just

before mixing. For the rest of the culture, homotypic pairs in both cultures were separated by pipetting them gently with a wide-bore pipette tip. Once all pairs had been separated, the two cultures were mixed together. This constitutes the experiment's 0-h time point. The conjugating culture was observed and samples collected for RNA isolation or cell fixation at 2 h, 6 h, 14 h, 18 h, 22 h, 26 h, 30 h and 38 h (Figure S8). Further details of the sample staging approach are described in [9] and [51]. At each time point including samples A1, H1, A2 and H2, 7 mL of culture was harvested for RNA-extraction using Trizol. The total RNA obtained was then separated into a small RNA fraction < 200 nt and a fraction with RNA fragments > 200 nt using the Zymo RNA Clean and Concentrator-5 kit according to the manufacturer's instructions. RNA-seq libraries were prepared by BGI according to their standard protocols and sequenced on a BGISeq 500 instrument.

Separate 2 mL aliquots of cells at each time point for which RNA was extracted were concentrated by centrifuging gently at 100 rcf. 50 µL of the concentrated cells were fixed with Carnoy's fixative (ethanol:acetic acid, 6:1), stained with DAPI and imaged to determine the state of nuclear development [9].

Cell fixation and imaging

B. stoltei cells were harvested as above ("Cell cultivation"), and fixed with an equal volume of "ZFAE" fixative, containing zinc sulfate (0.25 M, Sigma Aldrich), formalin, glacial acetic acid and ethanol (Carl Roth), freshly prepared by mixing in a ratio of 10:2:2:5. Fixed cells were pelleted (1000 g; 1 min), resuspended in 1% TritonX-100 in PHEM buffer to permeabilize (5 min; room temperature), pelleted and resuspended in 2% (w/v) formaldehyde in PHEM buffer to fix further (10 min; room temp.), then pelleted and washed twice with 3% (w/v) BSA in TBSTEM buffer

(~10 min; room temp.). For indirect immunofluorescence, washed cells were incubated with primary antibody rat anti-alpha tubulin (Abcam, ab6161; 1:100 dilution in 3% w/v BSA/TBSTEM; 60 min; room temp.) then secondary antibody goat anti-rat IgG H&L labeled with AlexaFluor 488 (Abcam, ab150157, 1:500 dilution in 3% w/v BSA/TBSTEM; 20 min; room temp.). Nuclei were counterstained with DAPI (1 µg/mL) in 3% (w/v) BSA/TBSTEM. A z-stack of images was acquired using a confocal laser scanning microscope (Leica TCS SP8), equipped with a HC PL APO 40× 1.30 Oil CS2 objective and a 1 photomultiplier tube and 3 HyD detectors, for DAPI (405 nm excitation, 420-470 nm emission) and Alexa Fluor 488 (488 nm excitation, 510-530 nm emission). Scanning was performed in sequential exposure mode. Spatial sampling was achieved according to Nyquist criteria. ImageJ (Fiji) [91] was used to adjust image contrast and brightness and overlay the DAPI and AlexaFluor 488 channels. The z-stack was temporally color-coded.

For a nuclear 3D reconstruction (Figure 1B), cells were fixed in 1% (w/v) formaldehyde and 0.25% (w/v) glutaraldehyde. Nuclei were stained with Hoechst 33342 (Invitrogen) (5 µM in the culture media), and imaged with a confocal laser scanning microscope (Zeiss, LSM780) equipped with an LD C-Apochromat 40x/1,1 W Korr objective and a 32 channel GaAsP array detector, with 405 nm excitation and 420-470 nm emission. Spatial sampling was achieved according to Nyquist criteria. The IMARIS (Bitplane) software v8.0.2 was used for three-dimensional reconstructions and contrast adjustments.

For scanning electron microscopy (SEM) cells were fixed in 0.5% osmium tetroxide/2% formaldehyde/2.5% glutaraldehyde in 0.06x PHEM for 5-10 minutes at room temperature. Cells were post-fixed with 2% formaldehyde/2.5% glutaraldehyde in 0.06x PHEM for 4-6 hours at room temperature. Subsequently, samples were dehydrated in a graded ethanol series with 1 day per step followed by critical point drying (Polaron) with CO_2. Finally, the cells were sputter-

coated with a 4 nm thick layer of platinum (CCU-010, Safematic) and examined with a field emission scanning electron microscope (Regulus 8230, Hitachi High Technologies) at an accelerating voltage of 3 kV.

Genome assembly

Two MAC genome assemblies for *B. stoltei* ATCC 30299 (70× and 76× coverage) were produced with Flye (version 2.7-b1585) [92] for the two separate PacBio Sequel II libraries (independent replicates) using default parameters and the switches: --pacbio-hifi -g 45m. The approximate genome assembly size was chosen based on preliminary Illumina genome assemblies of approximately 40 Mb. Additional assemblies using the combined coverage (145×) of the two libraries were produced using either Flye version 2.7-b1585 or 2.8.1-b1676, and the same parameters. Two rounds of extension and merging were then used, first comparing the 70× and 76× assemblies to each other, then comparing the 145× assembly to the former merged assembly. Assembly graphs were all relatively simple, with few tangles to be resolved (Figure S7). Minimap2 [93] was used for pairwise comparison of the assemblies using the parameters: -x asm5 --frag=yes --secondary=no, and the resultant aligned sequences were visually inspected and manually merged or extended where possible using Geneious (version 2020.1.2) [94].

Visual inspection of read mapping to the combined assembly was then used to trim off contig ends where there was little correspondence between the assembly consensus and the mapped reads - which we classify as "cruft". Read mapping to cruft regions was often lower or uneven, suggestive of repeats. Alternatively, these features could be due to trace MIC sequences, or sites of alternative chromosome breakage during development which lead to sequences that are

neither purely MAC nor MIC. A few contigs with similar dubious mapping of reads at internal locations, which were also clear sites of chromosome fragmentation (evident by abundant telomere-bearing reads in the vicinity) were split apart and trimmed back as for the contig ends. Telomere-bearing reads mapped to the non-trimmed region nearest to the trimmed site were then used to define contig ends, adding representative telomeric repeats from one of the underlying sequences mapped to each of the ends. The main genome assembly with gene predictions can be obtained from the European Nucleotide Archive (ENA) (PRJEB40285; accession GCA_905310155). “Cruft” sequences are also available from the same project accession.

Two separate assemblies were generated for *Blepharisma japonicum.* A genome assembly for *Blepharisma japonicum* strain R1072 was generated from Illumina reads, using SPAdes genome assembler (v3.14.0) [95]. An assembly with PacBio Sequel long reads was produced with Ra (v0.2.1) [96], which uses the Overlap-Layout-Consensus paradigm. The assembly produced with Ra was more contiguous, with 268 contigs, in comparison to 1510 contigs in the SPAdes assembly, and was chosen as the reference assembly for *Blepharisma japonicum* (ENA accession: ERR6474383).

Condylostoma magnum genomic reads (study accession PRJEB9019) from a previous study [97] were reassembled to improve contiguity and remove bacterial contamination. Reads were trimmed with bbduk.sh from the BBmap package v38.22 (https://sourceforge.net/projects/bbmap/), using minimum PHRED quality score 2 (both ends) and k-mer trimming for Illumina adapters and Phi-X phage sequence (right end), retaining only reads ≥25 bp. Trimmed reads were error-corrected and reassembled with SPAdes v3.13.0 [95]

using k-mer values 21, 33, 55, 77, 99. To identify potential contaminants, the unassembled reads were screened with phyloFlash v3.3b1 [98] against SILVA v132 [99]; the coding density under the standard genetic code and prokaryotic gene model were also estimated using Prodigal v2.6.3 [100]. Plotting the coverage vs. GC% of the initial assembly showed that most of the likely bacterial contigs (high prokaryotic coding density, lower coverage, presence of bacterial SSU rRNA sequences) had >=40% GC, so we retained only contigs with <40% GC as the final *C. magnum* genome bin. The final assembly is available from the ENA bioproject PRJEB48875 (accession GCA_920105805).

All assemblies were inspected with the quality assessment tool QUAST [101].

Variant calling

Illumina total genomic DNA-seq libraries for *B. stoltei* strains ATCC 30299 (ENA accession: ERR6061285) and HT-IV (ERR6064674) were mapped to the ATCC 30299 reference assembly with bowtie2 v2.4.2 [102]. Alignments were tagged with the MC tag (CIGAR string for mate/next segment) using samtools [103] fixmate. The BAM file was sorted and indexed, read groups were added with bamaddrg (commit 9baba65, https://github.com/ekg/bamaddrg), and duplicate reads were removed with Picard MarkDuplicates v2.25.1 (http://broadinstitute.github.io/picard/). Variants were called from the combined BAM file with freebayes v1.3.2 [104] in diploid mode, with maximum coverage 1000 (option -g). The resultant VCF file was combined and indexed with bcftools v1.12 [103], then filtered to retain only SNPs with quality score > 20, and at least one alternate allele.

Annotation of alternative telomere addition sites

Alternative telomere addition sites (ATASs) were annotated by mapping PacBio HiFi reads to the curated reference MAC assembly described above, using minimap2 and the following flags: -x asm20 --secondary=no --MD. We expect reads representing alternative telomere additions to have one portion mapping to the assembly (excluding telomeric regions), with the other portion containing telomeric repeats being soft-clipped in the BAM record. For each mapped read with a soft-clipped segment, we extracted the clipped sequence, and the coordinates and orientation of the clip relative to the reference. We searched for ≥ 24 bp tandem direct repeats of the telomere unit (i.e., ≥3 repeats of the 8 bp unit) in the clipped segment with NCRF v1.01.02 [105], which can detect tandem repeats in the presence of noise, e.g., from sequencing error. The orientation of the telomere sequence, the distance from the end of the telomeric repeat to the clip junction ('gap'), and the number of telomere-bearing reads vs. total mapped reads at each junction were also recorded. Junctions with zero gap between telomere repeat and clip junction were annotated as ATASs. The above procedure was implemented in the MILTEL module of the software package BleTIES v0.1.3 [106].

MILTEL output was processed with Python scripts depending on Biopython [107], pybedtools [108], Bedtools [109], and Matplotlib [110], to summarize statistics of junction sequences and telomere permutations at ATAS junctions, and to extract genomic sequences flanking ATASs for sequence logos. Logos were drawn with Weblogo v3.7.5 [111], with sequences oriented such that the telomere would be added on the 5' end of the ATAS junctions.

To calculate the expected minichromosome length, we assumed that ATASs were independent and identically distributed in the genome following a Poisson distribution. About 47×10^3 ATASs were annotated, supported on average by a single read. Given a genome of 42 Mbp at 145× coverage, the expected rate of encountering an ATAS is 47×10^3 / (145 × 42 Mbp), so the distance between ATASs (i.e., the minichromosome length) is exponentially distributed with expectation (145 × 42 Mbp) / 47×10^3 = 130 kbp.

RNA-seq read mapping

To permit correct mapping of tiny introns RNA-seq data was mapped to the *B. stoltei* ATCC 30299 MAC genome using a version of HISAT2 [112] with modified source code, with the static variable minIntronLen in hisat2.cpp lowered to 9 from 20 (change available in the HISAT2 github fork: https://github.com/Swart-lab/hisat2/; commit hash 86527b9). HISAT2 was run with default parameters and parameters --min-intronlen 9 --max-intronlen 500. It should be noted that RNA-seq from timepoints in which *B. stoltei* ATCC 30299 and *B. stoltei* HT-IV cells were mixed together were only mapped to the former genome assembly, and so reads for up to three alleles may map to each of the genes in this assembly.

Genetic code prediction

We used the program PORC (Prediction Of Reassigned Codons; available from https://github.com/Swart-lab/PORC) previously written to predict genetic codes in protist transcriptomes [97] to predict the *B. stoltei* genetic code. This program was used to translate the draft *B. stoltei* ATCC 30299 genome assembly in all six frames (with the standard genetic code). Like the program FACIL [113] that inspired PORC, the frequencies of amino acids in PFAM (version 34.0) protein domain profiles aligned to the six frame translation by HMMER

3.1b2 [114] (default search parameters; domains used for prediction with conditional E-values < 1e-20), and correspondingly also to the underlying codon, are used to infer the most likely amino acid encoded by each codon (Figure S5).

Gene prediction

We created a wrapper program, Intronarrator, to predict genes in *Blepharisma* and other heterotrichs, accommodating their tiny introns. Intronarrator can be downloaded and installed together with dependencies via Conda from GitHub (https://github.com/Swart-lab/Intronarrator). Intronarrator directly infers introns from spliced RNA-seq reads mapped by HISAT2 from the entire developmental time course we generated. RNA-seq reads densely cover almost the entire *Blepharisma* MAC genome, aside from intergenic regions, and most potential protein-coding genes (Figure 5A). After predicting the introns and removing them to create an intron-minus genome, Intronarrator runs AUGUSTUS (version 3.3.3) using its intronless model. It then adds back the introns to the intronless gene predictions to produce the final gene predictions.

Introns are inferred from “CIGAR” string annotations in mapped RNA-seq BAM files, using the regular expression “[0-9]+M([0-9][0-9])N[0-9]+M” to select spliced reads. For intron inference we only used primary alignments with: MAPQ >= 10; just a single “N”, indicating one potential intron, per read; and at least 6 mapped bases flanking both the 5’ and 3’ intron boundaries (to limit spurious chance matches of a few bases that might otherwise lead to incorrect intron prediction). The most important parameters for Intronarrator are a cut-off of 0.2 for the fraction of spliced reads covering a potential intron, and a minimum of 10 or more spliced reads to call an intron. The splicing fraction cut-off was chosen based on the overall distribution of splicing (Figure S6A-C). From our visual examination of mapped RNA-seq reads and gene predictions, values less than this were typically “cryptic” excision events [115] which remove potentially

essential protein-coding sequences, rather than genuine introns. Intronarrator classifies an intron as sense (7389 in total, excluding alternative splicing), when the majority of reads (irrespective of splicing) mapping to the intron are the same strand, and antisense (554 in total) when they are not. The most frequently spliced intron was chosen in rare cases of overlapping alternative intron splicing.

To eliminate spurious prediction of protein-coding genes overlapping ncRNA genes, we also incorporated ncRNA prediction in Intronarrator. Infernal [38] (default parameters; e-value < 1e-6) was used to predict a restricted set of conserved ncRNAs models (i.e., tRNAs, rRNAs, SRP, and spliceosomal RNAs) from RFAM 14.0 [116]. These ncRNAs were hard-masked (with “N” characters) before AUGUSTUS gene prediction. Both Infernal ncRNA predictions (excluding tRNAs) and tRNA-scan SE 2.0 [117] (default parameters) tRNA predictions are annotated in the *B. stoltei* ATCC 30299 assembly deposited in the European Nucleotide Archive.

Since we found that *Blepharisma stoltei*, like *Blepharisma japonicum* [97], uses a non-standard genetic code, with UGA codon translated as tryptophan, gene predictions use the “The Mold, Protozoan, and Coelenterate Mitochondrial Code and the Mycoplasma/Spiroplasma Code (transl_table=4)” from the NCBI genetic codes. The default AUGUSTUS gene prediction parameters override alternative (mitochondrial) start codons permitted by NCBI genetic code 4, other than ATG. So, all predicted *B. stoltei* gene coding sequences begin with ATG.

RNA-seq read mapping relative to gene predictions of Contig_1 of *B. stoltei* ATCC30299 was visualized with PyGenomeTracks [118].

Assessment of genome completeness

A BUSCO (version 4.0.2) [119] analysis of the assembled MAC genomes of *B. stoltei* and *B. japonicum* was performed on the set of predicted proteins (BUSCO mode -prot) using the BUSCO Alveolata database. The completeness of the *Blepharisma* genomes was compared to the protein-level BUSCO analysis of the published genome assemblies of ciliates *T. thermophila*, *P. tetraurelia*, *S. coeruleus* and *I. multifiliis* (Figure S1).

Gene annotation

Pannzer2 [120] (default parameters) and EggNog (version 2.0.1) [121] were used for gene annotation. Annotations were combined and are available from the Max Planck Society's Open Research Repository, Edmond (https://dx.doi.org/10.17617/3.8c). Protein domain annotations were performed using hmmscan from HMMER3 (version 3.3, Nov 2019) [114] vs. the PFAM database (Pfam-A.full, 33.0, retrieved on June 23, 2020) with default parameters.

Gene expression analysis

Features from RNA-seq reads mapped to the *B. stoltei* ATCC 30299 genome over the developmental time-course were extracted using featureCounts from the Subread package [122]. Further analysis was performed using the R software environment. Genes with a total read count of less than 50, across all timepoints, were filtered out of the dataset. The remaining genes were passed as a DGElist object to edgeR [123]. Each time point, representing one library, was normalized for library size using the edgeR function calcNormFactors. The normalized read counts were transformed into TPM (transcripts per million) values [124,125]. The TPM-values for different genes were compared across timepoints to examine changes in gene expression. Heatmaps showing log2(TPM) changes across timepoints were plotted using

the tidyverse collection of R packages (https://www.tidyverse.org/) and RColorBrewer (https://rdrr.io/cran/RColorBrewer/). Tabulated gene expression estimates together with protein annotations are available from Edmond (https://dx.doi.org/10.17617/3.8c).

Sequence visualization and analysis

Nucleotide and amino acid sequences were visualized using Geneious Prime (Biomatters Ltd.) [94]. Multiple sequence alignments were performed with MAFFT version 7.450 [126,127]. Phylogenetic trees were constructed with PhyML version 3.3.20180621 [128].

Orthogroup inference and analysis of orthogroup clusters

OrthoFinder version 2.5.2 with default parameters (i.e., using Diamond for searching, MAFFT for multiple alignment and FastTree for phylogenies) was used to define orthogroups, i.e., sets of genes descended from the last common ancestor of the chosen species. Proteomes for the following ciliate species were used: *Tetrahymena thermophila*, *Oxytricha trifallax*, *Stentor coeruleus* (data from ciliate.org [129]); *Euplotes octocarinatus* (EOGD [130]); *Paramecium tetraurelia*, *Paramecium caudatum* (data from ParameciumDB [131]); plus *Perkinsus marinus* ATCC 50983 (GenBank accession: AAXJ00000000) as a non-ciliate outgroup. Orthogroup clusters are available as Data S2, or from Edmond (https://dx.doi.org/10.17617/3.8c).

d_N/d_S estimation

We generated pairwise coding sequence alignments of PiggyMac paralog nucleotide sequences from *P. tetraurelia* and *P. octaurelia* using MAFFT version 7.450 [127] [126] (algorithm: “auto”, scoring matrix: 200PAM/k=2, gap open penalty 1.53, offset value 0.123) using the “translation align” panel of Geneious Prime (version 2020.1.2) [94]. PAML version 4.9 [132] was used to

963 estimate d_N/d_S values in pairwise mode (runmode = -2, seqtype = 1, CodonFreq = 2). For
964 *Blepharisma stoltei*, we generated pairwise coding sequence alignments of the *Blepharisma*
965 PiggyMac homolog, BPgm (Contig_49.g1063; BSTOLATCC_MAC17466), with the *Blepharisma*
966 Pgm-likes (BPgmLs) using ClustalW 2.1 [133] (Genetic code: *Blepharisma*, Protein alignment
967 options: ClustalW alignment, Cost matrix: BLOSUM, Gap open cost: 10, Gap open penalty: 0.1)
968 using "translation align" panel of Geneious Prime (version 2020.1.2). PAML version 4.9 was
969 used to estimate dN/dS values in pairwise mode (runmode = -2, seqtype = 1, CodonFreq = 2).

970 Phylogenetic analysis

971 Protein sequences of PBLEs and PGDBs were obtained from Bouallègue et al [61]. Protein
972 sequences of *Paramecium* and *Tetrahymena* Pgms and PgmLs were obtained from
973 ParameciumDB [131] (PGM, PGMLs1-5) and ciliate.org [129] (Tpb1, Tpb2, Tpb7, LIA5),
974 respectively. *Condylostoma* and *Blepharisma* Pgms and PgmLs were obtained from genome
975 assemblies (accessions GCA_920105805 and GCA_905310155, respectively). Other PiggyBac
976 protein sequences (*T. ni, D. purpureum*) were obtained from Uniprot [134]. Sequence
977 manipulation was done using Geneious (Biomatters Ltd.). The Geneious plug-in for
978 InterProScan [135] was used to identify DDE_Tnp_1_7 domains using the PFAM-A database
979 [136]. The DDE_Tnp_1_7 domains were extracted and aligned using the MAFFT plug-in
980 (v7.450) for Geneious [127] (Algorithm: Auto, Scoring matrix: BLOSUM62, Gap open penalty:
981 1.53, Offset value: 0.123). The best-fit model of evolution for each alignment was identified
982 using ModelTest-NG [137] (modeltest-ng -i <input_file>.phy -d aa -p 4 -T phyml -o
983 <output_file>.out). The best model according to Bayesian criteria (BIC) were used to create
984 phylogenetic trees using PhyML [128] [phyml -i <input_file>.phy -d aa -m LG -f m -v 0 -a e -c 4 -
985 o tlr]. Phylogenetic trees thus generated were visualized with FigTree (v1.4.4) (Andrew
986 Rambaut, http://tree.bio.ed.ac.uk/). Tree topology tests were performed using IQtree (v2.1.4-

beta) [138] (iqtree -s <input file> -m LG+G4 -z <unconstrained and constrained treefiles> -n 0 -zb 10000 -au -nt AUTO).

Repeat annotation

Interspersed repeat element families were predicted with RepeatModeler v2.0.1 (default settings, random number seed 12345) with the following dependencies: rmblast v2.9.0+ (http://www.repeatmasker.org/RMBlast.html), TRF 4.09 (Benson, 1999), RECON (Bao and Eddy, 2002), RepeatScout 1.0.6 (Price et al., 2005), RepeatMasker v4.1.1 (http://www.repeatmasker.org/RMDownload.html). Repeat families were also classified in the pipeline by RepeatClassifier v2.0.1 through comparison against RepeatMasker's repeat protein database and the Dfam database. Consensus sequences of the predicted repeat families, produced by RepeatModeler, were then used to annotate repeats with RepeatMasker, using rmblast as the search engine.

Terminal inverted repeats (TIRs) of selected repeat element families were identified by aligning the consensus sequence from RepeatModeler, and/or selected full-length elements, with their respective reverse complements using MAFFT (Katoh and Standley, 2013) (plugin version distributed with Geneious). TIRs from the Dfam DNA transposon termini signatures database (v1.1, https://www.dfam.org/releases/dna_termini_1.1/dna_termini_1.1.hmm.gz) (Storer et al., 2021) were searched with hmmsearch (HMMer v3.2.1) against the IES sequences, to identify matches to TIR signatures of major transposon subfamilies.

Data availability

The draft *Blepharisma stoltei* ATCC 30299 macronuclear genome assembly is accessible from bleph.ciliate.org and from the European Nucleotide Archive (ENA) bioproject PRJEB40285 under the accession GCA_905310155. PacBio CCS reads (ERR5873783 and ERR5873334) and subreads (ERR5962314) used to assemble the genome are also available from ENA. Illumina DNA-seq data for the *B. stoltei* ATCC 30299 and HT-IV strains is available from accessions ERR6061285 and ERR6064674, respectively. The RNA-seq developmental time course is available from the bioproject PRJEB45374 (accessions ERR6049461-ERR6049485).

Illumina and PacBio Sequel sequencing data for *Blepharisma japonicum* strain R1702 is available from the ENA bioproject PRJEB46921 (Illumina accessions: ERR6473251, ERR6474356; PacBio accession: ERR6474383).

Acknowledgements

This paper is dedicated in memory of Akio Miyake and his decades of inspirational *Blepharisma* research. We thank Federico Buonanno for the provision of *B. stoltei* ATCC 30299 cells and culturing advice, Christa Lanz and the MPI for Biology's genome center, Jürgen Berger for SEM imaging, and Sebastien Colin and the MPI for Biology's Light Microscopy Facility for the 3D nuclear reconstruction.

Bibliography

1. Martin WF, Garg S, Zimorski V. Endosymbiotic theories for eukaryote origin. Philos Trans R Soc Lond B Biol Sci. 2015;370: 20140330. doi:10.1098/rstb.2014.0330

2. Orias E. On the evolution of the karyorelict ciliate life cycle: heterophasic ciliates and the origin of ciliate binary fission. BioSystems. 1991;25: 67–73. doi:10.1016/0303-2647(91)90013-B

3. Prescott DM. The DNA of ciliated protozoa. Microbiol Rev. 1994;58: 233–267. doi:10.1128/mr.58.2.233-267.1994

4. Lauth MR, Spear BB, Heumann J, Prescott DM. DNA of ciliated protozoa: DNA sequence diminution during macronuclear development of Oxytricha. Cell. 1976;7: 67–74. doi:10.1016/0092-8674(76)90256-7

5. Chalker DL, Meyer E, Mochizuki K. Epigenetics of ciliates. Cold Spring Harb Perspect Biol. 2013;5: a017764. doi:10.1101/cshperspect.a017764

6. Vogt A, Goldman AD, Mochizuki K, Landweber LF. Transposon domestication versus mutualism in ciliate genome rearrangements. PLoS Genet. 2013;9: e1003659. doi:10.1371/journal.pgen.1003659

7. Lynn DH, editor. The Ciliated Protozoa. Dordrecht: Springer Netherlands; 2010. doi:10.1007/978-1-4020-8239-9

8. Giese AC. Blepharisma: The Biology of a Light-sensitive Protozoan. illustrated ed. Stanford University Press; 1973.

9. Miyake A, Rivola V, Harumoto T. Double paths of macronucleus differentiation at conjugation in Blepharisma japonicum. Eur J Protistol. 1991;27: 178–200. doi:10.1016/S0932-4739(11)80340-8

10. Slabodnick MM, Ruby JG, Reiff SB, Swart EC, Gosai S, Prabakaran S, et al. The Macronuclear Genome of Stentor coeruleus Reveals Tiny Introns in a Giant Cell. Curr Biol. 2017;27: 569–575. doi:10.1016/j.cub.2016.12.057

11. Slabodnick MM, Marshall WF. Stentor coeruleus. Curr Biol. 2014;24: R783-4. doi:10.1016/j.cub.2014.06.044

12. Zhang KS, Blauch LR, Huang W, Marshall WF, Tang SKY. Microfluidic guillotine reveals multiple timescales and mechanical modes of wound response in Stentor coeruleus. BMC Biol. 2021;19: 63. doi:10.1186/s12915-021-00970-0

13. Rapport EW, Rapport DJ, Berger J, Kupers V. Induction of conjugation in Stentor coeruleus. Trans Am Microsc Soc. 1976;95: 220–224. doi:10.2307/3225068

14. Miyake A, Harumoto T. Asymmetrical cell division in Blepharisma japonicum: difference between daughter cells in mating-type expression. Exp Cell Res. 1990;190: 65–68. doi:10.1016/0014-4827(90)90144-y

15. Terazima MN, Harumoto T. Defense function of pigment granules in the ciliate Blepharisma japonicum against two predatory protists, Amoeba proteus (Rhizopodea) and Climacostomum virens (Ciliata). Zool Sci. 2004;21: 823–828. doi:10.2108/zsj.21.823

16. Kumazawa H. Homopolar Grafting in Blepharisma japonicum. Journal of Experimental Zoology. 1979;207: 1–16.

17. Sugiura M, Shiotani H, Suzaki T, Harumoto T. Behavioural changes induced by the conjugation-inducing pheromones, gamone 1 and 2, in the ciliate Blepharisma japonicum. Eur J Protistol. 2010;46: 143–149. doi:10.1016/j.ejop.2010.01.002

18. Young D. Macronuclear reorganization in Blepharisma undulans. Doctoral dissertation. 1937.

19. Friedl E, Miyake A, Heckmann K. Requirement of successive protein syntheses for the

progress of meiosis in Blepharisma. Exp Cell Res. 1983;145: 105–113. doi:10.1016/s0014-4827(83)80013-5

20. Miyake A, Tulli M, Nobili R. Requirement of protein synthesis in the initiation of meiosis and other nuclear changes in conjugation of Blepharisma. Exp Cell Res. 1979;120: 87–93. doi:10.1016/0014-4827(79)90539-1

21. Inaba F. Conjugation between two strains of *Blepharisma*. J Protozool. 1965;12: 146–151. doi:10.1111/j.1550-7408.1965.tb01828.x

22. Harumoto T, Miyake A, Ishikawa N, Sugibayashi R, Zenfuku K, Iio H. Chemical defense by means of pigmented extrusomes in the ciliate Blepharisma japonicum. Eur J Protistol. 1998;34: 458–470. doi:10.1016/S0932-4739(98)80014-X

23. Kobayashi M, Miura M, Takusagawa M, Sugiura M, Harumoto T. Two possible barriers blocking conjugation between different megakaryotypes of Blepharisma. Zool Sci. 2015;32: 53–61. doi:10.2108/zs140151

24. Repak AJ. Encystment and Excystment of the Heterotrichous Ciliate Blepharisma stoltei Isquith. Journal of Protozoology. 1968;5: 407–412.

25. Salvini M, Durante M, Nobili R. Characterization of macronuclear DNA in Blepharisma japonicum. Protoplasma. 1983;117: 82–88. doi:10.1007/BF01281787

26. Kimball RF. The nature and inheritance of mating types in euplotes patella. Genetics. 1942;27: 269–285.

27. Katashima RYO. Mating Types in *Euplotes eurystomus*. J Protozool. 1959;6: 75–83. doi:10.1111/j.1550-7408.1959.tb03930.x

28. Luporini P, Miceli C, Ortenzi C. Evidence that the ciliate Euplotes raikovi releases mating-inducing factors (gamones). J Exp Zool. 1983;226: 1–9. doi:10.1002/jez.1402260102

29. Vallesi A, Giuli G, Bradshaw RA, Luporini P. Autocrine mitogenic activity of pheromones produced by the protozoan ciliate Euplotes raikovi. Nature. 1995;376: 522–524. doi:10.1038/376522a0

30. Braun V, Miyake A. Composition of blepharmone, a conjugation-inducing glycoprotein of the ciliate Blepharisma. FEBS Lett. 1975;53: 131–134. doi:10.1016/0014-5793(75)80003-2

31. Miyake A, Beyer J. Blepharmone: a conjugation-inducing glycoprotein in the ciliate blepharisma. Science. 1974;185: 621–623. doi:10.1126/science.185.4151.621

32. Sugiura M, Harumoto T. Identification, characterization, and complete amino acid sequence of the conjugation-inducing glycoprotein (blepharmone) in the ciliate Blepharisma japonicum. Proc Natl Acad Sci USA. 2001;98: 14446–14451. doi:10.1073/pnas.221457698

33. Kubota T, Tokoroyama T, Tsukuda Y, Koyama H, Miyake A. Isolation and structure determination of blepharismin, a conjugation initiating gamone in the ciliate blepharisma. Science. 1973;179: 400–402. doi:10.1126/science.179.4071.400

34. Klobutcher LA, Herrick G. Developmental genome reorganization in ciliated protozoa: the transposon link. Prog Nucleic Acid Res Mol Biol. 1997;56: 1–62. doi:10.1016/S0079-6603(08)61001-6

35. Arnaiz O, Mathy N, Baudry C, Malinsky S, Aury J-M, Denby Wilkes C, et al. The Paramecium germline genome provides a niche for intragenic parasitic DNA: evolutionary dynamics of internal eliminated sequences. PLoS Genet. 2012;8: e1002984. doi:10.1371/journal.pgen.1002984

36. Klobutcher LA, Herrick G. Consensus inverted terminal repeat sequence of Paramecium IESs: resemblance to termini of Tc1-related and Euplotes Tec transposons. Nucleic

Acids Res. 1995;23: 2006–2013. doi:10.1093/nar/23.11.2006

37. Chin C-S, Peluso P, Sedlazeck FJ, Nattestad M, Concepcion GT, Clum A, et al. Phased diploid genome assembly with single-molecule real-time sequencing. Nat Methods. 2016;13: 1050–1054. doi:10.1038/nmeth.4035

38. Nawrocki EP, Kolbe DL, Eddy SR. Infernal 1.0: inference of RNA alignments. Bioinformatics. 2009;25: 1335–1337. doi:10.1093/bioinformatics/btp157

39. Swart EC, Bracht JR, Magrini V, Minx P, Chen X, Zhou Y, et al. The Oxytricha trifallax macronuclear genome: a complex eukaryotic genome with 16,000 tiny chromosomes. PLoS Biol. 2013;11: e1001473. doi:10.1371/journal.pbio.1001473

40. Aeschlimann SH, Jönsson F, Postberg J, Stover NA, Petera RL, Lipps H-J, et al. The draft assembly of the radically organized Stylonychia lemnae macronuclear genome. Genome Biol Evol. 2014;6: 1707–1723. doi:10.1093/gbe/evu139

41. Zagulski M, Nowak JK, Le Mouël A, Nowacki M, Migdalski A, Gromadka R, et al. High coding density on the largest Paramecium tetraurelia somatic chromosome. Curr Biol. 2004;14: 1397–1404. doi:10.1016/j.cub.2004.07.029

42. Sheng Y, Duan L, Cheng T, Qiao Y, Stover NA, Gao S. The completed macronuclear genome of a model ciliate Tetrahymena thermophila and its application in genome scrambling and copy number analyses. Sci China Life Sci. 2020;63: 1534–1542. doi:10.1007/s11427-020-1689-4

43. Aury J-M, Jaillon O, Duret L, Noel B, Jubin C, Porcel BM, et al. Global trends of whole-genome duplications revealed by the ciliate Paramecium tetraurelia. Nature. 2006;444: 171–178. doi:10.1038/nature05230

44. Cheng Y-H, Liu C-FJ, Yu Y-H, Jhou Y-T, Fujishima M, Tsai IJ, et al. Genome plasticity in Paramecium bursaria revealed by population genomics. BMC Biol. 2020;18: 180.

doi:10.1186/s12915-020-00912-2

45. Yao MC, Yao CH, Monks B. The controlling sequence for site-specific chromosome breakage in Tetrahymena. Cell. 1990;63: 763–772. doi:10.1016/0092-8674(90)90142-2

46. Cavalcanti ARO, Dunn DM, Weiss R, Herrick G, Landweber LF, Doak TG. Sequence features of Oxytricha trifallax (class Spirotrichea) macronuclear telomeric and subtelomeric sequences. Protist. 2004;155: 311–322. doi:10.1078/1434461041844196

47. Lynch M. The origins of eukaryotic gene structure. Mol Biol Evol. 2006;23: 450–468. doi:10.1093/molbev/msj050

48. Roy SW, Hudson AJ, Joseph J, Yee J, Russell AG. Numerous fragmented spliceosomal introns, AT-AC splicing, and an unusual dynein gene expression pathway in Giardia lamblia. Mol Biol Evol. 2012;29: 43–49. doi:10.1093/molbev/msr063

49. Bondarenko VS, Gelfand MS. Evolution of the Exon-Intron Structure in Ciliate Genomes. PLoS ONE. 2016;11: e0161476. doi:10.1371/journal.pone.0161476

50. Csuros M, Rogozin IB, Koonin EV. A detailed history of intron-rich eukaryotic ancestors inferred from a global survey of 100 complete genomes. PLoS Comput Biol. 2011;7: e1002150. doi:10.1371/journal.pcbi.1002150

51. Sugiura M, Tanaka Y, Suzaki T, Harumoto T. Alternative gene expression in type I and type II cells may enable further nuclear changes during conjugation of Blepharisma japonicum. Protist. 2012;163: 204–216. doi:10.1016/j.protis.2011.07.007

52. Baudry C, Malinsky S, Restituito M, Kapusta A, Rosa S, Meyer E, et al. PiggyMac, a domesticated piggyBac transposase involved in programmed genome rearrangements in the ciliate Paramecium tetraurelia. Genes Dev. 2009;23: 2478–2483. doi:10.1101/gad.547309

53. Cheng C-Y, Vogt A, Mochizuki K, Yao M-C. A domesticated piggyBac transposase plays

key roles in heterochromatin dynamics and DNA cleavage during programmed DNA deletion in Tetrahymena thermophila. Mol Biol Cell. 2010;21: 1753–1762. doi:10.1091/mbc.e09-12-1079

54. Yuan Y-W, Wessler SR. The catalytic domain of all eukaryotic cut-and-paste transposase superfamilies. Proc Natl Acad Sci USA. 2011;108: 7884–7889. doi:10.1073/pnas.1104208108

55. Bischerour J, Bhullar S, Denby Wilkes C, Régnier V, Mathy N, Dubois E, et al. Six domesticated PiggyBac transposases together carry out programmed DNA elimination in Paramecium. eLife. 2018;7. doi:10.7554/eLife.37927

56. Chen X, Bracht JR, Goldman AD, Dolzhenko E, Clay DM, Swart EC, et al. The architecture of a scrambled genome reveals massive levels of genomic rearrangement during development. Cell. 2014;158: 1187–1198. doi:10.1016/j.cell.2014.07.034

57. Coyne RS, Hannick L, Shanmugam D, Hostetler JB, Brami D, Joardar VS, et al. Comparative genomics of the pathogenic ciliate Ichthyophthirius multifiliis, its free-living relatives and a host species provide insights into adoption of a parasitic lifestyle and prospects for disease control. Genome Biol. 2011;12: R100. doi:10.1186/gb-2011-12-10-r100

58. Guérineau M, Bessa L, Moriau S, Lescop E, Bontems F, Mathy N, et al. The unusual structure of the PiggyMac cysteine-rich domain reveals zinc finger diversity in PiggyBac-related transposases. Mob DNA. 2021;12: 12. doi:10.1186/s13100-021-00240-4

59. Yang Z, Nielsen R. Estimating synonymous and nonsynonymous substitution rates under realistic evolutionary models. Mol Biol Evol. 2000;17: 32–43. doi:10.1093/oxfordjournals.molbev.a026236

60. Mitra R, Fain-Thornton J, Craig NL. piggyBac can bypass DNA synthesis during cut and

paste transposition. EMBO J. 2008;27: 1097–1109. doi:10.1038/emboj.2008.41

61. Bouallègue M, Rouault J-D, Hua-Van A, Makni M, Capy P. Molecular Evolution of piggyBac Superfamily: From Selfishness to Domestication. Genome Biol Evol. 2017;9: 323–339. doi:10.1093/gbe/evw292

62. Kishino H, Miyata T, Hasegawa M. Maximum likelihood inference of protein phylogeny and the origin of chloroplasts. J Mol Evol. 1990;31: 151–160. doi:10.1007/BF02109483

63. Kishino H, Hasegawa M. Evaluation of the maximum likelihood estimate of the evolutionary tree topologies from DNA sequence data, and the branching order in hominoidea. J Mol Evol. 1989;29: 170–179. doi:10.1007/BF02100115

64. Ota R, Waddell PJ, Hasegawa M, Shimodaira H, Kishino H. Appropriate likelihood ratio tests and marginal distributions for evolutionary tree models with constraints on parameters. Mol Biol Evol. 2000;17: 798–803. doi:10.1093/oxfordjournals.molbev.a026358

65. Strimmer K, Rambaut A. Inferring confidence sets of possibly misspecified gene trees. Proc Biol Sci. 2002;269: 137–142. doi:10.1098/rspb.2001.1862

66. Shimodaira H. An approximately unbiased test of phylogenetic tree selection. Syst Biol. 2002;51: 492–508. doi:10.1080/10635150290069913

67. Tanaka Y, Nureki O, Kurumizaka H, Fukai S, Kawaguchi S, Ikuta M, et al. Crystal structure of the CENP-B protein-DNA complex: the DNA-binding domains of CENP-B induce kinks in the CENP-B box DNA. EMBO J. 2001;20: 6612–6618. doi:10.1093/emboj/20.23.6612

68. Casola C, Hucks D, Feschotte C. Convergent domestication of pogo-like transposases into centromere-binding proteins in fission yeast and mammals. Mol Biol Evol. 2008;25: 29–41. doi:10.1093/molbev/msm221

69. Hohmann S. Characterisation of PDC2, a gene necessary for high level expression of pyruvate decarboxylase structural genes in Saccharomyces cerevisiae. Mol Gen Genet. 1993;241: 657–666. doi:10.1007/BF00279908

70. Mojzita D, Hohmann S. Pdc2 coordinates expression of the THI regulon in the yeast Saccharomyces cerevisiae. Mol Genet Genomics. 2006;276: 147–161. doi:10.1007/s00438-006-0130-z

71. Gao B, Wang Y, Diaby M, Zong W, Shen D, Wang S, et al. Evolution of pogo, a separate superfamily of IS630-Tc1-mariner transposons, revealing recurrent domestication events in vertebrates. Mob DNA. 2020;11: 25. doi:10.1186/s13100-020-00220-0

72. Witherspoon DJ, Doak TG, Williams KR, Seegmiller A, Seger J, Herrick G. Selection on the protein-coding genes of the TBE1 family of transposable elements in the ciliates Oxytricha fallax and O. trifallax. Mol Biol Evol. 1997;14: 696–706. doi:10.1093/oxfordjournals.molbev.a025809

73. Williams K, Doak TG, Herrick G. Developmental precise excision of Oxytricha trifallax telomere-bearing elements and formation of circles closed by a copy of the flanking target duplication. EMBO J. 1993;12: 4593–4601. doi:10.1002/j.1460-2075.1993.tb06148.x

74. Nowacki M, Higgins BP, Maquilan GM, Swart EC, Doak TG, Landweber LF. A functional role for transposases in a large eukaryotic genome. Science. 2009;324: 935–938. doi:10.1126/science.1170023

75. Jahn CL, Doktor SZ, Frels JS, Jaraczewski JW, Krikau MF. Structures of the Euplotes crassus Tec1 and Tec2 elements: identification of putative transposase coding regions. Gene. 1993;133: 71–78. doi:10.1016/0378-1119(93)90226-s

76. Doak TG, Doerder FP, Jahn CL, Herrick G. A proposed superfamily of transposase

genes: transposon-like elements in ciliated protozoa and a common “D35E” motif. Proc Natl Acad Sci USA. 1994;91: 942–946. doi:10.1073/pnas.91.3.942

77. Dupeyron M, Baril T, Bass C, Hayward A. Phylogenetic analysis of the Tc1/mariner superfamily reveals the unexplored diversity of pogo-like elements. Mob DNA. 2020;11: 21. doi:10.1186/s13100-020-00212-0

78. Lewin HA, Graves JAM, Ryder OA, Graphodatsky AS, O’Brien SJ. Precision nomenclature for the new genomics. Gigascience. 2019;8. doi:10.1093/gigascience/giz086

79. Feng L, Wang G, Hamilton EP, Xiong J, Yan G, Chen K, et al. A germline-limited piggyBac transposase gene is required for precise excision in Tetrahymena genome rearrangement. Nucleic Acids Res. 2017;45: 9481–9502. doi:10.1093/nar/gkx652

80. Zufall RA, Sturm M, Mahon BC. Evolution of germline-limited sequences in two populations of the ciliate Chilodonella uncinata. J Mol Evol. 2012;74: 140–146. doi:10.1007/s00239-012-9493-4

81. Zufall RA, Katz LA. Micronuclear and macronuclear forms of beta-tubulin genes in the ciliate Chilodonella uncinata reveal insights into genome processing and protein evolution. J Eukaryot Microbiol. 2007;54: 275–282. doi:10.1111/j.1550-7408.2007.00267.x

82. Chen Q, Luo W, Veach RA, Hickman AB, Wilson MH, Dyda F. Structural basis of seamless excision and specific targeting by piggyBac transposase. Nat Commun. 2020;11: 3446. doi:10.1038/s41467-020-17128-1

83. Sarkar A, Sim C, Hong YS, Hogan JR, Fraser MJ, Robertson HM, et al. Molecular evolutionary analysis of the widespread piggyBac transposon family and related “domesticated” sequences. Mol Genet Genomics. 2003;270: 173–180.

doi:10.1007/s00438-003-0909-0

84. van Luenen HG, Colloms SD, Plasterk RH. The mechanism of transposition of Tc3 in C. elegans. Cell. 1994;79: 293–301. doi:10.1016/0092-8674(94)90198-8

85. Elick TA, Bauser CA, Fraser MJ. Excision of the piggyBac transposable element in vitro is a precise event that is enhanced by the expression of its encoded transposase. Genetica. 1996;98: 33–41. doi:10.1007/BF00120216

86. Cheng C-Y, Young JM, Lin C-YG, Chao J-L, Malik HS, Yao M-C. The piggyBac transposon-derived genes TPB1 and TPB6 mediate essential transposon-like excision during the developmental rearrangement of key genes in Tetrahymena thermophila. Genes Dev. 2016;30: 2724–2736. doi:10.1101/gad.290460.116

87. Miyake A, Beyer J. Cell interaction by means of soluble factors (gamones) in conjugation of Blepharisma intermedium. Exp Cell Res. 1973;76: 15–24. doi:10.1016/0014-4827(73)90413-8

88. Andersen RA. Algal Culturing Techniques. 1st Edition. 2004.

89. Miyake A, Harumoto T, Salvi B, Rivola V. Defensive function of pigment granules in Blepharisma japonicum. Eur J Protistol. 1990;25: 310–315. doi:10.1016/S0932-4739(11)80122-7

90. Miyake A. Cell interaction by gamones in blepharisma. Sexual interactions in eukaryotic microbes. Elsevier; 1981. pp. 95–129. doi:10.1016/B978-0-12-524160-1.50010-2

91. Schindelin J, Arganda-Carreras I, Frise E, Kaynig V, Longair M, Pietzsch T, et al. Fiji: an open-source platform for biological-image analysis. Nat Methods. 2012;9: 676–682. doi:10.1038/nmeth.2019

92. Kolmogorov M, Yuan J, Lin Y, Pevzner PA. Assembly of long, error-prone reads using repeat graphs. Nat Biotechnol. 2019;37: 540–546. doi:10.1038/s41587-019-0072-8

93. Li H. Minimap2: pairwise alignment for nucleotide sequences. Bioinformatics. 2018;34: 3094–3100. doi:10.1093/bioinformatics/bty191

94. Kearse M, Moir R, Wilson A, Stones-Havas S, Cheung M, Sturrock S, et al. Geneious Basic: an integrated and extendable desktop software platform for the organization and analysis of sequence data. Bioinformatics. 2012;28: 1647–1649. doi:10.1093/bioinformatics/bts199

95. Prjibelski A, Antipov D, Meleshko D, Lapidus A, Korobeynikov A. Using SPAdes de novo assembler. Curr Protoc Bioinformatics. 2020;70: e102. doi:10.1002/cpbi.102

96. Vaser R, Sikic M. Yet another de novo genome assembler. BioRxiv. 2019. doi:10.1101/656306

97. Swart EC, Serra V, Petroni G, Nowacki M. Genetic Codes with No Dedicated Stop Codon: Context-Dependent Translation Termination. Cell. 2016;166: 691–702. doi:10.1016/j.cell.2016.06.020

98. Gruber-Vodicka HR, Seah BKB, Pruesse E. phyloFlash: Rapid Small-Subunit rRNA Profiling and Targeted Assembly from Metagenomes. mSystems. 2020;5. doi:10.1128/mSystems.00920-20

99. Quast C, Pruesse E, Yilmaz P, Gerken J, Schweer T, Yarza P, et al. The SILVA ribosomal RNA gene database project: improved data processing and web-based tools. Nucleic Acids Res. 2013;41: D590-6. doi:10.1093/nar/gks1219

100. Hyatt D, Chen G-L, Locascio PF, Land ML, Larimer FW, Hauser LJ. Prodigal: prokaryotic gene recognition and translation initiation site identification. BMC Bioinformatics. 2010;11: 119. doi:10.1186/1471-2105-11-119

101. Gurevich A, Saveliev V, Vyahhi N, Tesler G. QUAST: quality assessment tool for genome assemblies. Bioinformatics. 2013;29: 1072–1075.

doi:10.1093/bioinformatics/btt086

102. Langmead B, Salzberg SL. Fast gapped-read alignment with Bowtie 2. Nat Methods. 2012;9: 357–359. doi:10.1038/nmeth.1923

103. Danecek P, Bonfield JK, Liddle J, Marshall J, Ohan V, Pollard MO, et al. Twelve years of SAMtools and BCFtools. Gigascience. 2021;10. doi:10.1093/gigascience/giab008

104. Garrison E, Marth G. Haplotype-based variant detection from short-read sequencing. v2 ed. arXiv; 2012 Jul p. arXiv:1207.3907 [q-bio.GN]. Available: https://arxiv.org/abs/1207.3907

105. Harris RS, Cechova M, Makova KD. Noise-cancelling repeat finder: uncovering tandem repeats in error-prone long-read sequencing data. Bioinformatics. 2019;35: 4809–4811. doi:10.1093/bioinformatics/btz484

106. Seah BKB, Swart EC. BleTIES: Annotation of natural genome editing in ciliates using long read sequencing. BioRxiv. 2021. doi:10.1101/2021.05.18.444610

107. Cock PJA, Antao T, Chang JT, Chapman BA, Cox CJ, Dalke A, et al. Biopython: freely available Python tools for computational molecular biology and bioinformatics. Bioinformatics. 2009;25: 1422–1423. doi:10.1093/bioinformatics/btp163

108. Dale RK, Pedersen BS, Quinlan AR. Pybedtools: a flexible Python library for manipulating genomic datasets and annotations. Bioinformatics. 2011;27: 3423–3424. doi:10.1093/bioinformatics/btr539

109. Quinlan AR, Hall IM. BEDTools: a flexible suite of utilities for comparing genomic features. Bioinformatics. 2010;26: 841–842. doi:10.1093/bioinformatics/btq033

110. Hunter JD. Matplotlib: A 2D Graphics Environment. Comput Sci Eng. 2007;9: 90–95. doi:10.1109/MCSE.2007.55

111. Crooks GE, Hon G, Chandonia JM, Brenner SE. WebLogo: a sequence logo generator. Genome Res. 2004;14: 1188–1190. doi:10.1101/gr.849004

112. Kim D, Paggi JM, Park C, Bennett C, Salzberg SL. Graph-based genome alignment and genotyping with HISAT2 and HISAT-genotype. Nat Biotechnol. 2019;37: 907–915. doi:10.1038/s41587-019-0201-4

113. Dutilh BE, Jurgelenaite R, Szklarczyk R, van Hijum SAFT, Harhangi HR, Schmid M, et al. FACIL: Fast and Accurate Genetic Code Inference and Logo. Bioinformatics. 2011;27: 1929–1933. doi:10.1093/bioinformatics/btr316

114. Eddy SR. Accelerated profile HMM searches. PLoS Comput Biol. 2011;7: e1002195. doi:10.1371/journal.pcbi.1002195

115. Saudemont B, Popa A, Parmley JL, Rocher V, Blugeon C, Necsulea A, et al. The fitness cost of mis-splicing is the main determinant of alternative splicing patterns. Genome Biol. 2017;18: 208. doi:10.1186/s13059-017-1344-6

116. Kalvari I, Argasinska J, Quinones-Olvera N, Nawrocki EP, Rivas E, Eddy SR, et al. Rfam 13.0: shifting to a genome-centric resource for non-coding RNA families. Nucleic Acids Res. 2018;46: D335–D342. doi:10.1093/nar/gkx1038

117. Chan PP, Lin BY, Mak AJ, Lowe TM. tRNAscan-SE 2.0: Improved Detection and Functional Classification of Transfer RNA Genes. BioRxiv. 2019. doi:10.1101/614032

118. Lopez-Delisle L, Rabbani L, Wolff J, Bhardwaj V, Backofen R, Grüning B, et al. pyGenomeTracks: reproducible plots for multivariate genomic datasets. Bioinformatics. 2021;37: 422–423. doi:10.1093/bioinformatics/btaa692

119. Waterhouse RM, Seppey M, Simão FA, Manni M, Ioannidis P, Klioutchnikov G, et al. BUSCO applications from quality assessments to gene prediction and phylogenomics. Mol Biol Evol. 2018;35: 543–548. doi:10.1093/molbev/msx319

120. Törönen P, Medlar A, Holm L. PANNZER2: a rapid functional annotation web server. Nucleic Acids Res. 2018;46: W84–W88. doi:10.1093/nar/gky350

121. Huerta-Cepas J, Szklarczyk D, Heller D, Hernández-Plaza A, Forslund SK, Cook H, et al. eggNOG 5.0: a hierarchical, functionally and phylogenetically annotated orthology resource based on 5090 organisms and 2502 viruses. Nucleic Acids Res. 2019;47: D309–D314. doi:10.1093/nar/gky1085

122. Liao Y, Smyth GK, Shi W. featureCounts: an efficient general purpose program for assigning sequence reads to genomic features. Bioinformatics. 2014;30: 923–930. doi:10.1093/bioinformatics/btt656

123. Robinson MD, McCarthy DJ, Smyth GK. edgeR: a Bioconductor package for differential expression analysis of digital gene expression data. Bioinformatics. 2010;26: 139–140. doi:10.1093/bioinformatics/btp616

124. Li B, Ruotti V, Stewart RM, Thomson JA, Dewey CN. RNA-Seq gene expression estimation with read mapping uncertainty. Bioinformatics. 2010;26: 493–500. doi:10.1093/bioinformatics/btp692

125. Wagner GP, Kin K, Lynch VJ. Measurement of mRNA abundance using RNA-seq data: RPKM measure is inconsistent among samples. Theory Biosci. 2012;131: 281–285. doi:10.1007/s12064-012-0162-3

126. Katoh K, Misawa K, Kuma K, Miyata T. MAFFT: a novel method for rapid multiple sequence alignment based on fast Fourier transform. Nucleic Acids Res. 2002;30: 3059–3066. doi:10.1093/nar/gkf436

127. Katoh K, Standley DM. MAFFT multiple sequence alignment software version 7: improvements in performance and usability. Mol Biol Evol. 2013;30: 772–780. doi:10.1093/molbev/mst010

128. Guindon S, Dufayard J-F, Lefort V, Anisimova M, Hordijk W, Gascuel O. New algorithms and methods to estimate maximum-likelihood phylogenies: assessing the performance of PhyML 3.0. Syst Biol. 2010;59: 307–321. doi:10.1093/sysbio/syq010

129. Stover NA, Punia RS, Bowen MS, Dolins SB, Clark TG. Tetrahymena Genome Database Wiki: a community-maintained model organism database. Database (Oxford). 2012;2012: bas007. doi:10.1093/database/bas007

130. Wang R-L, Miao W, Wang W, Xiong J, Liang A-H. EOGD: the Euplotes octocarinatus genome database. BMC Genomics. 2018;19: 63. doi:10.1186/s12864-018-4445-z

131. Arnaiz O, Meyer E, Sperling L. ParameciumDB 2019: integrating genomic data across the genus for functional and evolutionary biology. Nucleic Acids Res. 2020;48: D599–D605. doi:10.1093/nar/gkz948

132. Yang Z. PAML 4: phylogenetic analysis by maximum likelihood. Mol Biol Evol. 2007;24: 1586–1591. doi:10.1093/molbev/msm088

133. Larkin MA, Blackshields G, Brown NP, Chenna R, McGettigan PA, McWilliam H, et al. Clustal W and Clustal X version 2.0. Bioinformatics. 2007;23: 2947–2948. doi:10.1093/bioinformatics/btm404

134. UniProt Consortium. UniProt: the universal protein knowledgebase in 2021. Nucleic Acids Res. 2021;49: D480–D489. doi:10.1093/nar/gkaa1100

135. Jones P, Binns D, Chang H-Y, Fraser M, Li W, McAnulla C, et al. InterProScan 5: genome-scale protein function classification. Bioinformatics. 2014;30: 1236–1240. doi:10.1093/bioinformatics/btu031

136. Mistry J, Chuguransky S, Williams L, Qureshi M, Salazar GA, Sonnhammer ELL, et al. Pfam: The protein families database in 2021. Nucleic Acids Res. 2021;49: D412–D419. doi:10.1093/nar/gkaa913

137. Darriba D, Posada D, Kozlov AM, Stamatakis A, Morel B, Flouri T. ModelTest-NG: A New and Scalable Tool for the Selection of DNA and Protein Evolutionary Models. Mol Biol Evol. 2020;37: 291–294. doi:10.1093/molbev/msz189

138. Minh BQ, Schmidt HA, Chernomor O, Schrempf D, Woodhams MD, von Haeseler A, et al. IQ-TREE 2: New Models and Efficient Methods for Phylogenetic Inference in the Genomic Era. Mol Biol Evol. 2020;37: 1530–1534. doi:10.1093/molbev/msaa015

139. Suzuki S. Parthenogenetic conjugation in Blepharisma undulans japonicus Suzuki. Bull Yamagata Univ Natural Sci. 1957;4: 69–84.

140. Kriventseva EV, Kuznetsov D, Tegenfeldt F, Manni M, Dias R, Simão FA, et al. OrthoDB v10: sampling the diversity of animal, plant, fungal, protist, bacterial and viral genomes for evolutionary and functional annotations of orthologs. Nucleic Acids Res. 2019;47: D807–D811. doi:10.1093/nar/gky1053

141. Wick RR, Schultz MB, Zobel J, Holt KE. Bandage: interactive visualization of de novo genome assemblies. Bioinformatics. 2015;31: 3350–3352. doi:10.1093/bioinformatics/btv383

Figure captions

Figure 1. *Blepharisma* cells and properties of ciliate MAC genomes. **A.** *B. stoltei* ATCC 30299 cell stained with anti-alpha tubulin-Alexa488 (depth-color coded red to yellow) and DAPI (cyan). **B.** Snapshot of a 3D reconstruction (Imaris, Bitplane) from CLSM images of Hoechst 33342 (dsDNA dye, Invitrogen™) fluorescence (Ex405 nm / Em420-470 nm). **C.** Scanning electron microscope (SEM) image of a *B. stoltei* ATCC 30299 cell (false color).

Figure 2. Nuclear development during *Blepharisma stoltei* conjugation. A. Cell development cycle with inset showing the four main kinds of nuclei, highlighted with arrows. Illustration of various cell stages adapted from [139]). Detailed staging collected for an RNA-seq time course is provided in Figure S9. **B.** Schematic of nuclear processes occurring during conjugation (classified according to, and modified from [9]). Nuclear events occurring before and up to, but not including fusion of the gametic nuclei (syngamy) are classified into sixteen pre-gamic stages where the MICs undergo meiosis and the haploid products of meiotic MICs are exchanged between the conjugating cells, followed by karyogamy. After karyogamy, cells are classified into 10 stages S (synkaryon), D1 (1st mitosis), I1 (1st interphase), D2 (2nd mitosis), I2 (2nd interphase), D3 (3rd mitosis), I3 (3rd interphase), D4 (4th mitosis), E1 (1st embryonic stage), E2 (2nd embryonic stage). After E2, the exconjugants divide further and are classified into 6 stages of cell division (CD1-6) which we did not follow here.

Figure 3. Basic properties of ciliate MAC genomes. In cell diagrams MACs are green and MICs are small black dots in close proximity to MACs. Citations for genome properties are in Data S1.

Figure 4. **Alternative telomere addition sites. A.** Mapping of a subset telomere-containing

HiFi reads to a *B. stoltei* MAC genome contig region, with alternative telomere addition sites (ATASs) shown by blue (5') or mauve (3') arrows. Pink bars at read ends indicate soft-masking by minimap2, typically of telomeric repeats. **B.** Mean base frequencies in +/- 1 kbp flanking ATAS junctions.

Figure 5. A gene-dense somatic genome with tiny introns. A. HiFi (DNA) and RNA-seq coverage across a representative *B. stoltei* ATCC30299 MAC genome contig (Contig_1). Y scale is linear for HiFi reads and logarithmic (base 10) for RNA-seq. Plus strand (relative to the contig) RNA-seq coverage is green; minus strand RNA-seq coverage is blue. Between the RNA-seq coverage graphs each arrow represents a predicted gene, colored green when transcribed from the sense strand and blue from the antisense one. Two orthogroups classified by OrthoFinder are shown in orange and pink, respectively. **B.** Distribution of intron lengths from predicted genes. **C.** Sequence logos for 15 bp introns (splicing frequency > 0.5). **D.** Clustered orthogroups (Data S2) in the *B. stoltei* MAC genome.

Figure 6. MAC genome-encoded transposases in ciliates and properties of a putative *Blepharisma* IES excisase. A. Presence/absence matrix of PFAM transposase domains detected in predicted MAC genome-encoded ciliate proteins. Ciliate classes are indicated before the binomial species names. Note that *Ichthyophthirius multifiliis* is not shown because no domains with i-E-values < 1e-4 were detected. PiggyBac homolog phylogeny with PFAM domain architecture and gene expression heatmap for *Blepharisma*. **B**. DDE_Tnp_1_7 domain phylogeny with PFAM domain architecture and gene expression heatmap for *Blepharisma*. **C.** Cysteine-rich domains of PiggyBac homologs. PBLE transposases: Ago (*Aphis gossypii*); Bmo (*Bombyx mori*); Cag (*Ctenoplusia agnata*); Har (*Helicoverpa armigera*); Hvi (*Heliothis virescens*); PB-Tni (*Trichoplusia ni*); Mlu (PiggyBat from *Myotis lucifugus*); PLE-wu (*Spodoptera frugiperda*). Domesticated PGBD transposases: Oni (*Oreochromis niloticus*); Pny (*Pundamilia nyererei*);

Lia5, Tpb1, Tpb2, Tpb6 and Tpb7 (*Tetrahymena thermophila*); Pgm, PgmL1, PgmL2, PgmL3a/b/c, PgmL4a/b, PgmL5a/b (*Paramecium tetraurelia*); Tru (*Takifugu rubripes*); Pgbd2, Pgbd3 and Pgbd4 (*Homo sapiens*).

Figure 7. Phylogeny of ciliate PiggyBac homologs, eukaryotic PBLEs and PGBD5 homologs. Colors indicate eukaryotic lineages: purple=Alveolata, green=Stramenopiles, cyan=Archaeplastida, yellow=Opisthokonta, blue=Amoebozoa. Clade highlighted in pink represents all heterotrich Pgms and PgmLs. aBayes values generated by PhyML are represented as line widths and branch colors. aBayes values lower than 0.9 are represented in red-grey, with lower values appearing more red. The tree is rooted at the PiggyBac-like element of *Entamoeba invadens.*

Supplementary figure captions

Figure S1. Analysis of assembly completeness by Benchmarking Universal Single-Copy Orthologs (BUSCO). Completeness of the *B. stoltei* ATCC 30299 MAC assembly was estimated by the percentage of BUSCOs found in the assembly with reference to the OrthoDB v10 alveolate database [140]. The nature of the ortholog-matches is indicated by characters followed by counts: C (complete orthologs) - light blue, D (duplicated orthologs) - dark blue, F (fragmented orthologs) - yellow and M (missing orthologs) - red.

Figure S2. Properties of minichromosomes, telomeres, and alternative telomere addition sites. A. Length distribution of telomeres of telomere-bearing HiFi reads. **B.** Length distribution of HiFi reads delimited by telomeres. **C**. Diagram of a telomere-bearing read mapped onto genome reference at an ATAS. Sequence which is ambiguously chromosomal or telomeric is "junction sequence"; junction coordinate which maximizes telomere repeat length on the read is the "first identifiable breakpoint"; the coordinate maximizing alignment length to reference is the "last identifiable breakpoint". The last telomeric unit permutation at the last identifiable breakpoint is underlined (length 8 bp). **D.** Sequence logos of chromosomal sequence at ATAS junctions, sorted by which permutation of the telomeric repeat is present (plot labels). Logos are aligned to the "last identifiable breakpoint" between positions 20 and 21; telomeric repeats on telomere-bearing reads begin to the left of the breakpoint. **E**. Frequencies of 2-mers in whole genome (blue), in telomeres (green), and at ATAS junctions (chromosomal side after last identifiable breakpoint, orange). **F.** Histogram of junction sequence lengths for ATASs in *B. stoltei*. **G.** Counts of each telomere repeat permutation at ATAS junctions (last identifiable breakpoint).

Figure S3. **Femto Pulse analyses of *B. stoltei* MAC DNA and mapping of *T. thermophila***

telomere-bearing reads. A. Mapping of PacBio CLR reads with 3 consecutive telomeric repeats to a representative *T. thermophila* MAC chromosome (Chr_001 from ciliate.org). **B.** Length distribution of input MAC DNA sizes prior to fragmentation and library preparation (Femto Pulse; LM = lower maker) - replicate 1. RFU=relative fluorescent units. **C.** Length distribution of input MAC DNA sizes prior to fragmentation and library preparation (Femto Pulse; LM = lower maker) - replicate 2.

Figure S4. POT1 paralog phylogeny, PFAM domain architecture, and gene expression in *Blepharisma*. Diagram elements as described in Figure 6B.

Figure S5. *Blepharisma stoltei* genetic code. Prediction for *B. stoltei* ATCC 30299 MAC genome by PORC; codons that are stops in the standard genetic code are highlighted in orange.

Figure S6. Intron splicing. A. Distribution of intron splicing fraction of candidate sense introns in the *B. stoltei* MAC genome. **B**. Distribution of intron splicing fractions of introns according to intron lengths. **C.** Distribution of intron splicing fraction of candidate antisense introns. **D.** Sequence logos for all predicted 16 nt introns, and 16 nt introns with “A” at either position -7 or -6 (counting from the 3’ end). The number of introns underlying the logos are indicated to the right. **E.** Distribution of intron splicing fractions of introns according to intron lengths. **F.** Sample of RNA-seq reads mapped to a GT-GG intron from gene BSTOLATCC_MAC21551 (Contig_57.g761). Translation in alternative reading frames downstream of the predicted intron leads to premature stop codons soon after the intron.

Figure S7. ***B. stoltei* ATCC30299 MAC genome assembly graph.** Bandage [141] representation of Flye 2.8.1 assembly graph. Edges corresponding to contigs are colored by coverage (brightest pink = 160×, black=0×).

Figure S8. Experimental approach for conjugation RNA-seq time series. Complementary mating type strains of *Blepharisma stoltei* were harvested and cleaned by starving overnight. The cleaned cultures were treated in a time-staggered format, with gamones of the complementary mating type, where gamone 2 was a solution of the synthetic gamone 2 calcium salt and gamone 1 was provided as the cell-free fluid (CFF) harvested from mating-type I cells. Two sets of time-staggered gamone-treated cultures were used for the time series. Set I, indicated by the solid line, was mixed and used to observe and collect samples at 0 hours, 2 hours, 6 hours, 26 hours and 30 hours after mixing. Set II, indicated by the dashed lines, was mixed and used to observe and collect samples at 14 hours, 18 hours, 22 hours and 38 hours after mixing. Test tubes indicate Trizol samples prepared for RNA-extraction which were stored at -80 ˚C before processing. Cells collected for imaging were obtained shortly before the remainder were transferred into Trizol.

Figure S9. Developmental staging of *B. stoltei* for RNA-seq. A. The classification of nuclear morphology into stages has been done according to previous descriptions [9]. Nuclear events occurring before and up to, but not including fusion of the gametic nuclei (syngamy) are classified into sixteen stages indicated by roman numerals. These are the pre-gamic stages of conjugation where the MICs undergo meiosis and the haploid products of meiotic MICs are exchanged between the conjugating cells. Stages after syngamy are classified into 10 stages, stage S (synkaryon), D1 (1st mitosis), I1(1st interphase), D2 (2nd mitosis), I2 (2nd interphase), D3 (3rd mitosis), I3 (3rd interphase), D4 (4th mitosis), E1 (1st embryonic stage), E2 (2nd embryonic stage). After E2, the exconjugants divide further and are classified into 6 stages of cell division (CD1-6) which we did not follow here. Illustration of various cell stages adapted from [139]). Stacked bars show the proportion of cells at each time point at different stages of development, preceded by the number of cells inspected (n).

Figure S10. DDE_1 and DDE_3 domain transposases in *Blepharisma*. A. DDE_1 domain phylogeny with PFAM domain architecture and gene expression heatmap for *Blepharisma*. **B.** DDE_3 domain phylogeny with PFAM domain architecture and gene expression heatmap for *Blepharisma*.

Figure S11. DDE_Tnp_IS1595 and MULE domain transposases in *Blepharisma*. A. DDE_Tnp_IS1595 domain phylogeny with PFAM domain architecture and gene expression heatmap for *Blepharisma*. **B.** MULE domain phylogeny with PFAM domain architecture and gene expression heatmap for *Blepharisma*.

Figure S12. Small RNA-related proteins in *Blepharisma*. A. ResIII, Helicase_c and Ribonuclease_3 domain phylogeny with PFAM domain architecture and gene expression heatmap for *Blepharisma*. **B.** PIWI domain phylogeny with PFAM domain architecture and gene expression heatmap for *B. stoltei*.

Figure S13. Histones and histone-domain-containing proteins in *Blepharisma*. Gene expression heatmaps are shown as in previous figures, are clustered according to major histone type as classified using HistoneDB domain models. Domains from PFAM and HistoneDB are shown to the right.

Figure 1.

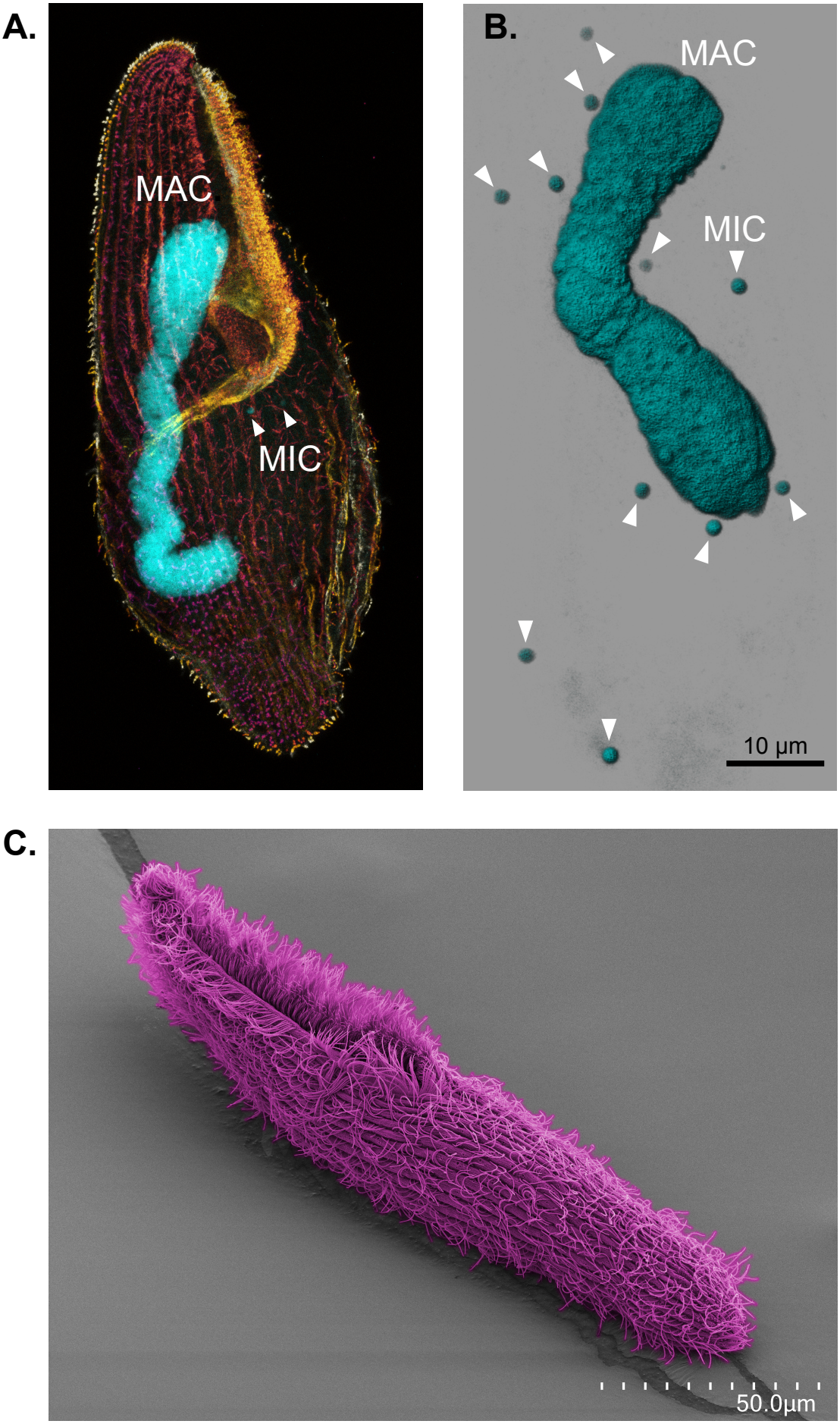

Figure 2.

A.

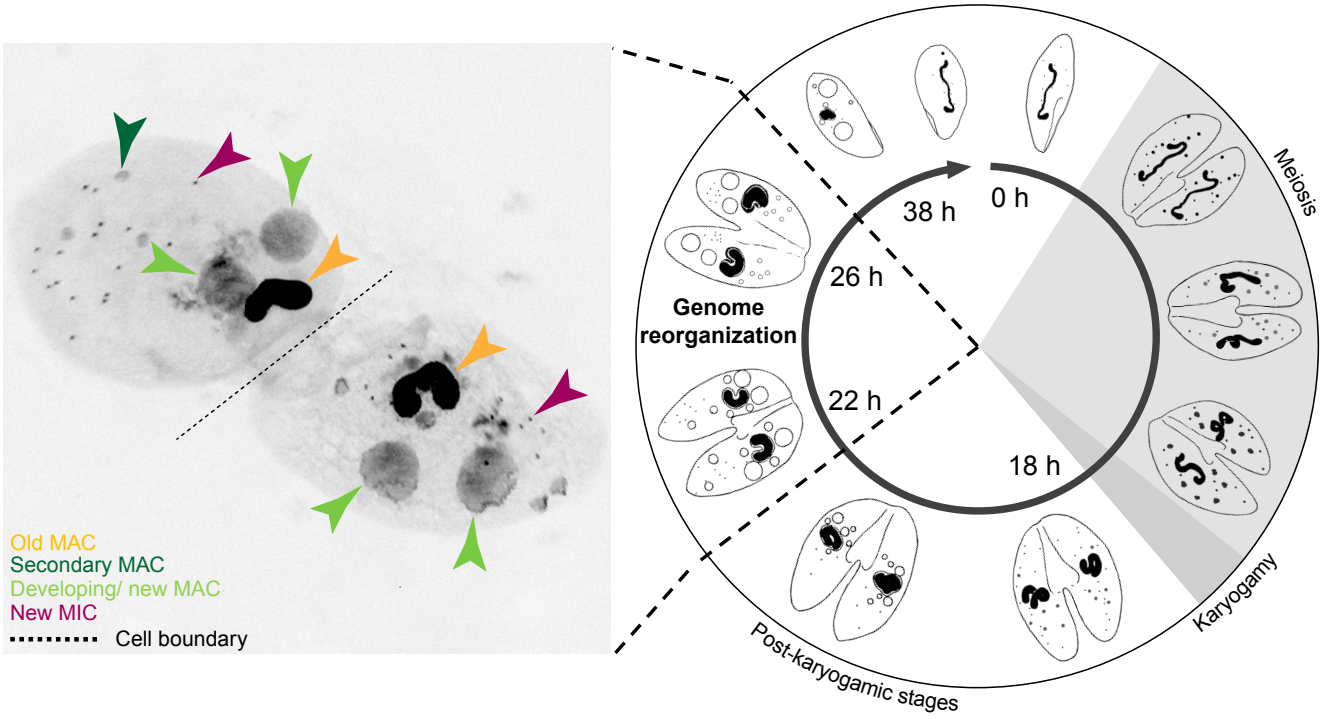
Old MAC
Secondary MAC
Developing/ new MAC
New MIC
Cell boundary
0 h
18 h
22 h
26 h
38 h
Genome reorganization
Meiosis
Karyogamy
Post-karyogamic stages

B.

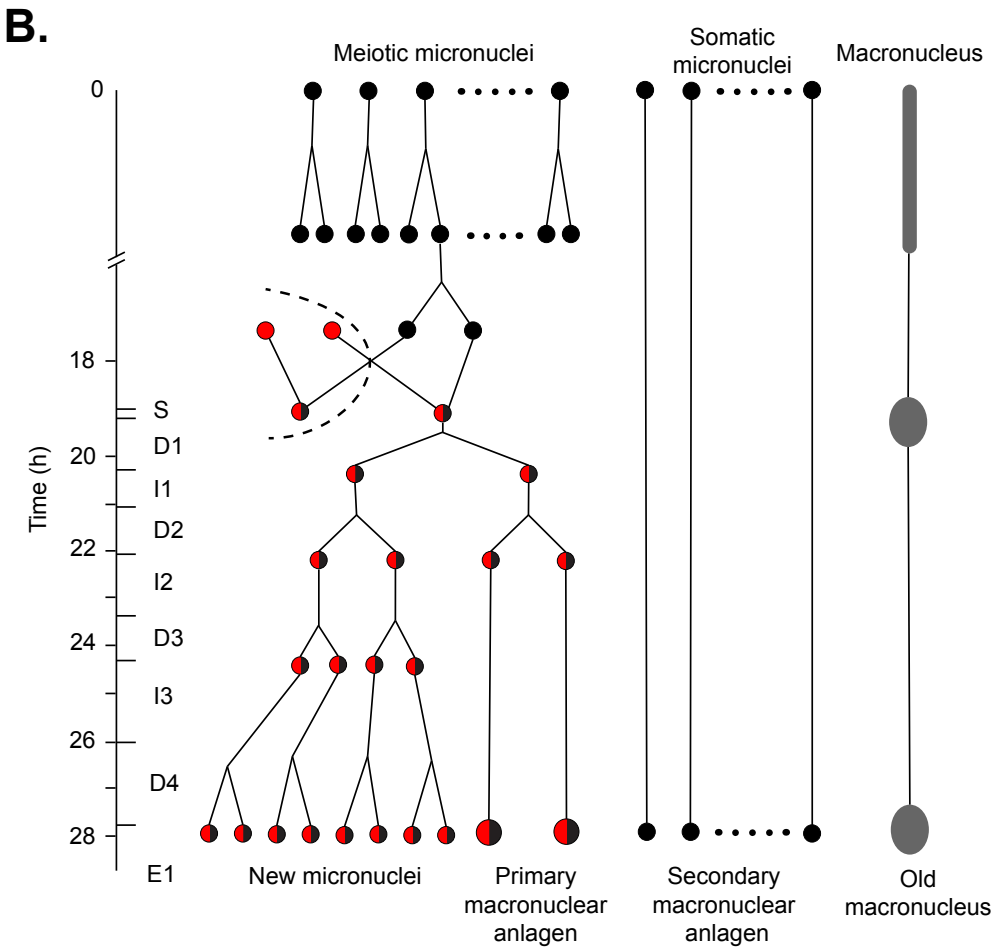
Meiotic micronuclei
Somatic micronuclei
Macronucleus
Time (h)
0
18
20
22
24
26
28
S
D1
I1
D2
I2
D3
I3
D4
E1
New micronuclei
Primary macronuclear anlagen
Secondary macronuclear anlagen
Old macronucleus

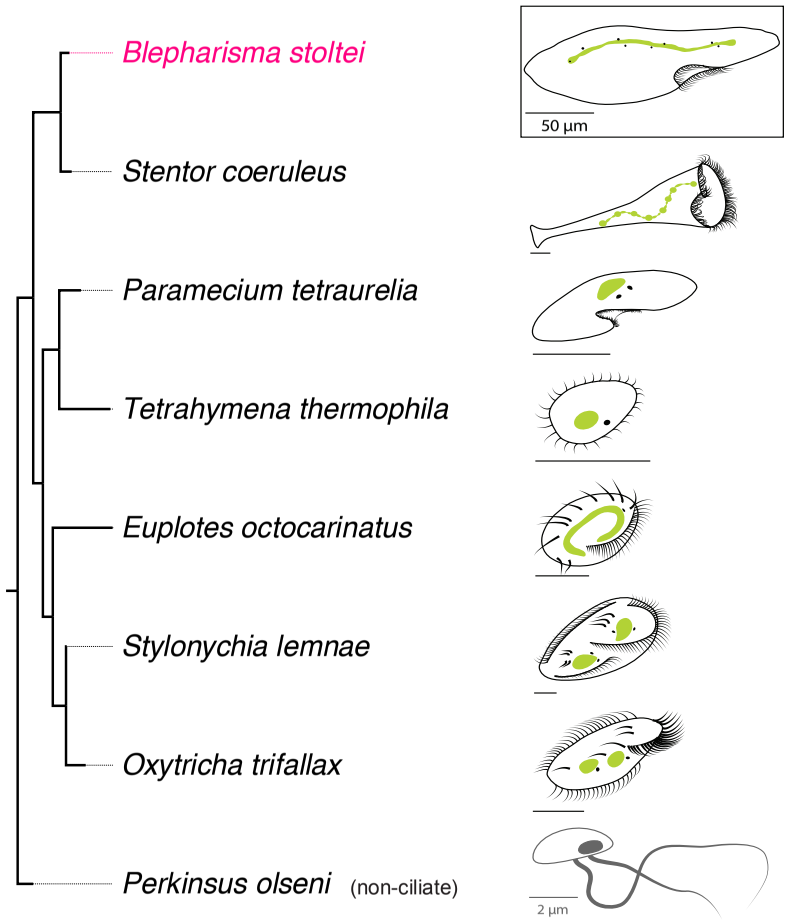

Species	Genome size (~Mb)	Genome architecture	Genes (zygosity)	Codon reassignments		
				UAA	UAG	UGA
***Blepharisma stoltei* (ATCC 302099)**	**41**	**Mini-chromosomes**	**25726 (n)**	*	*	W
Stentor coeruleus	77	?	31426 (?)	*	*	*
Paramecium tetraurelia	72	Chromosomes	39642 (n)	Q	Q	*
Tetrahymena thermophila	103	Chromosomes	26258 (n)	Q	Q	*
Euplotes octocarinatus	88	Nano-chromosomes	29076 (n)	*	*	C
Stylonychia lemnae	52	Nano-chromosomes	15102 (n)	Q	Q	*
Oxytricha trifallax	50	Nano-chromosomes	18400 (n)	Q	Q	*
Perkinsus olseni	63	Chromosomes	17342 (4n)	*	*	*

Figure 3.

Figure 4.

A.

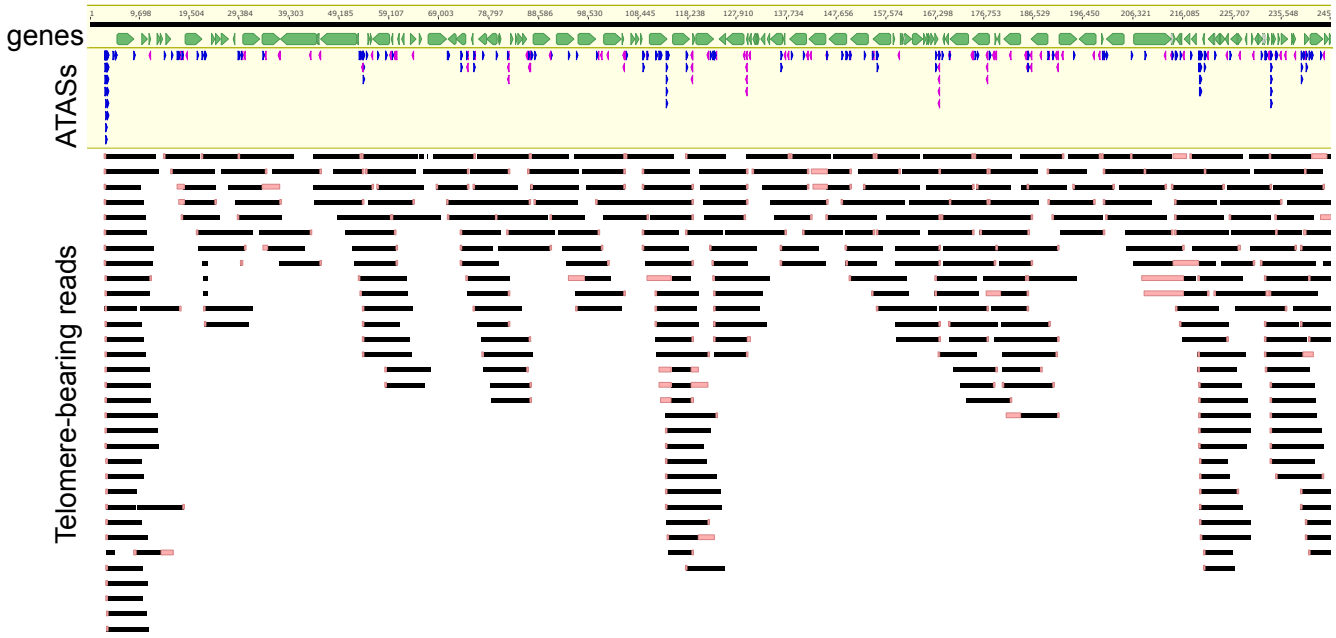
genes
ATASs
Telomere-bearing reads

B.

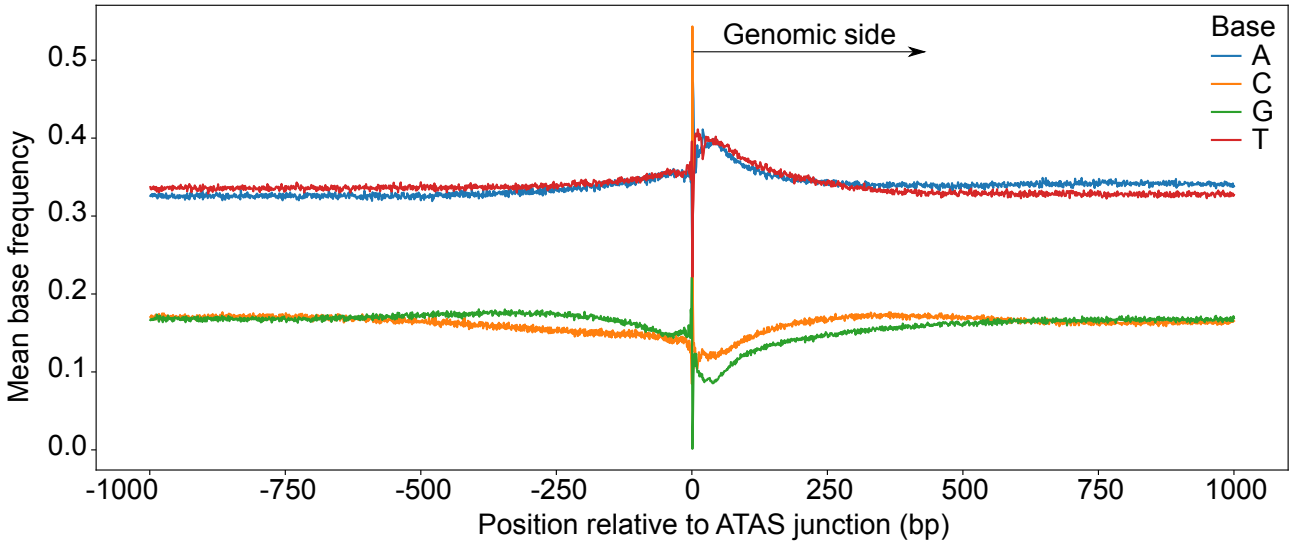
Genomic side
Base
A
C
G
T
Mean base frequency
0.0
0.1
0.2
0.3
0.4
0.5
-1000
-750
-500
-250
0
250
500
750
1000
Position relative to ATAS junction (bp)

Figure 5.

A.

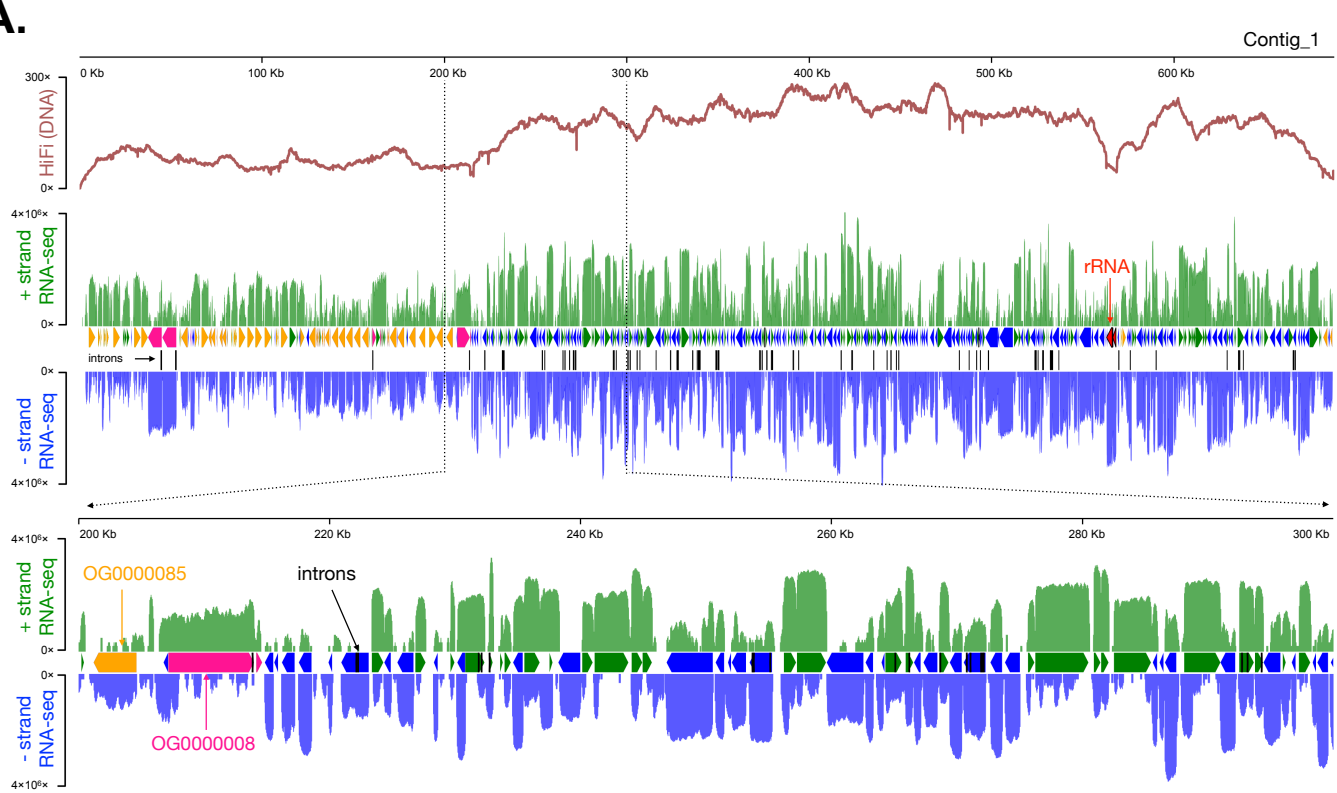

B.

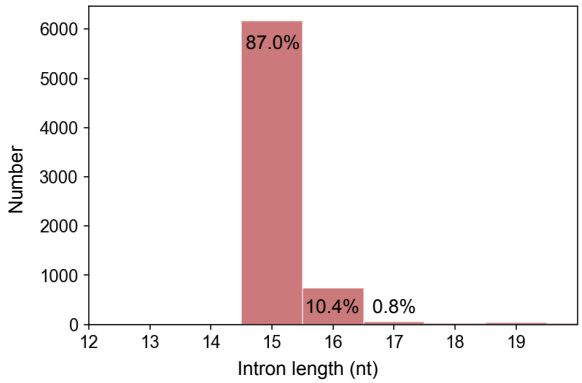

C.

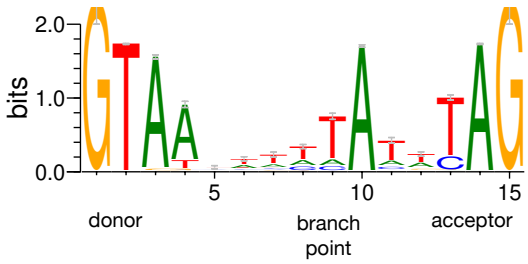

D.

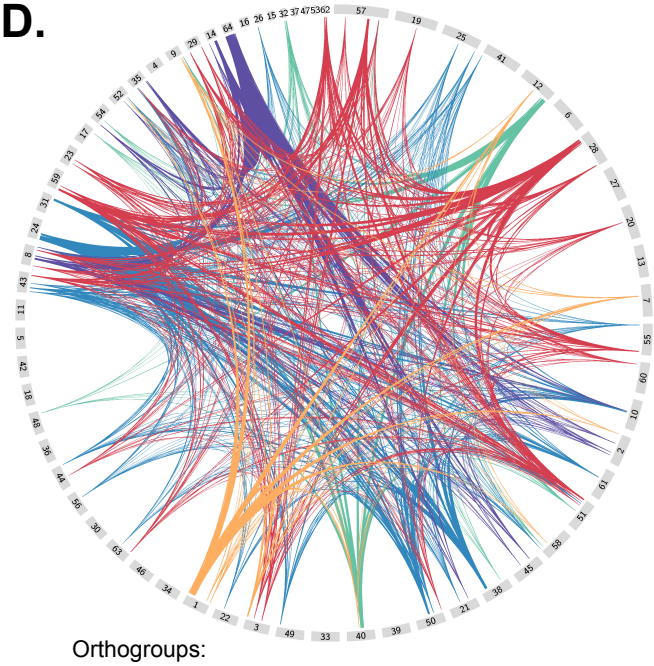

Orthogroups:

OG0000085 OG0000018 OG0000019

OG0000014 OG0000052

Figure 6.

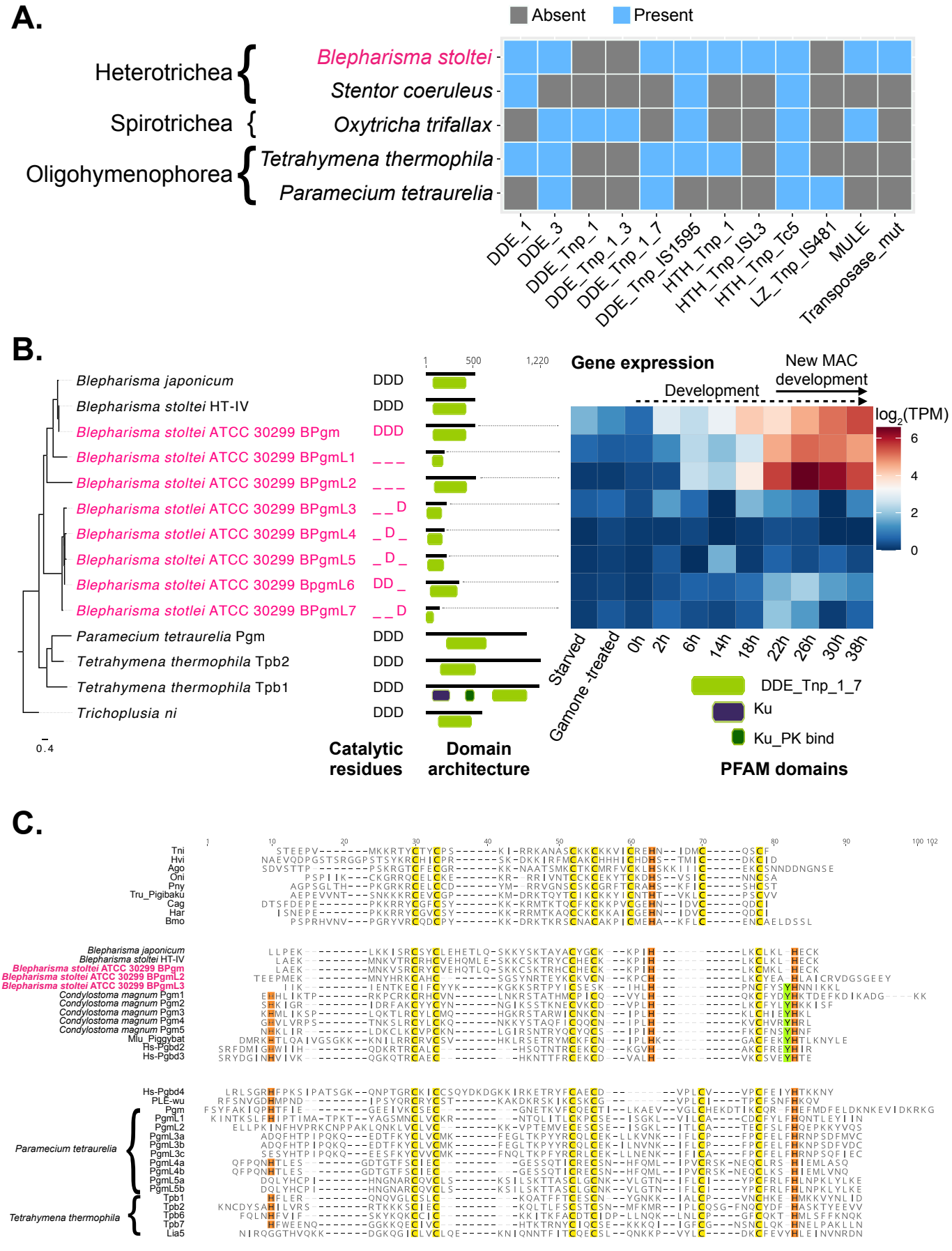
A.
Absent
Present
Heterotrichea
Spirotrichea
Oligohymenophorea
Blepharisma stoltei
Stentor coeruleus
Oxytricha trifallax
Tetrahymena thermophila
Paramecium tetraurelia
DDE_1
DDE_3
DDE_Tnp_1
DDE_Tnp_1_3
DDE_Tnp_1_7
DDE_Tnp_IS1595
HTH_Tnp_1
HTH_Tnp_ISL3
HTH_Tnp_Tc5
LZ_Tnp_IS481
MULE
Transposase_mut
B.
Blepharisma japonicum
Blepharisma stoltei HT-IV
Blepharisma stoltei ATCC 30299 BPgm
Blepharisma stoltei ATCC 30299 BPgmL1
Blepharisma stoltei ATCC 30299 BPgmL2
Blepharisma stoltei ATCC 30299 BPgmL3
Blepharisma stoltei ATCC 30299 BPgmL4
Blepharisma stoltei ATCC 30299 BPgmL5
Blepharisma stoltei ATCC 30299 BpgmL6
Blepharisma stoltei ATCC 30299 BPgmL7
Paramecium tetraurelia Pgm
Tetrahymena thermophila Tpb2
Tetrahymena thermophila Tpb1
Trichoplusia ni
0.4
Catalytic residues
Domain architecture
Gene expression
Development
New MAC development
log2(TPM)
Starved
Gamone -treated
0h
2h
6h
14h
18h
22h
26h
30h
38h
DDE_Tnp_1_7
Ku
Ku_PK bind
PFAM domains
C.
Tni
Hvi
Ago
Oni
Pny
Tru_Pigibaku
Cag
Har
Bmo
Blepharisma japonicum
Blepharisma stoltei HT-IV
Blepharisma stoltei ATCC 30299 BPgm
Blepharisma stoltei ATCC 30299 BPgmL2
Blepharisma stoltei ATCC 30299 BPgmL3
Condylostoma magnum Pgm1
Condylostoma magnum Pgm2
Condylostoma magnum Pgm3
Condylostoma magnum Pgm4
Condylostoma magnum Pgm5
Mlu_Piggybat
Hs-Pgbd2
Hs-Pgbd3
Hs-Pgbd4
PLE-wu
Pgm
PgmL1
PgmL2
PgmL3a
PgmL3b
PgmL3c
PgmL4a
PgmL4b
PgmL5a
PgmL5b
Paramecium tetraurelia
Tpb1
Tpb2
Tpb6
Tpb7
Lia5
Tetrahymena thermophila

Figure 7.

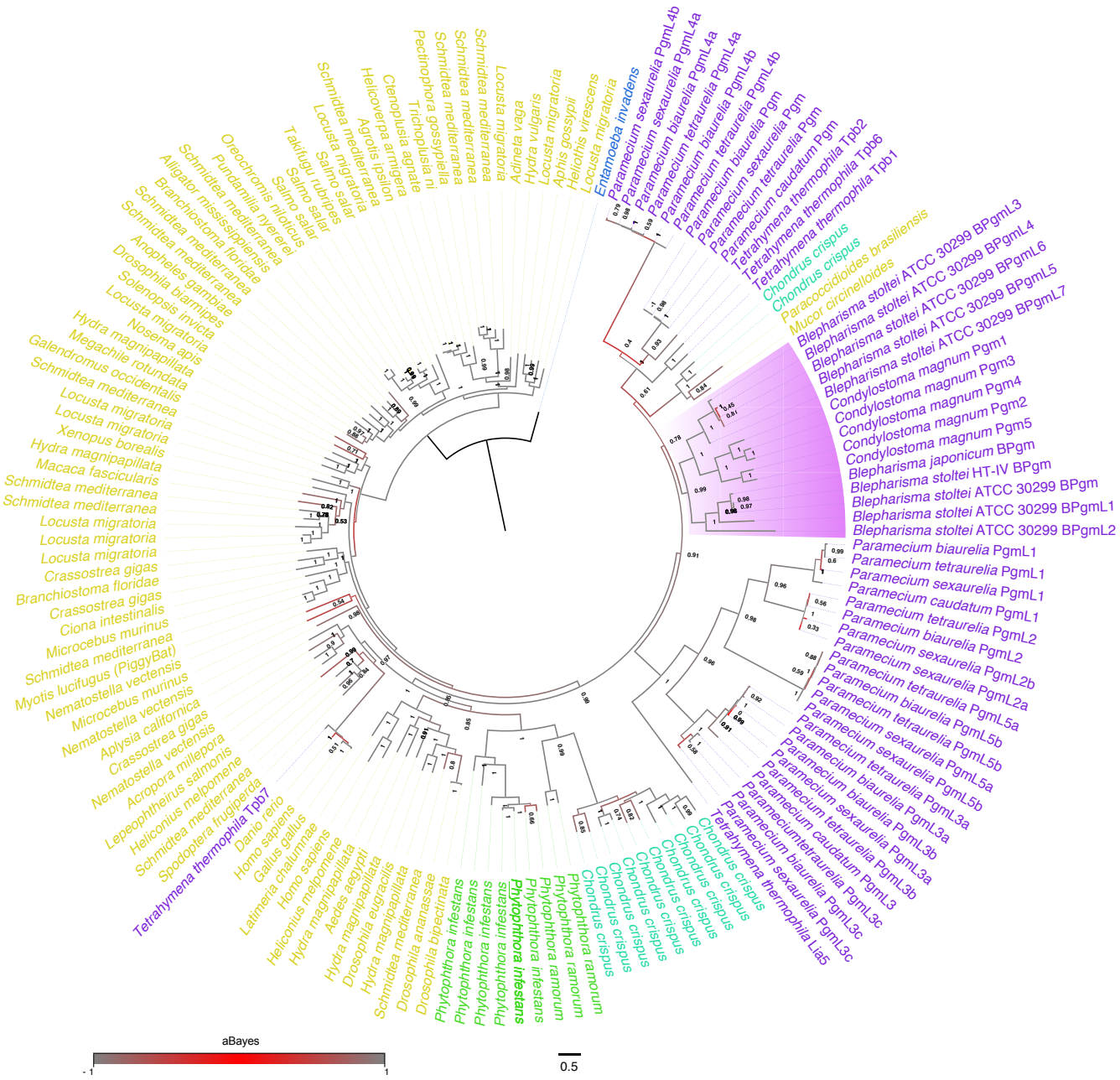
Entamoeba invadens
Paramecium sexaurelia PgmL4b
Paramecium sexaurelia PgmL4a
Paramecium biaurelia PgmL4a
Paramecium tetraurelia PgmL4a
Paramecium biaurelia PgmL4b
Paramecium tetraurelia PgmL4b
Paramecium sexaurelia Pgm
Paramecium tetraurelia Pgm
Paramecium caudatum Pgm
Tetrahymena thermophila Tpb2
Tetrahymena thermophila Tpb6
Tetrahymena thermophila Tpb1
Chondrus crispus
Paracoccidioides brasiliensis
Mucor circinelloides
Blepharisma stoltei ATCC 30299 BPgmL3
Blepharisma stoltei ATCC 30299 BPgmL4
Blepharisma stoltei ATCC 30299 BPgmL6
Blepharisma stoltei ATCC 30299 BPgmL5
Blepharisma stoltei ATCC 30299 BPgmL7
Blepharisma stoltei ATCC 30299 Pgm1
Condylostoma magnum Pgm3
Condylostoma magnum Pgm4
Condylostoma magnum Pgm2
Condylostoma magnum Pgm5
Blepharisma japonicum BPgm
Blepharisma stoltei HT-IV BPgm
Blepharisma stoltei ATCC 30299 BPgm
Blepharisma stoltei ATCC 30299 BPgmL1
Blepharisma stoltei ATCC 30299 BPgmL2
Paramecium biaurelia PgmL1
Paramecium tetraurelia PgmL1
Paramecium sexaurelia PgmL1
Paramecium caudatum PgmL1
Paramecium tetraurelia PgmL2
Paramecium biaurelia PgmL2
Paramecium sexaurelia PgmL2b
Paramecium tetraurelia PgmL2a
Paramecium biaurelia PgmL5a
Paramecium tetraurelia PgmL5b
Paramecium sexaurelia PgmL5b
Paramecium tetraurelia PgmL5a
Paramecium biaurelia PgmL5b
Paramecium sexaurelia PgmL3a
Paramecium tetraurelia PgmL3a
Paramecium biaurelia PgmL3b
Paramecium sexaurelia PgmL3b
Paramecium caudatum PgmL3
Paramecium tetraurelia PgmL3c
Paramecium biaurelia PgmL3c
Paramecium sexaurelia PgmL3c
Tetrahymena thermophila Lia5
Chondrus crispus
Chondrus crispus
Chondrus crispus
Chondrus crispus
Chondrus crispus
Chondrus crispus
Chondrus crispus
Chondrus crispus
Chondrus crispus
Chondrus crispus
Chondrus crispus
Chondrus crispus
Phytophthora ramorum
Phytophthora ramorum
Phytophthora ramorum
Phytophthora infestans
Phytophthora infestans
Phytophthora infestans
Phytophthora infestans
Phytophthora infestans
Phytophthora infestans
Phytophthora infestans
Phytophthora infestans
Drosophila bipectinata
Drosophila ananassae
Drosophila mediterranea
Schmidtea mediterranea
Hydra magnipapillata
Drosophila eugracilis
Hydra magnipapillata
Aedes aegypti
Hydra magnipapillata
Homo sapiens
Heliconius melpomene
Hydra magnipapillata
Latimeria chalumnae
Homo sapiens
Gallus gallus
Danio rerio
Spodoptera frugiperda
Schmidtea mediterranea
Heliconius melpomene
Lepeophtheirus salmonis
Acropora millepora
Nematostella vectensis
Crassostrea gigas
Aplysia californica
Nematostella vectensis
Microcebus murinus
Myotis lucifugus (PiggyBat)
Schmidtea mediterranea
Microcebus murinus
Nematostella vectensis
Ciona intestinalis
Crassostrea gigas
Branchiostoma floridae
Crassostrea gigas
Locusta migratoria
Locusta migratoria
Locusta migratoria
Schmidtea mediterranea
Schmidtea mediterranea
Macaca fascicularis
Hydra magnipapillata
Xenopus borealis
Locusta migratoria
Locusta migratoria
Schmidtea mediterranea
Galendromus occidentalis
Megachile rotundata
Hydra magnipapillata
Nosema apis
Locusta migratoria
Solenopsis invicta
Drosophila biarmipes
Anopheles gambiae
Schmidtea mediterranea
Schmidtea mediterranea
Branchiostoma floridae
Alligator mississippiensis
Schmidtea mediterranea
Pundamilia nyererei
Oreochromis niloticus
Salmo salar
Salmo salar
Takifugu rubripes
Locusta migratoria
Salmo salar
Schmidtea mediterranea
Agrotis ipsilon
Helicoverpa armigera
Ctenoplusia agnate
Trichoplusia ni
Pectinophora gossypiella
Schmidtea mediterranea
Schmidtea mediterranea
Schmidtea mediterranea
Locusta migratoria
Adineta vaga
Hydra vulgaris
Locusta migratoria
Aphis gossypii
Heliothis virescens
Locusta migratoria
Tetrahymena thermophila Tpb7
aBayes
- 1
1
0.5

Figure S1.

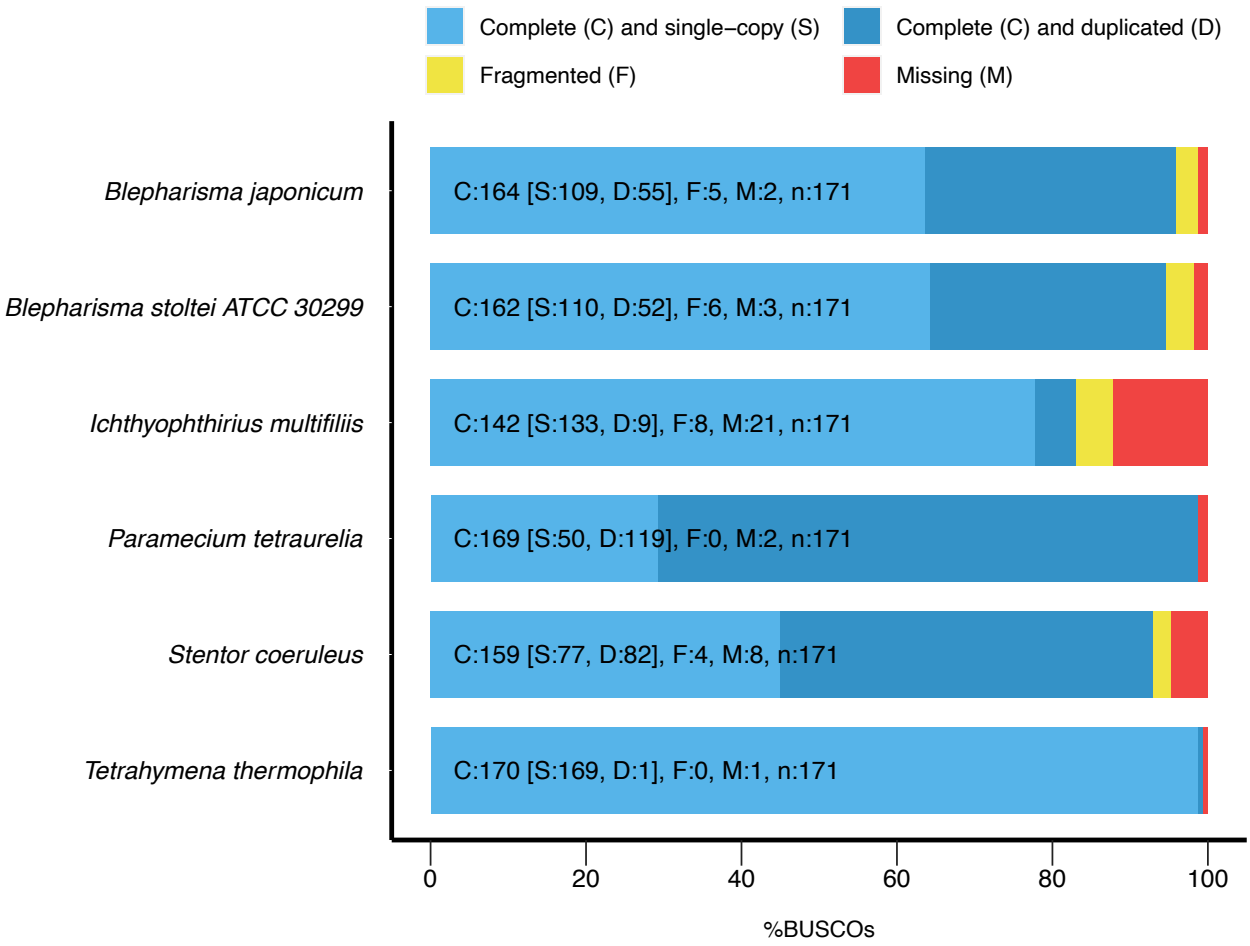
Complete (C) and single−copy (S)
Complete (C) and duplicated (D)
Fragmented (F)
Missing (M)
Blepharisma japonicum
C:164 [S:109, D:55], F:5, M:2, n:171
Blepharisma stoltei ATCC 30299
C:162 [S:110, D:52], F:6, M:3, n:171
Ichthyophthirius multifiliis
C:142 [S:133, D:9], F:8, M:21, n:171
Paramecium tetraurelia
C:169 [S:50, D:119], F:0, M:2, n:171
Stentor coeruleus
C:159 [S:77, D:82], F:4, M:8, n:171
Tetrahymena thermophila
C:170 [S:169, D:1], F:0, M:1, n:171
0
20
40
60
80
100
%BUSCOs

Figure S2.

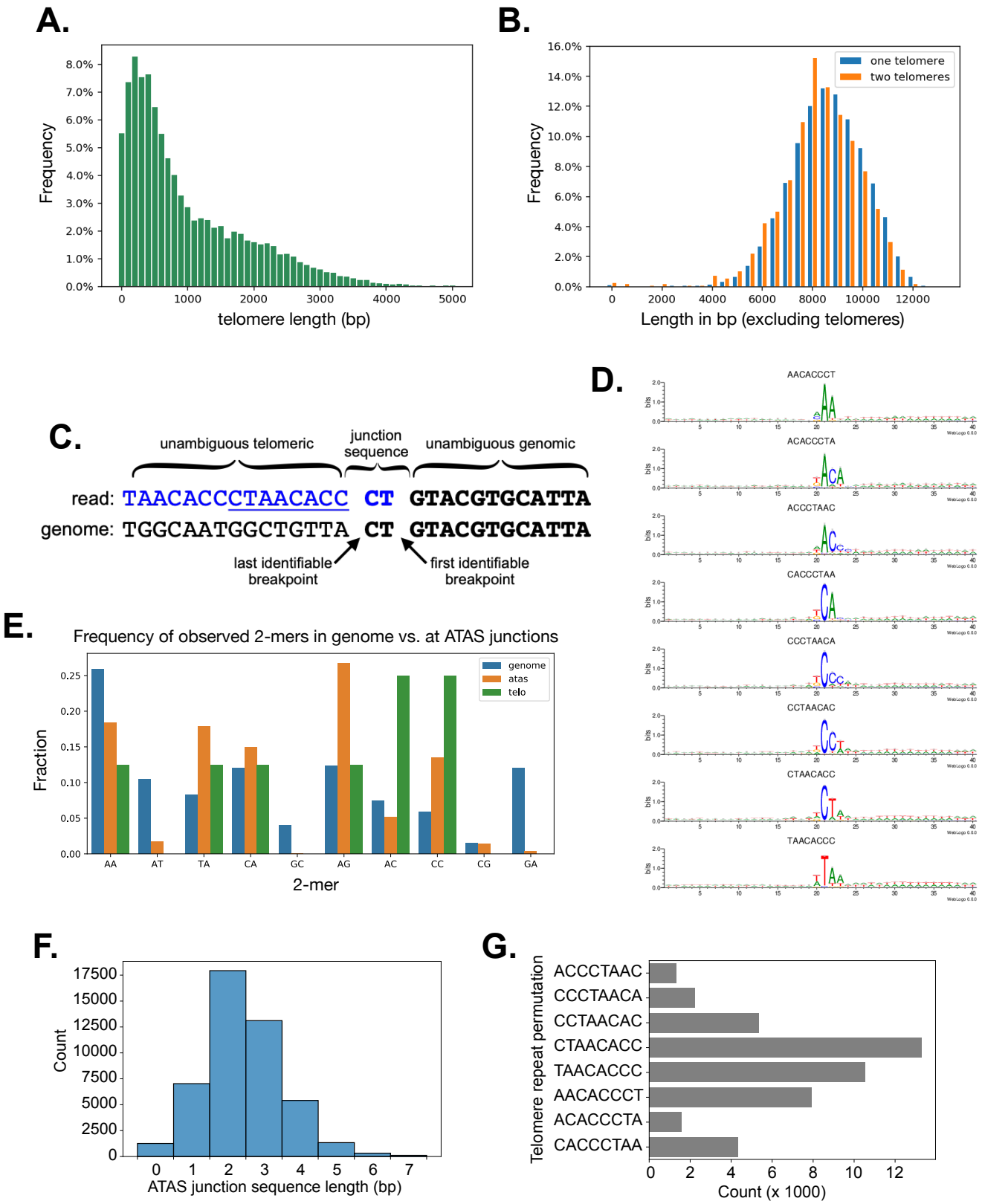
A.
Frequency
telomere length (bp)
B.
one telomere
two telomeres
Frequency
Length in bp (excluding telomeres)
C.
unambiguous telomeric
junction sequence
unambiguous genomic
read: TAACACCCTAACACC CT GTACGTGCATTA
genome: TGGCAATGGCTGTTA CT GTACGTGCATTA
last identifiable breakpoint
first identifiable breakpoint
D.
AACACCCT
ACACCCTA
ACCCTAAC
CACCCTAA
CCCTAACA
CCTAACAC
CTAACACC
TAACACCC
E.
Frequency of observed 2-mers in genome vs. at ATAS junctions
genome
atas
telo
Fraction
AA
AT
TA
CA
GC
AG
AC
CC
CG
GA
2-mer
F.
Count
ATAS junction sequence length (bp)
G.
Telomere repeat permutation
ACCCTAAC
CCCTAACA
CCTAACAC
CTAACACC
TAACACCC
AACACCCT
ACACCCTA
CACCCTAA
Count (x 1000)

Figure S3.

A.

C.

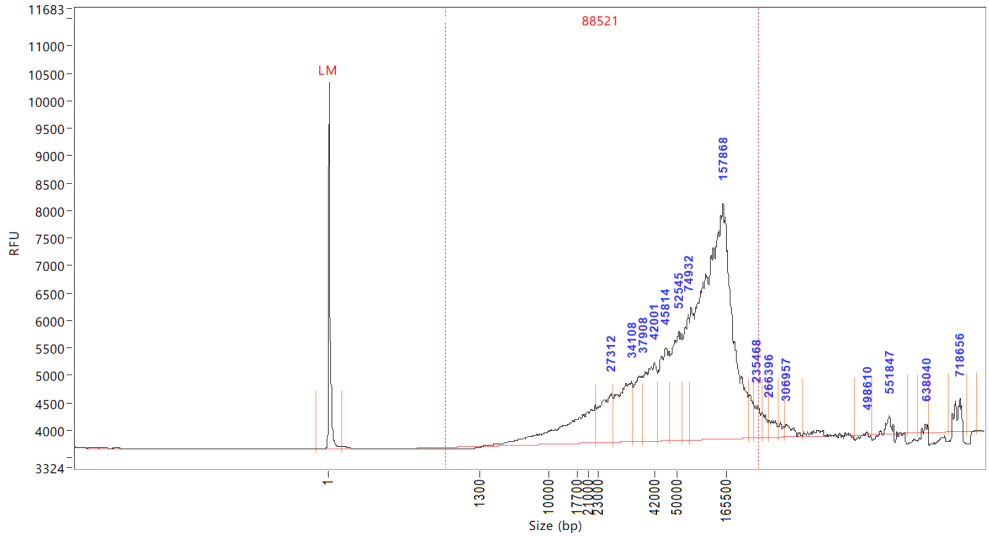

D.

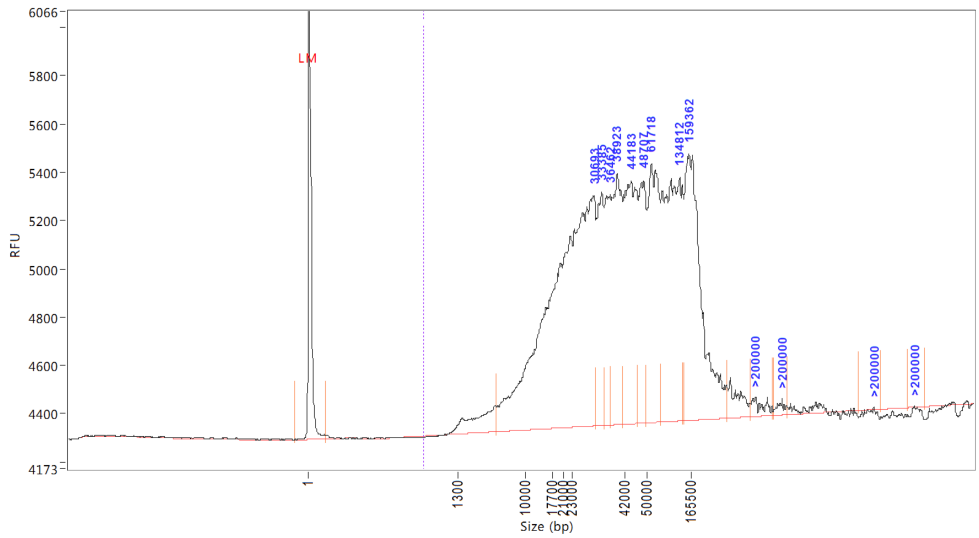

Figure S4.

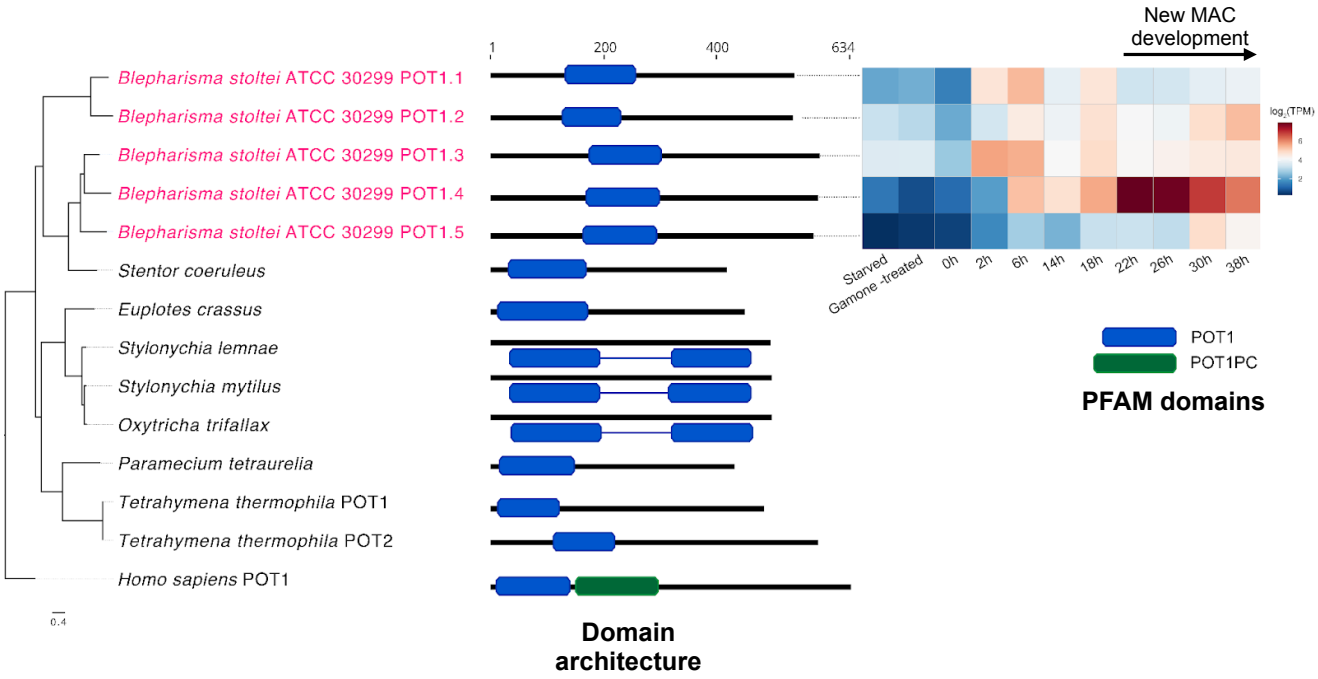
Blepharisma stoltei ATCC 30299 POT1.1
Blepharisma stoltei ATCC 30299 POT1.2
Blepharisma stoltei ATCC 30299 POT1.3
Blepharisma stoltei ATCC 30299 POT1.4
Blepharisma stoltei ATCC 30299 POT1.5
Stentor coeruleus
Euplotes crassus
Stylonychia lemnae
Stylonychia mytilus
Oxytricha trifallax
Paramecium tetraurelia
Tetrahymena thermophila POT1
Tetrahymena thermophila POT2
Homo sapiens POT1
0.4
1
200
400
634
Domain architecture
New MAC development
Starved
Gamone -treated
0h
2h
6h
14h
18h
22h
26h
30h
38h
log2(TPM)
POT1
POT1PC
PFAM domains

Figure S5.

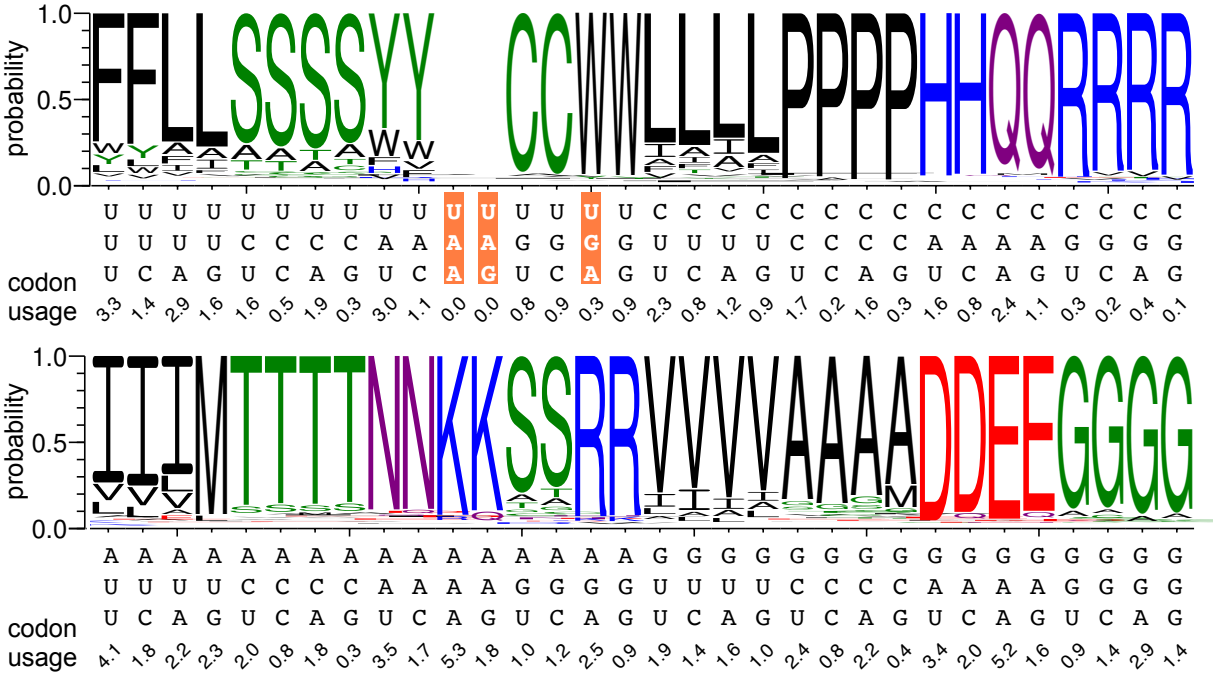
probability
1.0
0.5
0.0
codon
usage
U U U U U U U U U U U U U U U U C C C C C C C C C C C C C C C C
U U U U C C C C A A A A G G G G U U U U C C C C A A A A G G G G
U C A G U C A G U C A G U C A G U C A G U C A G U C A G U C A G
3.3 1.4 2.9 1.6 1.6 0.5 1.9 0.3 3.0 1.1 0.0 0.0 0.8 0.9 0.3 0.9 2.3 0.8 1.2 0.9 1.7 0.2 1.6 0.3 1.6 0.8 2.4 1.1 0.3 0.2 0.4 0.1
probability
1.0
0.5
0.0
codon
usage
A A A A A A A A A A A A A A A A G G G G G G G G G G G G G G G G
U U U U C C C C A A A A G G G G U U U U C C C C A A A A G G G G
U C A G U C A G U C A G U C A G U C A G U C A G U C A G U C A G
4.1 1.8 2.2 2.3 2.0 0.8 1.8 0.3 3.5 1.7 5.3 1.8 1.0 1.2 2.5 0.9 1.9 1.4 1.6 1.0 2.4 0.8 2.2 0.4 3.4 2.0 5.2 1.6 0.9 1.4 2.9 1.4

Figure S6.

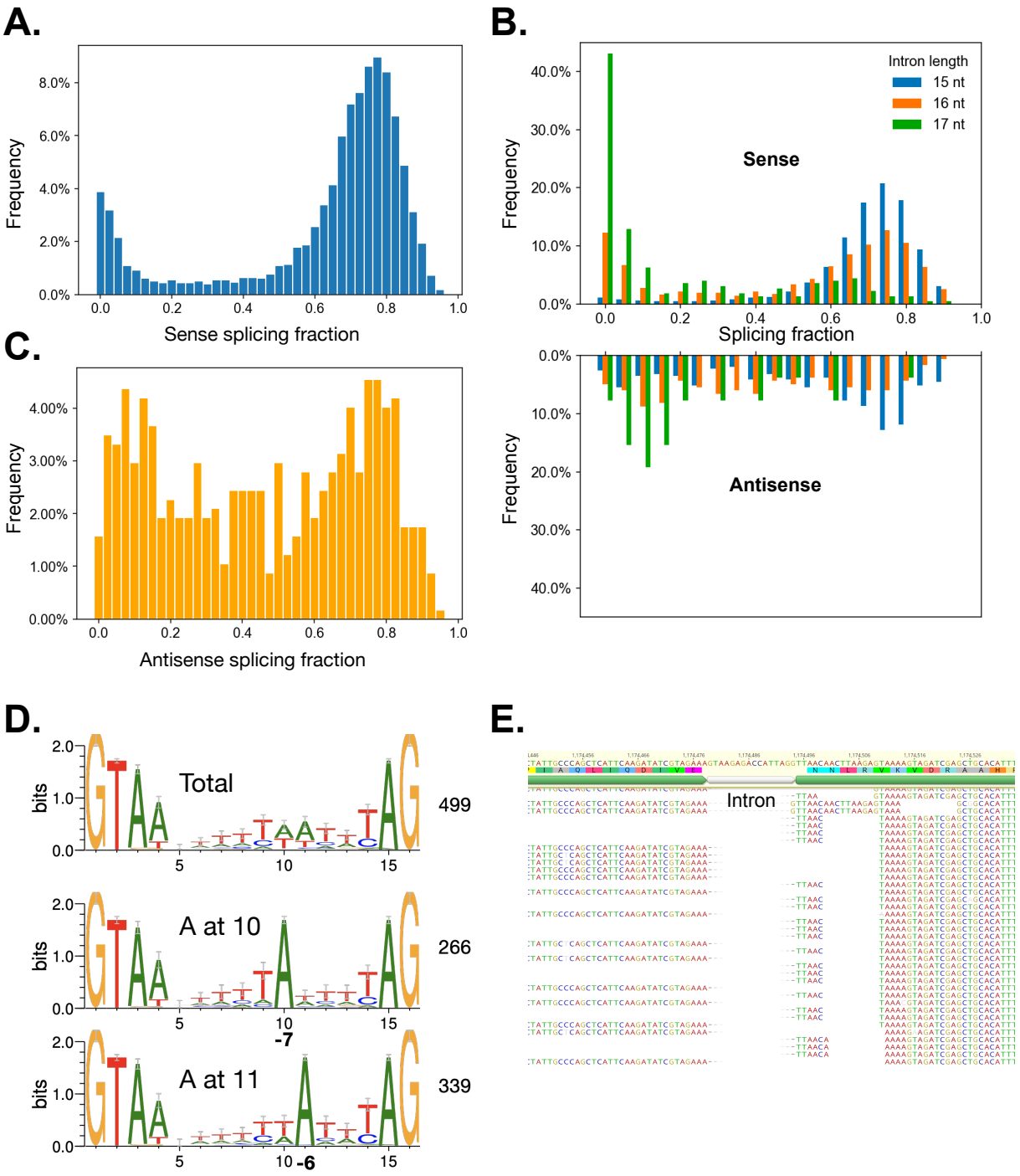
A.
Frequency
8.0%
6.0%
4.0%
2.0%
0.0%
0.0
0.2
0.4
0.6
0.8
1.0
Sense splicing fraction
B.
Intron length
15 nt
16 nt
17 nt
Sense
Frequency
40.0%
30.0%
20.0%
10.0%
0.0%
Splicing fraction
Antisense
C.
Frequency
4.00%
3.00%
2.00%
1.00%
0.00%
Antisense splicing fraction
D.
Total
499
A at 10
266
A at 11
339
bits
2.0
1.0
0.0
5
10
15
-7
-6
E.
Intron

Figure S7.

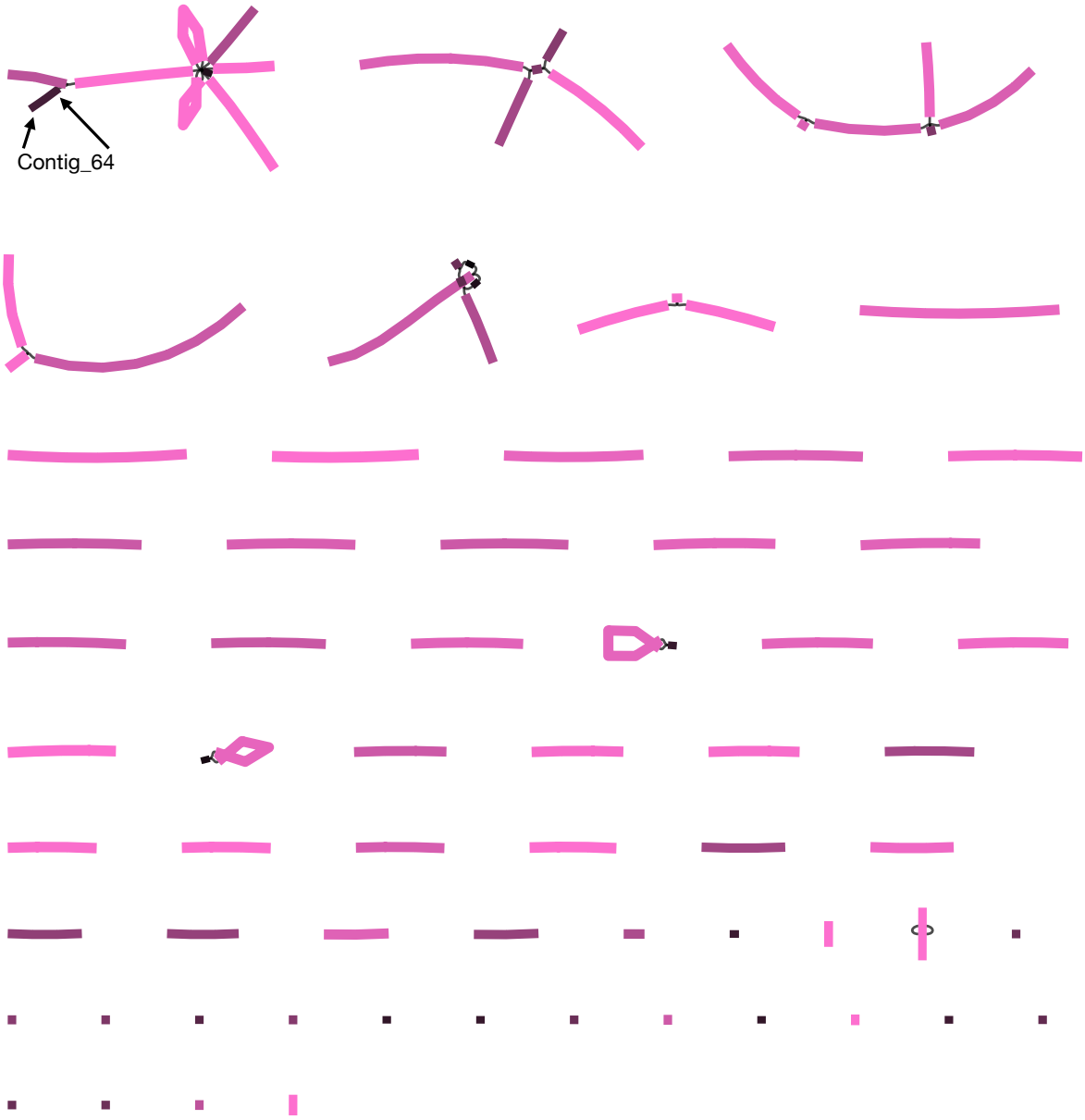

Figure S8.

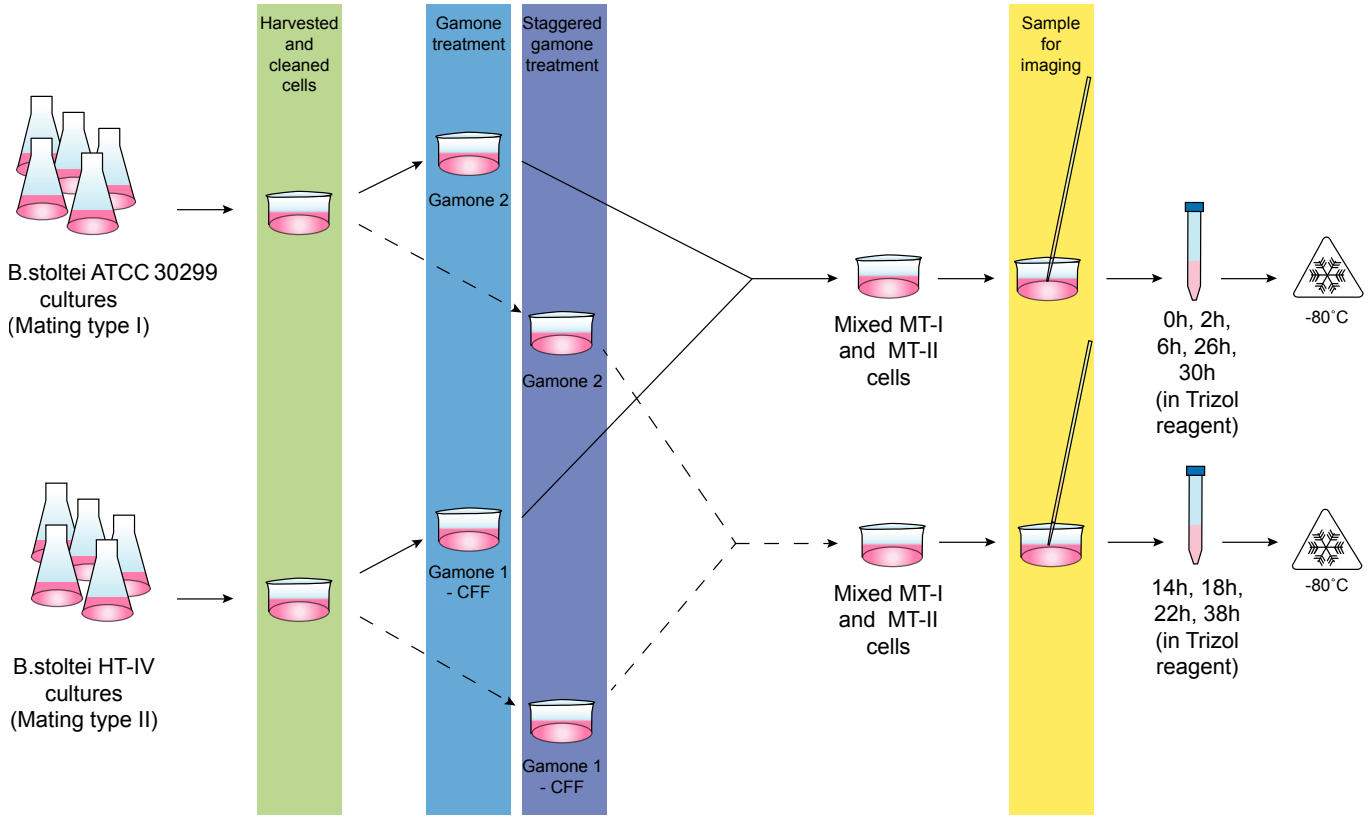
Harvested and cleaned cells
Gamone treatment
Staggered gamone treatment
Sample for imaging
B.stoltei ATCC 30299 cultures (Mating type I)
B.stoltei HT-IV cultures (Mating type II)
Gamone 2
Gamone 2
Gamone 1 - CFF
Gamone 1 - CFF
Mixed MT-I and MT-II cells
Mixed MT-I and MT-II cells
0h, 2h, 6h, 26h, 30h (in Trizol reagent)
14h, 18h, 22h, 38h (in Trizol reagent)
-80˚C
-80˚C

Figure S9.

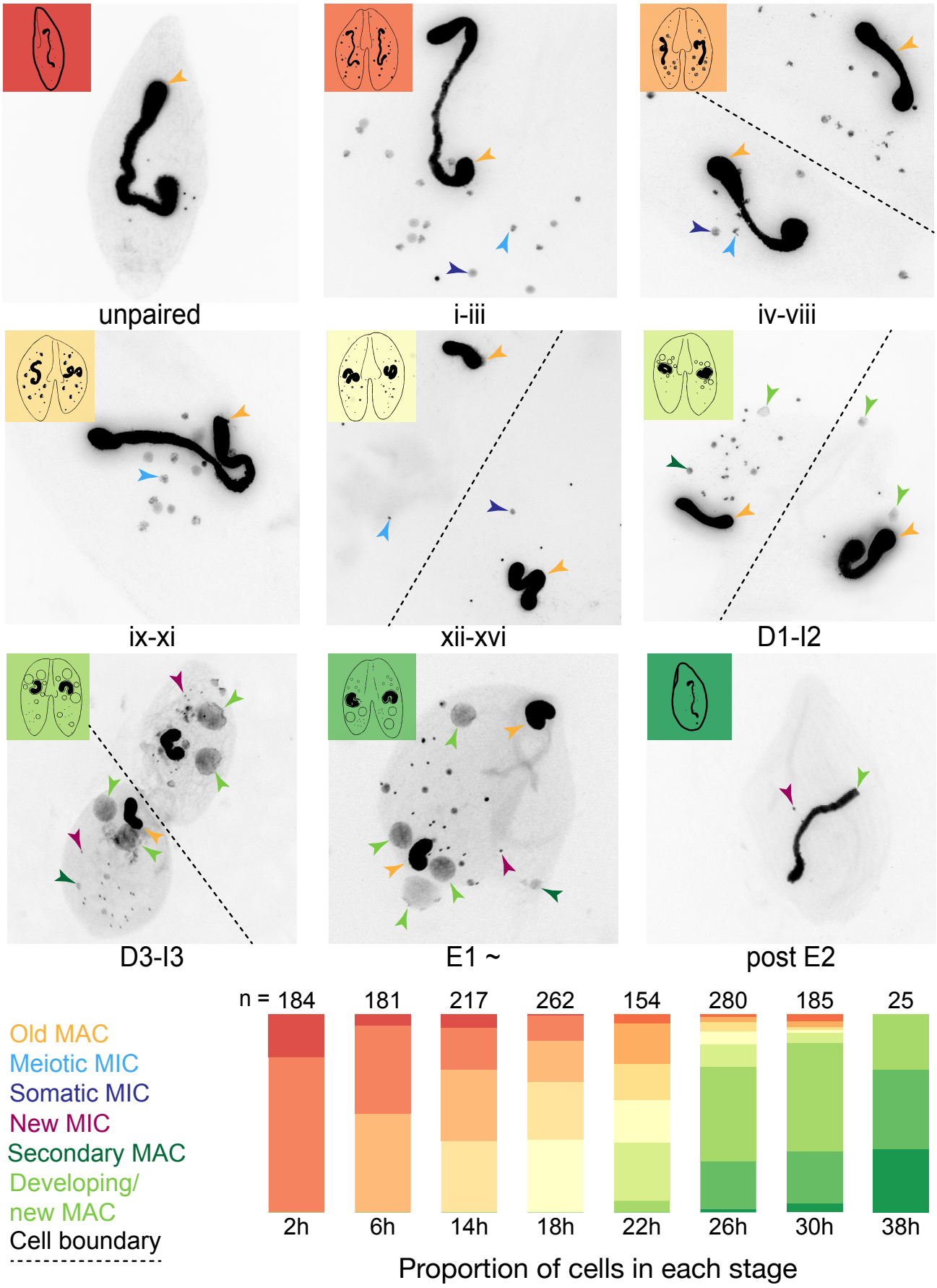
unpaired
i-iii
iv-viii
ix-xi
xii-xvi
D1-I2
D3-I3
E1 ~
post E2
n = 184
181
217
262
154
280
185
25
Old MAC
Meiotic MIC
Somatic MIC
New MIC
Secondary MAC
Developing/
new MAC
Cell boundary
2h
6h
14h
18h
22h
26h
30h
38h
Proportion of cells in each stage

Figure S10.

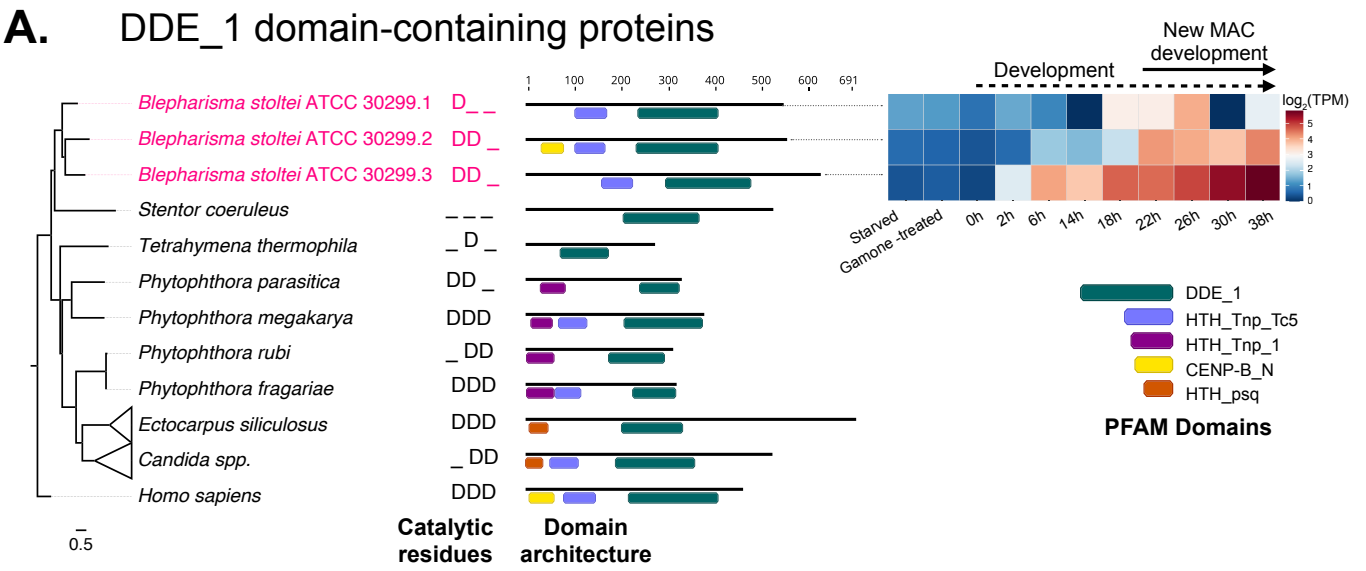
A.
DDE_1 domain-containing proteins
Blepharisma stoltei ATCC 30299.1
Blepharisma stoltei ATCC 30299.2
Blepharisma stoltei ATCC 30299.3
Stentor coeruleus
Tetrahymena thermophila
Phytophthora parasitica
Phytophthora megakarya
Phytophthora rubi
Phytophthora fragariae
Ectocarpus siliculosus
Candida spp.
Homo sapiens
0.5
D_ _
DD _
DD _
_ _ _
_ D _
DD _
DDD
_ DD
DDD
DDD
_ DD
DDD
Catalytic residues
Domain architecture
1
100
200
300
400
500
600
691
New MAC development
Development
log2(TPM)
Starved
Gamone -treated
0h
2h
6h
14h
18h
22h
26h
30h
38h
DDE_1
HTH_Tnp_Tc5
HTH_Tnp_1
CENP-B_N
HTH_psq
PFAM Domains

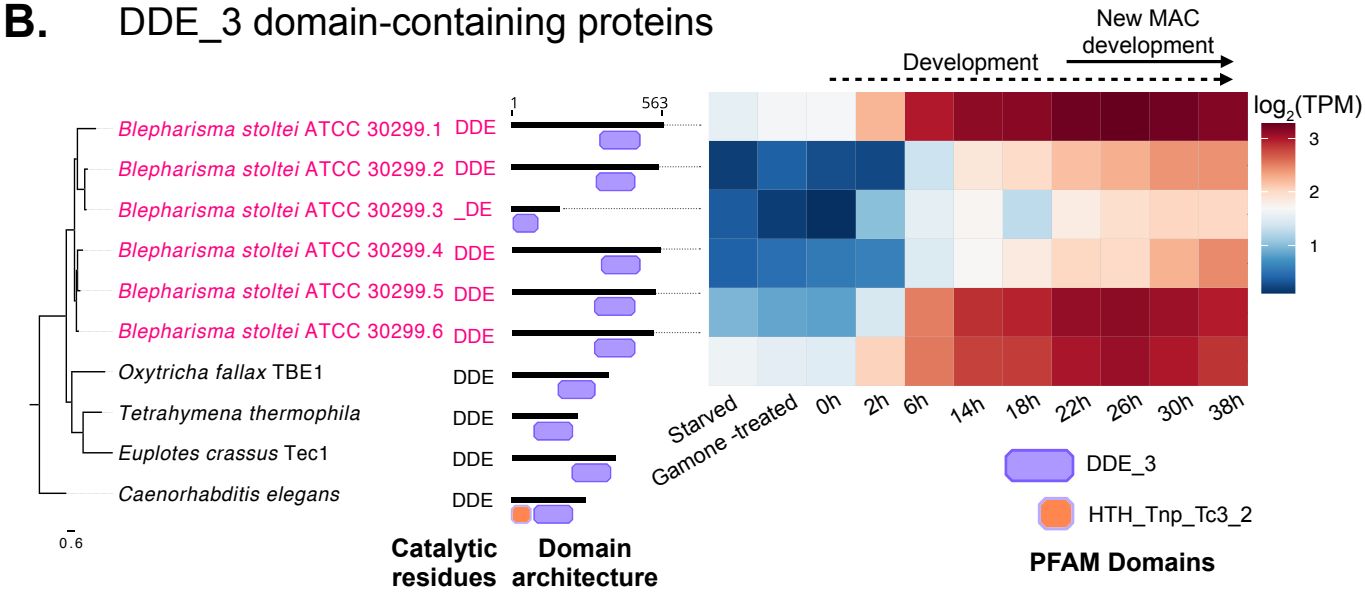
B.
DDE_3 domain-containing proteins
Blepharisma stoltei ATCC 30299.1
Blepharisma stoltei ATCC 30299.2
Blepharisma stoltei ATCC 30299.3
Blepharisma stoltei ATCC 30299.4
Blepharisma stoltei ATCC 30299.5
Blepharisma stoltei ATCC 30299.6
Oxytricha fallax TBE1
Tetrahymena thermophila
Euplotes crassus Tec1
Caenorhabditis elegans
0.6
DDE
DDE
_DE
DDE
DDE
DDE
DDE
DDE
DDE
Catalytic residues
Domain architecture
1
563
New MAC development
Development
log2(TPM)
3
2
1
Starved
Gamone -treated
0h
2h
6h
14h
18h
22h
26h
30h
38h
DDE_3
HTH_Tnp_Tc3_2
PFAM Domains

Figure S11.

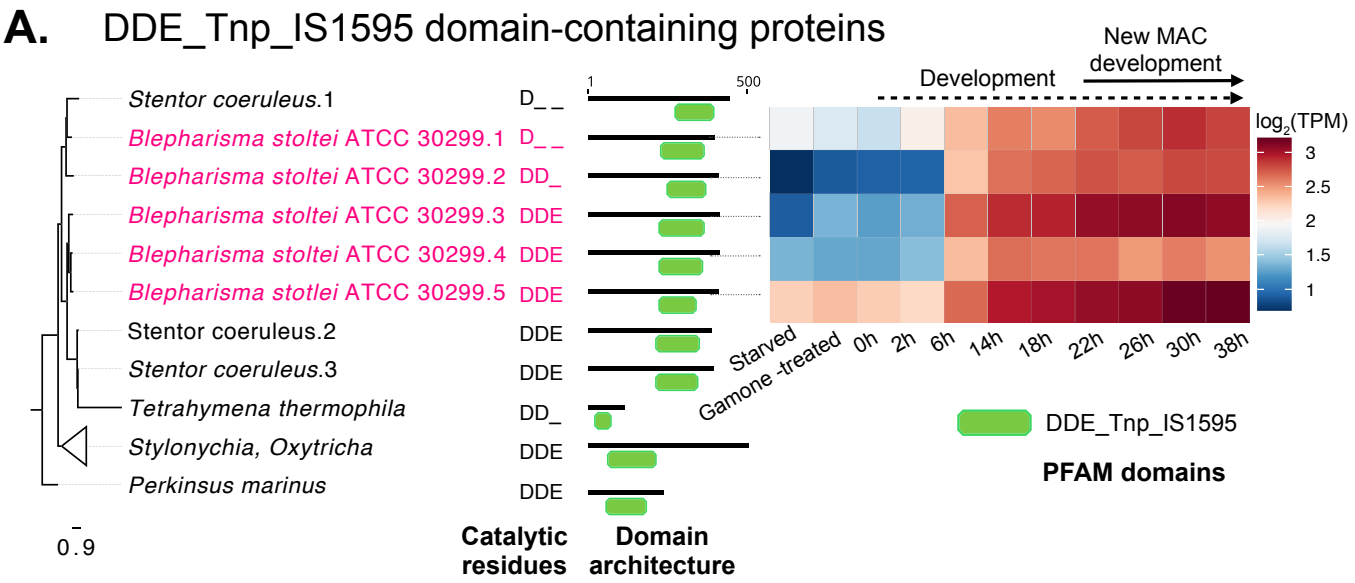
A.
DDE_Tnp_IS1595 domain-containing proteins
Stentor coeruleus.1
Blepharisma stoltei ATCC 30299.1
Blepharisma stoltei ATCC 30299.2
Blepharisma stoltei ATCC 30299.3
Blepharisma stoltei ATCC 30299.4
Blepharisma stotlei ATCC 30299.5
Stentor coeruleus.2
Stentor coeruleus.3
Tetrahymena thermophila
Stylonychia, Oxytricha
Perkinsus marinus
0.9
D_ _
D_ _
DD_
DDE
DDE
DDE
DDE
DDE
DD_
DDE
DDE
Catalytic residues
1
500
Domain architecture
Development
New MAC development
log2(TPM)
3
2.5
2
1.5
1
Starved
Gamone -treated
0h
2h
6h
14h
18h
22h
26h
30h
38h
DDE_Tnp_IS1595
PFAM domains

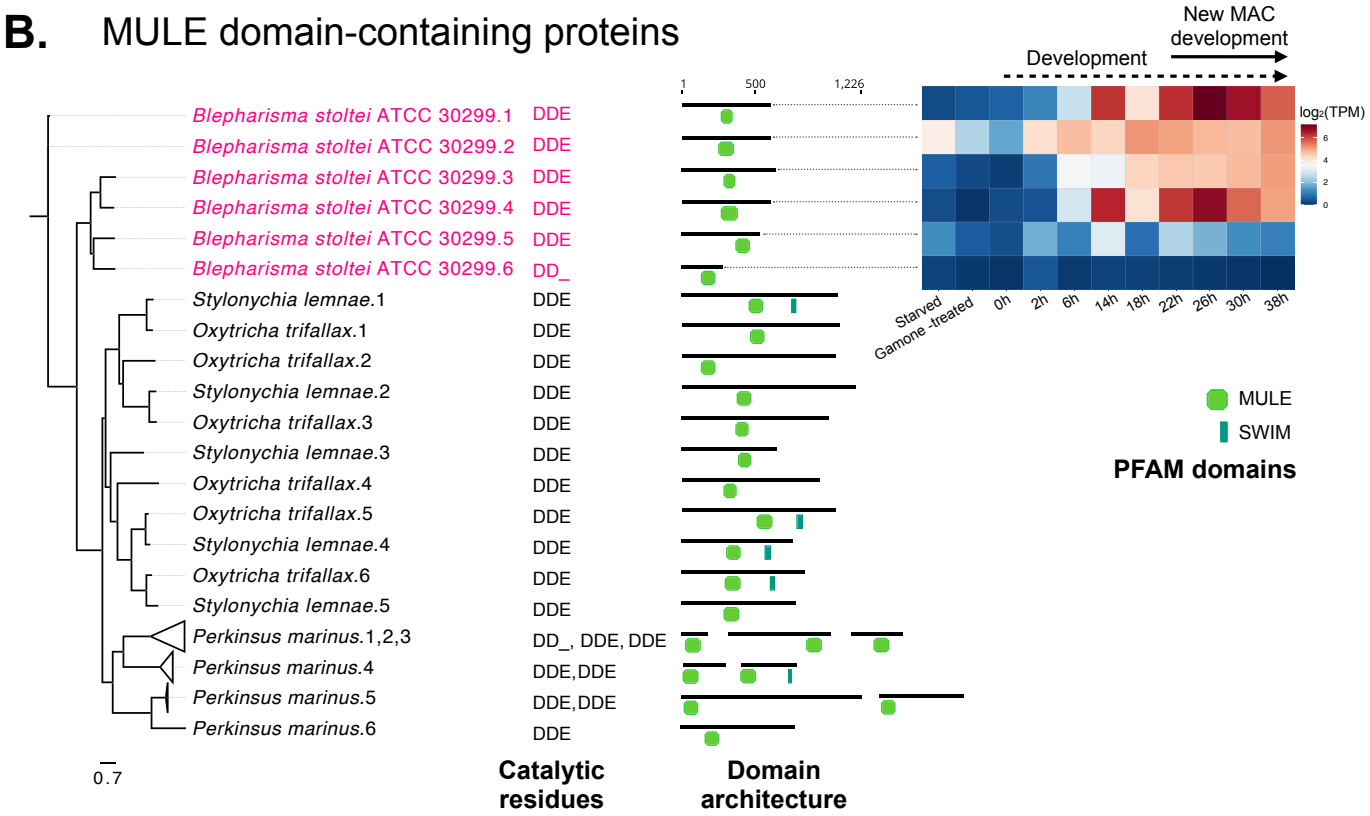
B.
MULE domain-containing proteins
Blepharisma stoltei ATCC 30299.1
Blepharisma stoltei ATCC 30299.2
Blepharisma stoltei ATCC 30299.3
Blepharisma stoltei ATCC 30299.4
Blepharisma stoltei ATCC 30299.5
Blepharisma stoltei ATCC 30299.6
Stylonychia lemnae.1
Oxytricha trifallax.1
Oxytricha trifallax.2
Stylonychia lemnae.2
Oxytricha trifallax.3
Stylonychia lemnae.3
Oxytricha trifallax.4
Oxytricha trifallax.5
Stylonychia lemnae.4
Oxytricha trifallax.6
Stylonychia lemnae.5
Perkinsus marinus.1,2,3
Perkinsus marinus.4
Perkinsus marinus.5
Perkinsus marinus.6
0.7
DDE
DDE
DDE
DDE
DDE
DD_
DDE
DDE
DDE
DDE
DDE
DDE
DDE
DDE
DDE
DD_, DDE, DDE
DDE,DDE
DDE,DDE
DDE
Catalytic residues
1
500
1,226
Domain architecture
Development
New MAC development
log2(TPM)
6
4
2
0
Starved
Gamone -treated
0h
2h
6h
14h
18h
22h
26h
30h
38h
MULE
SWIM
PFAM domains

Figure S12.

A. Dicers, Dicer-likes and Dicer-derivatives

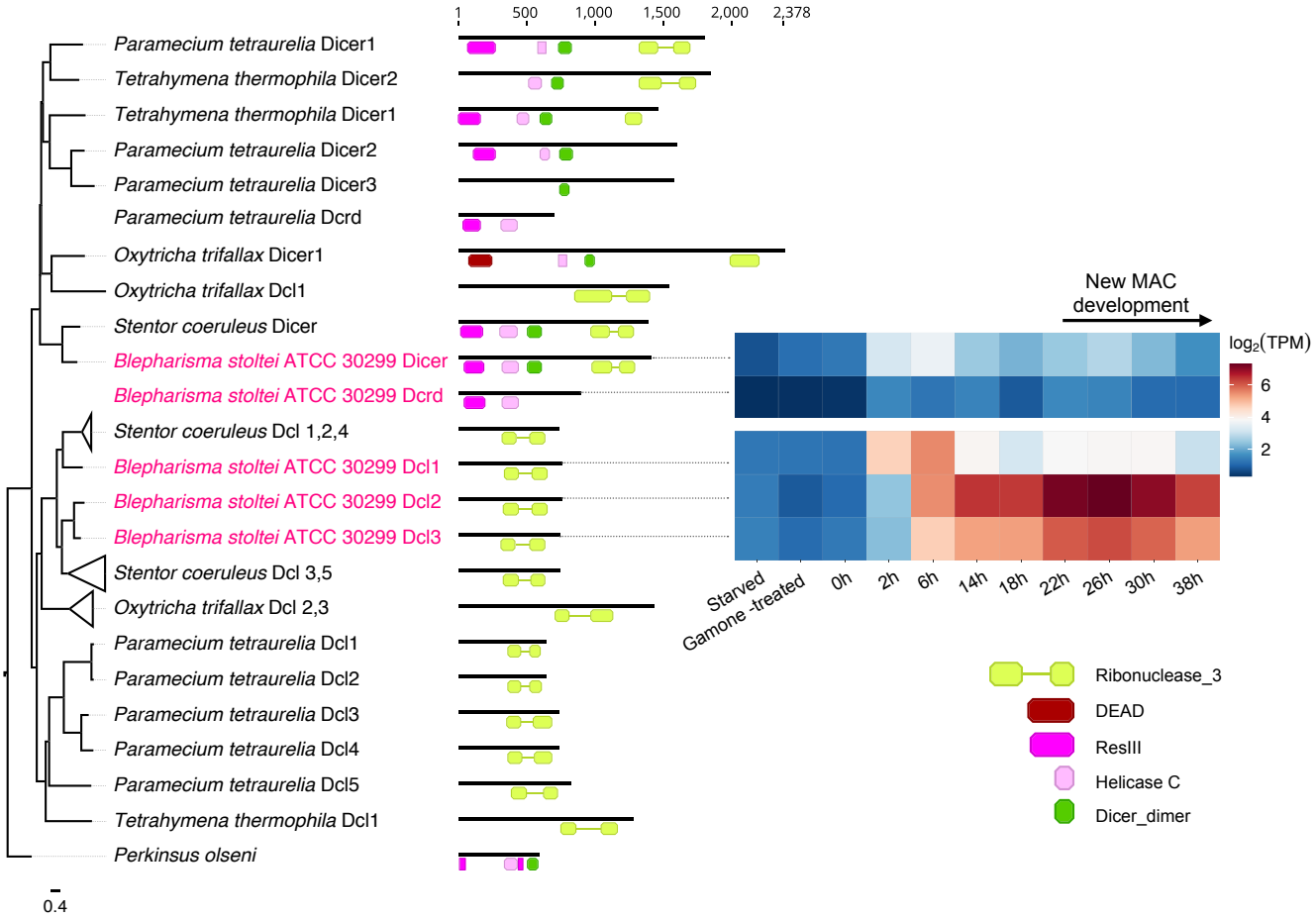

B. Piwi proteins

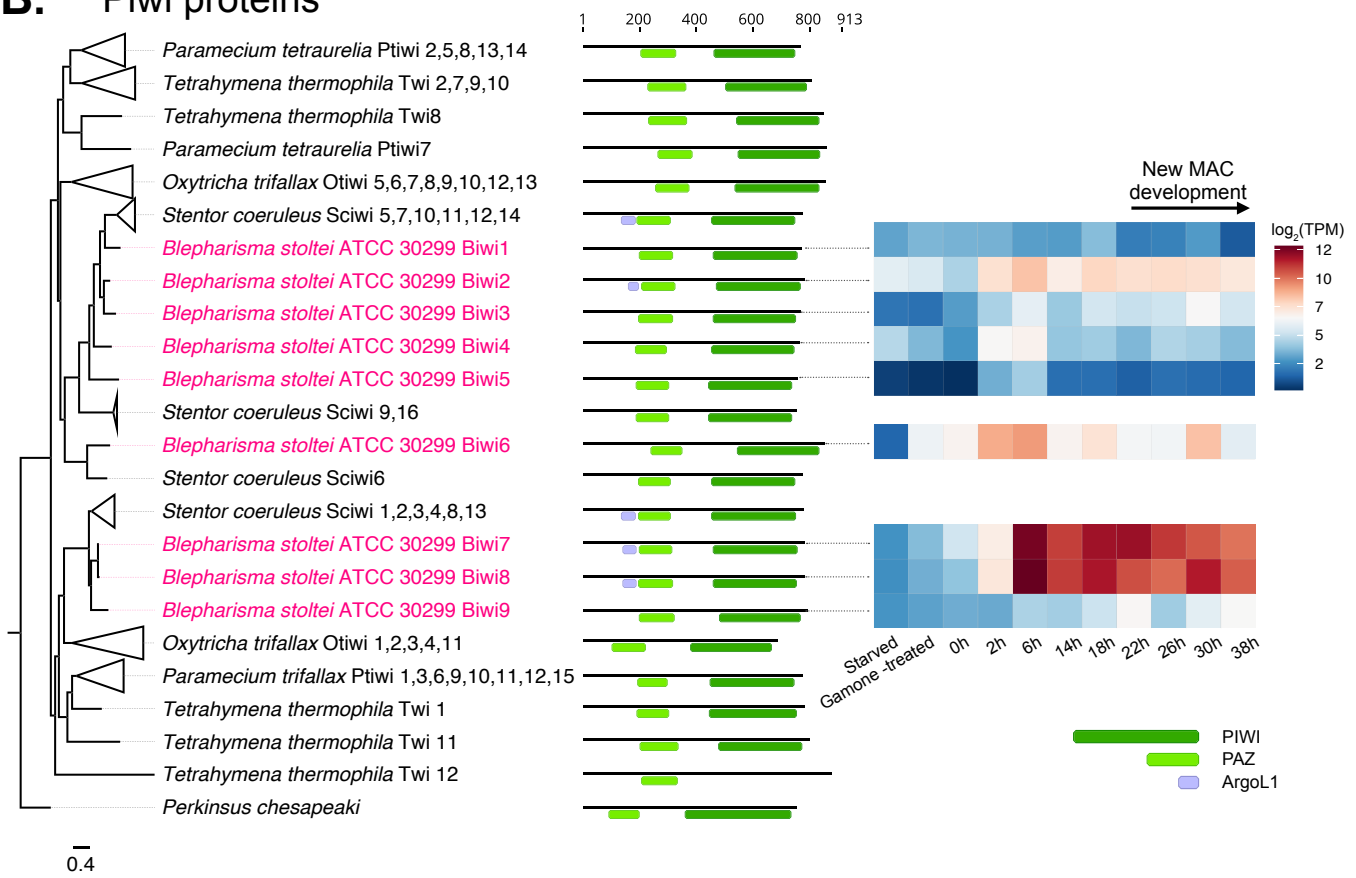

Figure S13.

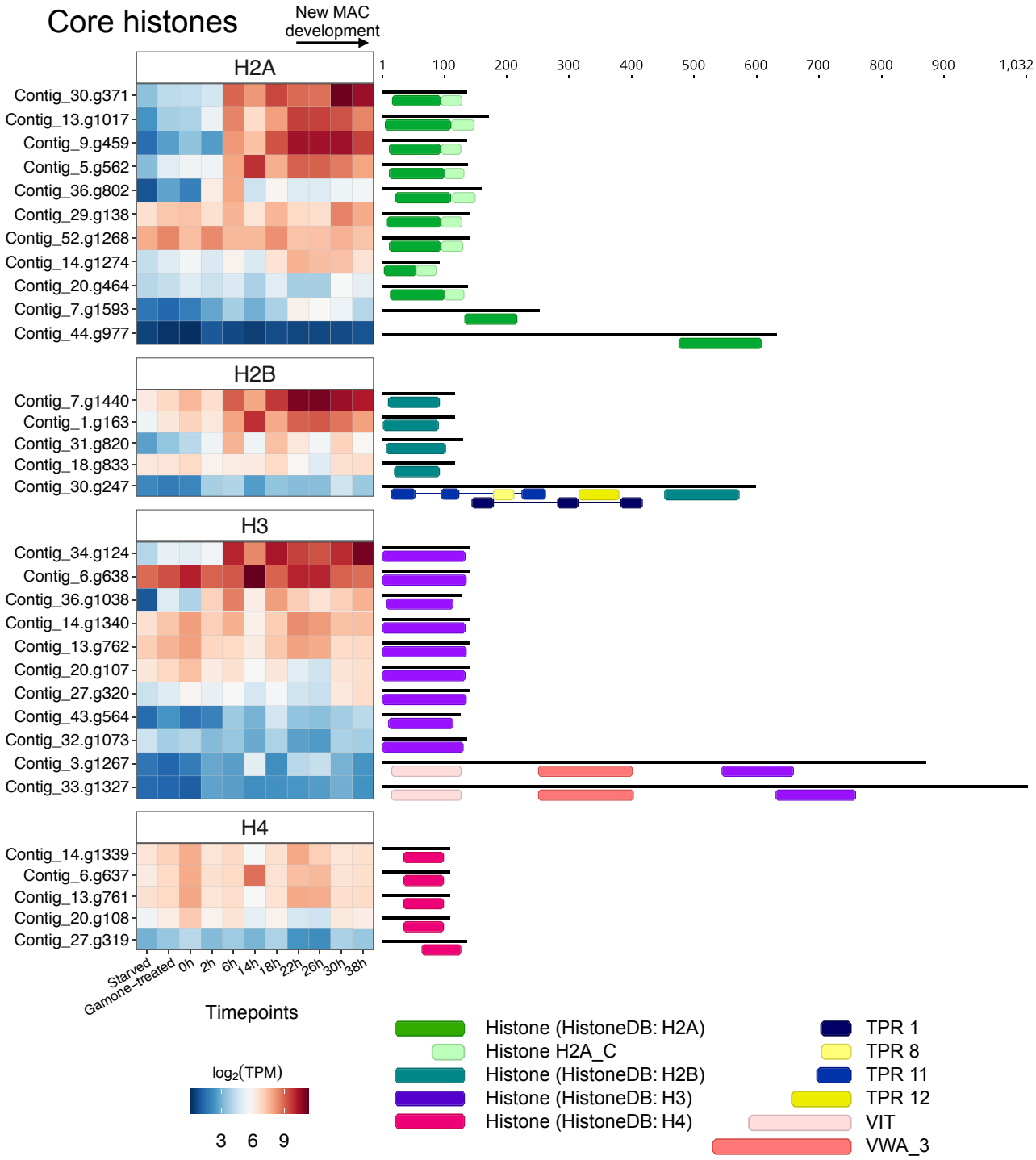
Core histones
New MAC development
H2A
Contig_30.g371
Contig_13.g1017
Contig_9.g459
Contig_5.g562
Contig_36.g802
Contig_29.g138
Contig_52.g1268
Contig_14.g1274
Contig_20.g464
Contig_7.g1593
Contig_44.g977
1
100
200
300
400
500
600
700
800
900
1,032
H2B
Contig_7.g1440
Contig_1.g163
Contig_31.g820
Contig_18.g833
Contig_30.g247
H3
Contig_34.g124
Contig_6.g638
Contig_36.g1038
Contig_14.g1340
Contig_13.g762
Contig_20.g107
Contig_27.g320
Contig_43.g564
Contig_32.g1073
Contig_3.g1267
Contig_33.g1327
H4
Contig_14.g1339
Contig_6.g637
Contig_13.g761
Contig_20.g108
Contig_27.g319
Starved
Gamone-treated
0h
2h
6h
14h
18h
22h
26h
30h
38h
Timepoints
log2(TPM)
3
6
9
Histone (HistoneDB: H2A)
Histone H2A_C
Histone (HistoneDB: H2B)
Histone (HistoneDB: H3)
Histone (HistoneDB: H4)
TPR 1
TPR 8
TPR 11
TPR 12
VIT
VWA_3